UNIVERSITY OF SOUTHAMPTON
Faculty of Physical Sciences and Engineering
School of Electronics and Computer Science

Development of an Electrodeposited PdNi-Si Schottky Barrier Hydrogen Sensor

by

Longtao Dong

A thesis submitted for the
degree of Doctor of Philosophy

February 2015

Supervisor: Prof Cornelis H. de Groot

UNIVERSITY OF SOUTHAMPTON

ABSTRACT

FACULTY OF PHYSICAL SCIENCE AND ENGINEERING
SCHOOL OF ELECTRONICS AND COMPUTER SCIENCE

Doctor of Philosophy

by Longtao Dong

This thesis presents the development of low power electrodeposited PdNi-Si Schottky barrier hydrogen sensors with the purpose of enabling distributed sensor networks allowing the further development of hydrogen as a renewable alternative to carbon-based fuels. In this work a Schottky barrier based PdNi-Si hydrogen sensor is introduced which can compete with available sensors in terms of sensitivity and selectivity, while at the same time having extremely low power consumption. It is shown that variation of the electrodeposition potential is capable of creating PdNi alloys with the ratio of Pd to Ni spanning almost the entire range. Based on this possibility we present a new technique of composition-modulated PdNi films, in which each part of the PdNi film is separately optimized within a single electrodeposition process for use in a Schottky barrier hydrogen sensor. Back to back PdNi-Si Schottky barrier hydrogen sensor have been fabricated. The Current-Voltage characteristic of back to back Pd-Si Schottky barrier in both hydrogen and nitrogen ambient clearly demonstrate that the back to back Schottky barrier have a good sensitivity to hydrogen. The sensors have been integrated in a printed circuit board (PCB) for aqueous measurement to take advantage of the low power consumption of the hydrogen sensors to allow the fabrication of ubiquitous distributed unpowered sensor network.

It is shown that the pure Ni films do not show evidence of response to hydrogen and that adding a thin layer of Pd on top allows those sensors to function, but that an alloy of both materials is required to prevent the formation of the destructive β Pd phase. The increase in current with hydrogen can be explained by a decrease of the Schottky barrier height. The sensors have full selectivity with respect to nitrogen and oxygen. It is shown that sensitivity is optimum for $Pd_{1-x}Ni_x$ with x around 0.4 whereas time response is optimum for x around 0.1. This conundrum is solved by the composition-modulated technique. The time response results for the $Pd_{1-x}Ni_x$ composition modulated surface layer and constant Pd-Ni ratio in

the bulk layer prove that the speed of hydrogen dissociation at the surface scales near exponential with an increase of Pd concentration indicating that as high Pd concentration in the surface layer should be selected which is compatible with the prevention of the β-phase during cycling. The sensitivity response results for the composition modulated barrier layer with constant Pd-Ni ratio in the bulk layer and 10% Ni in the surface layer agrees with the previous results on uniform films with x=0.4 giving the highest sensitivity. It is hence concluded that a $Pd_{1-x}Ni_x$ film with x=0.1, 0.3, 0.4 for the surface, bulk, and barrier layer, respectively, is the optimum composition.

The relation between response time and hydrogen concentration was tested and showed a drastically fall with increasing hydrogen concentration. The quickest time response was achieved as the concentration reach to 5000ppm and a power law relation of -0.76 was found. A dissociation limited rate equation would follow Sievert's law and result in a slope of -0.5 while limitation in number of trap states at the PdNi-Si interface would result in a slope of -1.0. Our results on response time versus hydrogen concentration indicate that both dissociation and number of traps state at the Schottky barrier interface are of importance in the determination of the sensitivity of the sensor.

Temperature dependent measurements show that these sensors function properly at both slightly elevated and below zero temperature. The temperature dependence characteristic of the Schottky barrier height shows that the sensor have a good fit with the equation describing the current as function of temperature in terms of spatial variation of the barrier height. Minimizing this spatial variation is essential for reliable operation of the sensor.

Contents

Declaration of Authorship

I, Longtao Dong, declare that this thesis and the work presented in it are my own and has been generated by me as the result of my own original research.

"Development of an electrodeposited PdNi-Si Schottky barrier hydrogen sensor."

I confirm that:

- This work was done wholly or mainly while in candidature for a research degree at this University;
- Where any part of this thesis has previously been submitted for a degree or any other qualification at this University or any other institution, this has been clearly stated;
- Where I have consulted the published work of others, this is always clearly attributed;
- where I have quoted from the work of others, the source is always given. With the exception of such quotations, this thesis is entirely my own work.
- I have acknowledged all main sources of help;
- where the thesis is based on work done by myself jointly with others, I have made clear what was done by others and what I have contributed myself
- Either none of this work has been published before submission, or parts of this work have been published as: A list of publications is provided with this manuscript.

Signed:

Date:

List of Publications

Conference Presentations

Electrodeposited PdNi-Si Schottky barrier hydrogen sensors with improved time response.

Dong, Longtao, de Groot, C.H., Usgaocar, A. and Chavagnac, V.,Eurosensors 2012: The 26th European Conference on Solid-State Transducers, Krakow, Poland (09 - 12 Sep 2012).

Effect of interfacial PdNi concentration on time response of Si-based electrodeposited hydrogen sensors.

Dong, L., de Groot, C.H., Usgaocar, A. and Chavagnac, V., At Transducers 2013 and Eurosensors XXVII: The 17th International Conference on Solid-State Sensors, Actuators, and Microsystems,Barcelona, ES, 16 - 20 Jun 2013. 4pp.

Journal

Composition-modulated electrodeposited PdNi-Si Schottky barrier hydrogen sensors L. Dong , C.H. de Groot. Sensors and Actuators B: Chemical [to be submitted]

Acknowledgements

Although obtaining a PhD degree requires mostly the individual effort and dedication in scientific research, without many people who have supported me in different aspects to the completion of thesis would have made it impossible. I want to reckon a few words in the frontline of my thesis to express my great appreciation.

Firstly and most importantly, I would like to express my sincere gratitude to my supervisor Prof. Kees de Groot for his excellent guidance, non-stop encouragement, support and occasionally criticism in my research. His experimental and methodical approach to the science was profoundly educational and inspirational. During my PhD period, he was very patient to guide and inspire me to overcome my weakness. Special thanks to Dr. Ashwin Usgaocar for his help with electrodeposition of the PdNi alloy and the initial help on probe station to measure the sensor in the beginning of my PhD and Dr Maurits de Planque for his assessments and contributions during my internal viva. I also have to thank Kian for his help on lithography, machine lift-off process; Peter Ayliffe for all his training and help on SEM and EDX; Owain and James for their help on e-beam evaporator and wet room process; Richard for his help on the thermal oxidation process. Yan Zhao for his help on the preparation of PDMS. Xiaoli for her training on the C-V measurement and discussion on my project.; Ruomeng, Yunpeng, Shuojin, Yudong, Xingzhao, Suhana, Ibrahim, Sara, Hwanjit, Feras, Taha, Ken, for all the help and best time spent altogether in the cleanroom and office. Of course, the Nano group secretary Glenys, who helped me a lot in terms of all the administrative issues.

Finally, I want to give a big thank you to my girlfriend Yi Qu. Since we met at my first year of PhD, my life was totally changed. Without her encouragement in the life style, I would probably still is a fat boy. For my parents who always supported and gave me this opportunity to study abroad, and I hope my accomplishment could make them proud and fulfill.

I Dedicated this study to my whole family

Chapter 1

Introduction

1.1 Hydrogen Sensor

Oil based fuels are finite and environmentally hazardous, and the search for alternatives is driven by increasing concern about the negative effects of CO_2 emissions on climate change. Liquid Hydrogen already has been utilized in rockets as a powerful fuel. Furthermore, in the industrialized sectors such as the chemical-, food-, semiconductor- and transportation-sector, hydrogen has turned out to be one of the most useful gases. For the next generation of conversion from fossil fuel energy source to renewable energy, a clean source of hydrogen will be paramount in the utilization of hydrogen as an alternative source of raw material or fuel. The key property of hydrogen as renewable alternative to carbon-based fuels, is its clean combustion without harmful emission.

Hydrogen sensors are critical to insure the safety of hydrogen systems due to hydrogen's combustion characteristics which include

- Low minimum ignition energy:0.015mJ
- High heat of combustion:147kJ/g H_2
- Wide flammable range:4-75%
- High diffusivity:0.61 cm^2s^{-1}
- lightest element:0.08988 g/L
- Autoignition temperature:500^oC

The other special properties of hydrogen are its absence of colour, odour and taste, so hydrogen gas can not be discovered by the human sense function. In 1937, the airship Hindenburg, powered by hydrogen gas, flew from Germany to USA, caught fire and exploded resulting in 36 fatalities. An urgent need of hydrogen safety sensor was commissioned as a result of this accident and other similar explosions, but even though this accident is more than 75 years ago, the safety of hydrogen gas has not recovered in the human mind.

Currently, people use natural gas fuels boilers and cooking stoves in their homes. Hydrogen as an end use fuel could replace natural gas, as well as the fuel cell based micro-CHP (combined heat and power) boilers which fueled by the hydrogen can also produce volumes of decentralized electricity during peak demand time [1]. With the developing hydrogen fuel cell industry, the consumption of hydrogen gas has a drastic potential to expand. Due to hydrogen gas having the characteristic of low mass, high diffusivity, and extremely low liquefaction point, the storage of hydrogen gas is not easy. Meanwhile, the dimension of a hydrogen molecule is very small which makes it difficult to seal any container hermetically and prevent leaks. So, with the continuous research and development in hydrogen technology both as an energy carrier and for other industrial uses, there is clear need for advanced hydrogen sensors for the measurement and monitoring of hydrogen concentration during production, storage, and transport. Furthermore, accurate measurement of gas composition and in-situ monitoring of hydrogen is of great economic value for the energy industry. For a hydrogen fuel cell, the mixture and distribution of hydrogen gas are vital for the efficiency of the fuel cell. Therefore, a highly sensitive hydrogen detecting technology becomes even more crucial.

1.2 PdNi-Si Hydrogen Sensor

Hydrogen sensors are needed that can be operated at temperatures from -30 to 1000 ^{o}C, and this results in the use of unique designs and new sensor materials. For many widespread applications, a sensor with simplicity and low cost as well as small size and minimal power consumption is desired. The fundamentals of palladium based sensor technology for sensing applications is its independence from the local environment as well as its small size and ability to be used at high pressures. Electrochemical approaches to sensing hydrogen can provide one of the lowest power approaches for gas monitoring combined with good analytical performance.

In the last years, many hydrogen sensors use palladium as transducer. Most solid state hydrogen sensors measure the resistance change in Pd/Pd-alloy films and current changes in Pt/Pd-semiconductor Schottky barriers on exposure to hydrogen [2]. Palladium catalyzes the dissociation of hydrogen molecules and exhibits changes in its properties on hydrogen absorption. The effect of alloying with Nickel is making the Palladium film more robust in handling multiple hydrogen exposures. The low reverse bias current of PdNi-Si Schottky barrier is used to fabricate low power hydrogen sensor. Recent research in Southampton, has resulted in PdNi-Si Schottky barrier sensors in which the critical process is the electro-deposition of the metal on Si. These electrodeposited Ni-Si Schottky diodes presented low reverse bias current and higher on/off ratios compared to evaporated Schottky diode. The sensor was designed as a back to back Schottky diode pair which can draw very low idle current and exhibit large percentage increases in current on hydrogen exposure. However, these sensors respond much too slow to be of any practical use. It is the object of the research presented in this thesis to understand the time response of this sensor and improve the structure such that the response time is significantly improved.

1.3 Thesis Outline

In this PhD thesis the work is presented as follows:

- In chapter 2, a review of current hydrogen sensing technologies is introduced. This chapter not only lists the advantages and disadvantages of particular hydrogen sensors, but explains the use metal semiconductor Schottky barrier structures as object of our research.
- Chapter 3 describes the fundamentals of electrodeposition as well as the process to deposit PdNi alloys with desirable concentrations. The concept of the Schottky barrier is also introduced in this chapter. Basic theory of the current-voltage (I-V) and capacitance-voltage (C-V) characteristics of Schottky diodes is explained in terms of ideality factor and barrier height.
- Chapter 4 introduces the design and fabrication process of the Schottky barrier hydrogen sensor. The sensor was designed as a back to back Schottky diode which results in very low idle current.
- In Chapter 5, hydrogen sensors with uniform PdNi alloy composition were characterized by full of C-V and I-V technique both at room temperature

and as function of temperature. Using a combination of measurement, the best alloy composition was found to be used as the bulk of the thin film.

- In Chapter 6, the sensor is further improved by using an innovative electrodeposition process to create surface and interface layers of different alloy composition than the bulk. This techniques allows individual parts of the thin film to be optimized for response time, sensitivity and cyclability. The optimized sensor is subsequently tested in different hydrogen concentrations and at different temperatures to fully characterize the response.

Chapter 2

Hydrogen Sensor Reviews

2.1 Sensor Specifications

Currently, there exists a broad range of hydrogen sensing technologies and it is therefore complicated to select an appropriate sensing technology for a proper application. There are numerous different types of hydrogen safety sensors commercially available and new technologies continue to be developed and are expected to be commercialized successfully. In the following sections, some hydrogen sensor which are already commercially available will be described together with the most promising research activities. The current mature and commercial available hydrogen sensor technologies include the following different types [3].

- Electrochemical sensors
- "Pellistor"-type combustible sensors
- Thermal conductivity sensors
- Semiconductive metal-oxide sensors
- MEMS type and acoustic sensors
- Resistive Pd-film and Pd-alloy films sensors
- Metal Oxide Semiconductor sensors
- Schottky barrier hydrogen sensors

The gas sensor sensitivity is the key characteristic to describe the performance. Generally, sensitivity for a gas sensor is expressed as the ratio of current change or resistance change between nitrogen and hydrogen ambient at a certain hydrogen concentration, but this generates different values for each hydrogen concentration [4]. In order to have a reasonable fair comparison between different sensor techniques, we define two sensitivities for the PdNi Schottky barrier hydrogen sensor; the high hydrogen concentration was defined as concentration above 1% and the low concentration as between 0 to 1%. The equations are 2.1, 2.2, respectively.

$$S_{high} = \frac{I_{1\%} - I_{0\%}}{I_{0\%}} \tag{2.1}$$

$$S_{low} = \frac{I_{5000ppm} - I_{0ppm}}{I_{0ppm}} \tag{2.2}$$

The gas selectivity α_{AB} is defined as the ratio of the permeability coefficient of the gas A (P_A) to the permeability coefficient of the gas B (P_B). Normally, A is the most permeable gas resulting in $\alpha_{AB} > 1$. This value of the selectivity is unit-less [5]. This value also can be interpreted as that the gas sensor is more sensitive to gas A than to gas B by a factor of α_{AB} . Therefore, the selectivity of a hydrogen sensor can be expressed as Eq. 2.3.

$$\alpha_{H_2B} = \frac{\Delta I_{H_2}/N_2}{\Delta I_B/N_2} \tag{2.3}$$

For response time of the hydrogen sensor, the widely accepted definition is the time it takes to reach 90% of the difference in steady-state current from nitrogen or vacuum ambient to the hydrogen ambient [6, 7].

2.2 Electrochemical Sensors

For the electrochemical hydrogen sensor, hydrogen is oxidized at a sensing electrode surface which is coated with a platinum catalyst. The oxidation reaction at the electrode surface results in a potential difference between the sensing electrode and the reference electrode [8]. Electrochemical sensors are classified into two categories of sensors: amperometric and potentiometric.

The basic schematic of an amperometric sensor is illustrated in Fig. 2.1. The electrolyte in this figure is sandwiched between the sensing electrode and another

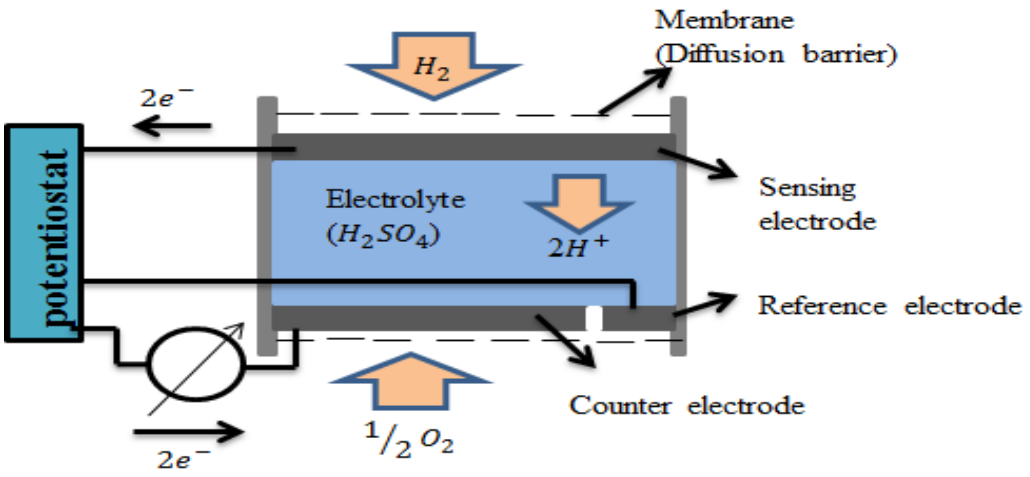

FIGURE 2.1: Schematic of a 3-electrode amperometric sensor [9].

electrode called the counter electrode. The electrolyte normally is a solid form of Hydrogen Uranyl Phosphate ($HUO_2PO_4.4H_2O$) which is a good conductor for H^+ ions. Operationally, the electrochemical hydrogen sensor undergoes an electrochemical reaction when subjected to hydrogen gas, resulting in an electrical current that is proportion to the hydrogen gas concentration. The hydrogen molecules experience a variation in oxidation state which lead to a transition from the molecule as displayed in Eq. 2.4 in which the hydrogen gas after the catalytic process is changed to hydrogen ions. Two electrons are freed during this process. The reduction of oxygen takes place at the counter electrode simultaneously as displayed in Eq. 2.5 .

$$H_2 \rightarrow 2H^+ + 2e^- \tag{2.4}$$

$$1/2O_2 + 2H^+ + 2e^- \rightarrow H_2O \tag{2.5}$$

When the sensor senses the hydrogen gas in the actual situation, the hydrogen gas diffuses through a permeable hydrophobic gas barrier (membrane) and reaches the surface of the electrode. This barrier is utilized to control the amount of gas which will react at the sensing electrode. The barrier not only controls the amount of gas to achieve a sufficient electrical signal, but can also prevent the electrolyte to leak out of the sensor [10].

As Fig. 2.1 shows, these sensors are typically managed by an external electronic circuit or a potentiostat. The potentiostat does not only control the electrochemical conditions of the sensor but also provides stable ambient to measure the current. The applied potential between working and reference electrode set by the

potentiostat fixes the thermodynamic operating potential for the working reaction [11]. It is critical for both the observed sensitivity and the selectivity of the sensor. Moreover, a selection of operating potential is an effective way to change or optimize the performance of the sensor. Amperometric gas sensors have a good sensitivity with wide linear range. Amperometric sensors exhibit cross sensitivity to various species, including some hydrocarbons and a number of approaches have been investigated to improve this. As mentioned above, the gas permeable barrier was adapted to improve the selectivity by filtering other gases and prevent them from diffusing into the sensor.

In order to achieve a good selectivity, Chao.Y *et al.* [12] mounted a FEP (fluorinated ethylene propylene) membrane at the gas inlet of the sensor. The hydrogen can rapidly pass through the FEP membrane and react with Pt at the working electrode. The cross sensitivity to gases such as carbon monoxide, ammonia and hydrogen sulphide was eliminated with nearly 100% efficiency in the short term. Also Sakthivel and Weppner reported a sensor with Pd diffusion barrier to freeze the CO and CO_2 contaminated electrode [13]. A hydrogen sensor combining the working principles of amperometric and field effect transistors was developed by Huck.C [14]. This type of combination provide a more accurate and more reliable sensor which gives a warning at the early stage of hydrogen dissolving. The sensor shows a good detection of high concentration in the range from 0.1 to 3%, and good sensitivity of 198 $\pm$ 14 nA/1% hydrogen.

The difference between potentiometric sensors and amperometric sensors is that the potentiometric sensor works at zero current, and the measured quantity is related to the potential between the sensing and the reference electrode [15]. The hydrogen concentration though has a non-linear relationship to the potential difference. In potentiometric sensors, the open circuit potential is typically proportional to the logarithm of the concentration of analyte [16]. The relationship expressed from the Nernst equation is shown in Eq. 2.6,

$$E = E^0 + [\frac{RT}{zF}] \ln(\frac{a}{a_0}) \tag{2.6}$$

where E is the electrode potential, E^0 is standard electrode potential, R is universal gas constant, T is absolute temperature, F is Faraday constant, z is number of electrons taking part in the reaction, a is chemical activity of the analytes, and a_0 is the activity of the reference. A potentiometric sensor can measure analyte concentration over a range of more than 10 decades. The sensing principle is

thermodynamic, it assumes that all reactions relating to the sensing are at equilibrium [16]. In potentiometry, the process of diffusion and reaction must be at equilibrium conditions in the sensor for a thermodynamically accurate signal to be observed. Potentiometric sensors have a similar structure as the amperometric sensor which consists of two electrodes and contact with an electrolyte on both side. The electrodes are often made of noble elements such as Pd, Pt, Au or Ag [17].

The detection signal from a potentiometric sensor is not dependent on the size and geometry of the sensor. This leads to an advantage from the standpoint of sensor miniaturization. However, the response of potentiometric sensor shows a logarithmic relationship with hydrogen concentration, which results in a lower accuracy at higher hydrogen concentration compared with the linear response of amperometric sensors [18]. Both potentiometric and amperometric sensors have a numbers of merits and demerits: they can work at low temperature environment, low power consumption, high selectivity and sensitivity. However, the concentration of electrolytes between the electrodes can change with the humidity of the environment. Electrochemical sensors are used to measure the hydrogen in the range of 100 to 1000 ppm. Response time can be as quick as several seconds. Electrochemical sensor offers the advantage of low power consumption and perform well at room temperature. Nowadays, electrochemical hydrogen sensors are one of the commercial sensors in the market.

2.3 Pellistor-type Combustible Gas Sensor

Pellistor type combustible gas sensor are ultimately assembled by two coils, which are inserted in a ceramic bead and provide a catalytic surface for hydrogen gas in air combustion [15]. Physically, the coil has two functions. Firstly, the coil act as a heater and secondly as a resistive thermometer in the system while the surface of one bead is activated with a metal catalyst such as platinum or Pd. The other surface of inactive bead without catalyst has the responsibility to act as a compensating element. The coated surface catalyzes combustion during the device exposure to hydrogen or other combustible vapours. The air combustion taking place on the surface of coils leads to a certain temperature increase on the combustible gas sensor. This type of sensor detects the hydrogen gas concentration by the difference of the resistance of coil surface where the gas combustion take place.

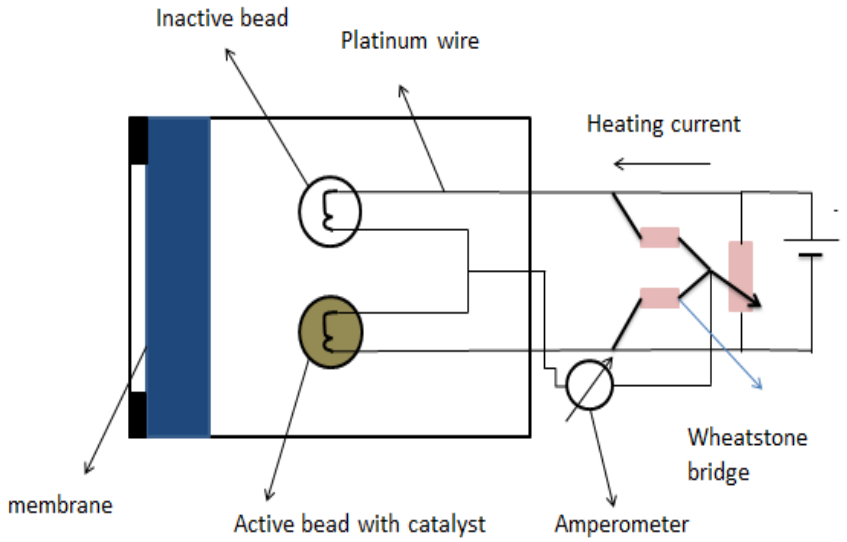

FIGURE 2.2: Pellistor consists of an active bead and inactive bead which connecting with a Wheatstone bridge circuit.

Although pellistors have been developed for a long period and are commercially available, they still have drawbacks. The basic pellistor type sensor is not exclusive selective to hydrogen but can also respond to other gases such as hydrocarbons and CO_2. A filter or molecular sieve can be used to improve the selectivity. Pellistor type hydrogen sensors offers high power consumption from 0.5 to 3W, because of the pellistor need to heat up to its operating temperature. Furthermore, oxygen concentration from 5% to 10% is required for the oxidation process.

As with other solid state sensors, improvement in power requirement and response time is possible with miniaturized thin film structures that use modern MEMS technology for fabrication. A planar catalytic combustion hydrogen sensor has been fabricated based on MEMS technology [19]. The size of chip is 5.76 mm^2 and the sensor showed a high response to hydrogen at 1V operating voltage. The response time and recovery time to 1000 ppm hydrogen is 0.36s and 1.29s, respectively. Katti *et al.* also developed a catalytic type hydrogen sensor with a Pd film deposit on alumina which can operate at temperatures of 120^{o}C with enlarged area of catalytic surface [20]. This type of sensor consists of a glass encapsulated Pt-heater coated with the catalytic thick film and a compensating element without the active film. The sensor also uses a Polytetrafluoroethylene (PTFE) thin film on the active element to improve the resistance of the sensor against poisoning with HDMS and iodine etc. The sensor shows linear response up to 10% of hydrogen in 40 standard cm^3/min air flow with response time of 30s and recovery time of 50s.

2.4 Thermal Conductivity Sensors

A thermal conductivity sensor senses gas composition by comparing the conductivity of a sample gas with that of either a flowing or stationary reference gas [21]. In thermal conductivity sensors, thermal conductivity of the gas is measured from monitoring the temperature of heated elements in both measurement cell and a reference cell in a similar way as pellistors. These heated elements form part of a Wheatstone bridge with changes in sample gas thermal conductivity yielding a change in resistance of the sample cell heated element. The resistance change signal can be correlated to the composition of the sample gas. These detectors can operate from 100 ppm to 100% H_2 in most of considered applications. Thermal conductivity sensor requires a lower power consumption than the combustion sensor. However, the production signal from thermal conductivity under hydrogen ambient is not independent of the environment gas and may be affected by the flow rate. Miniaturization of thermal conductivity sensors also results in rapid response time, being significantly smaller than 1 second [22].

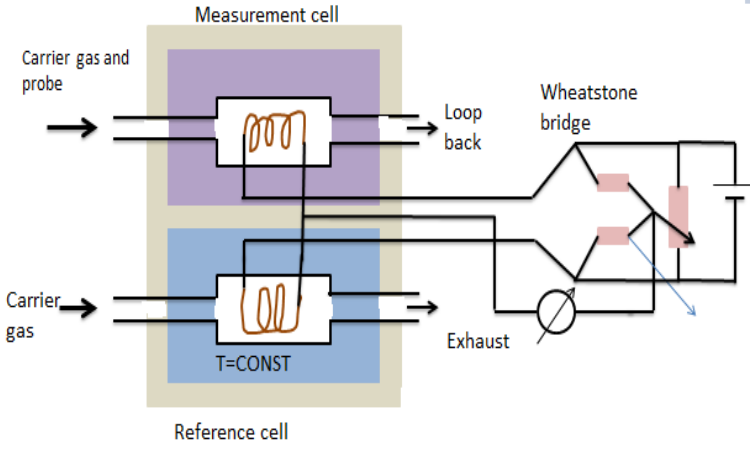

FIGURE 2.3: A thermal conductivity sensor connected with a Wheatstone bridge circuit.

2.5 Semiconducting Metal Oxide Sensors

Metal oxide sensors are fabricated with a wide band gap semiconductor material as the active element of the sensor [23]. Currently, doped tin dioxide (SnO_2) being an n-type semiconductor is the most widely accepted and most completely characterized sensing material. Typically a metal oxide film is deposited on an insulating substrate material and connected to two electrodes.

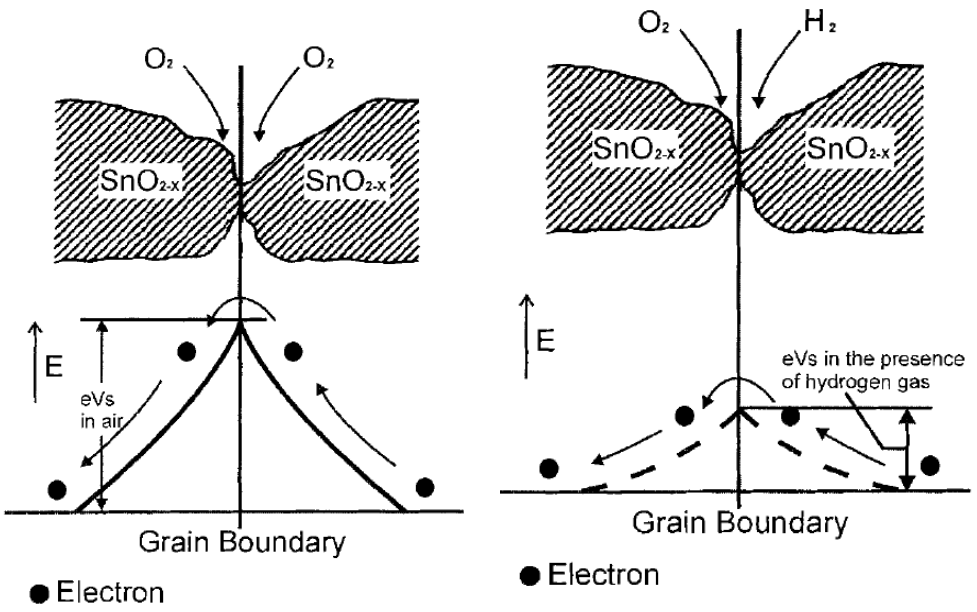

FIGURE 2.4: Model of Semiconducting metal oxide sensor. (a) Without hydrogen (b) with hydrogen [24].

The metal oxide crystal is heated to 300 to 500 ^{o}C when oxygen will be adsorbed on the crystal surface to give a negative charge. The oxygen creates a potential barrier at the grain boundaries which prevents the flow of electrons and results in an increase of surface resistance [24]. When hydrogen gas arrive at the sensor, it will be adsorbed and merge with the negatively charged oxygen with the reaction between hydrogen and adsorbed oxygen expressed as Eq. 2.7, 2.8. As a result, the barrier height in the grain boundary is reduced, which decrease the resistance.

$$O_2 + 2e^- \rightarrow 2O^- \tag{2.7}$$

$$H_2 + O^- \rightarrow H_2O + e^- \tag{2.8}$$

Semiconducting oxide sensors offer a good sensitivity that is as lower even lower than 50 ppm and the time response can be reduced to less than 10 seconds. However, semiconducting oxide sensors have a major problem in the aspect of selectivity. The method of doping with a noble metal such as Pd and Pt in SnO_2 does improve the selectivity. The test results exhibits a 2 seconds response time and 10 seconds of recovery time, as well as good sensitivity to hydrogen at 100^{o}C [25]. Currently, the widest hydrogen concentration range that can be detected by the

semiconducting metal oxide sensor is from 300 ppm to 1500 ppm at a temperature of 250^{o}C by a design of single wall carbon nanotube reinforced nanocrystalline tin oxide [26]. Due to the required heating, the sensor consumes a considerable amount of power.

2.6 Mass sensitive sensors

2.6.1 Acoustic sensor

Acoustic hydrogen sensor use surface acoustic wave (SAW) which travel through the surface of a piezoelectric substrate such as $LiNbO_3$ and $LiTaO_3$. The piezoelectric substrate possesses high electromechanical coupling coefficient [27]. As the (hydrogen) molecules are absorbed into a Pd layer coated on a SAW material, this leads to a perturbation of the surface acoustic waves. As a consequence, hydrogen gas can be monitored by the variation in frequency, amplitude as well as phase of the transmitted waves of the SAW [28]. Recently, Phan *et al.* investigated a SAW hydrogen sensor by incorporating ZnO nanoparticles with a Pt catalyst for hydrogen gas detection [29]. The sensor demonstrated that by using Pt and ZnO as sensing layer, the sensor can detect 1% H_2 concentration with frequency shift of 55kHz. SAW hydrogen sensors are compatible with microelectronic fabrication and array integration. On the other hand, the sensitivity is limited by baseline noise and the sensor has a poor temperature stability.

2.6.2 MEMS type sensor

In MEMS type hydrogen sensor, the hydrogen gas exposure to a thin Pd layer deposited on surface of quartz crystal leads to a decrease in resonance frequency [30]. Alternatively, an optical fiber is coated with essentially a Pd Layer. While the hydrogen is absorbed on the Pd layer, the optical properties will be changed. The optical properties normally include absorbance, reflectance, or scattering [31]. Optical fiber sensors have developing rapidly and are divided into several kinds of technologies, for instance evanescent, micromirror, surface plasmon resonance, and fiber Bragg grating sensor [32]. Wester waal *et al.* demonstrate a Pd-Au alloy thin film as hydrogen sensitive layer in a fiber optic sensor [33]. The sensor presents a 15 seconds time response during absorption and desorption.

2.7 Pd-film and Pd-alloy Films Hydrogen Sensor

The simplest hydrogen sensors are Pd films in which the resistivity or volume change due to hydrogen absorption is measured. Palladium is a noble metal and has already been used as catalyst in hydrogen production and hydrogen fuel cells. The hydrogen absorption by Pd during electrolysis was first found by Graham T in 1868 [34]. Hydrogen molecules dissociated on their surface followed by the atomic hydrogen which gets absorbed into the metal. Palladium can absorbed large volumes of hydrogen gas equal to many times its own volume [35]. For this absorption from the gas phase to occur, the surface of the metals should be sufficiently clean for the $H_2 \rightarrow 2H$ reaction readily to happen.

Pd hydride systems is one of the most well studied metal-hydride. Despite its name, it is not an ionic hydride but rather an alloy of palladium with metallic hydrogen(see also fig. 6.14. The phase diagram of Pd-H is shown in Fig. 2.5. Pd has a face centered cubic (FCC) structure at room temperature with a lattice parameter of 0.3890 nm; with hydrogen absorption, the lattice undergoes an isotropic expansion but retains its FCC structure. In the dilute α-phase, the lattice parameter of PdH_α is 0.3894 nm, corresponding to the ratio of the hydrogen to Pd atoms of 0.0015. For the hydrogen Pd ratio larger than 0.7, the lattice is in the β phase with a lattice parameter of 0.4040nm. As the H/Pd ratio is between 0.0015 and 0.7, the α phase and β phased co-exist. The volume expansion from the α to the β phase is 10.4% [36]. This large expansion stresses the Pd film causes film embrittlement and fracture during hydrogen absorption. Theoretically, after removal of the Pd from the hydrogen ambient the film should recover to the original situation. However, the Pd film can be easily physical damaged by the volume change which lead to the phase change being irreversible.

2.7.1 Volume Change Related Pd-film Sensors

Thin Pd films coated on a micro-cantilever based hydrogen sensor have demonstrated high selectivity and sensitivity. By using the quartz crystal micro-balance and volumetric technology, it was observed that when the Pd thickness was below 70 nm the onset of the Pd β phase due to hydrogen pressure, increased the thickness of the film [37] (for explanation see the next section). Ollaginer *et al.* utilize silicon cantilevers with dimensions of 250 μm $\times$ 35μm width, and 1μm thickness. Either 10 or 30nm Pd was deposited on the cantilever by using thermal evaporation [38]. As the hydrogen molecules were introduced into the device chamber,

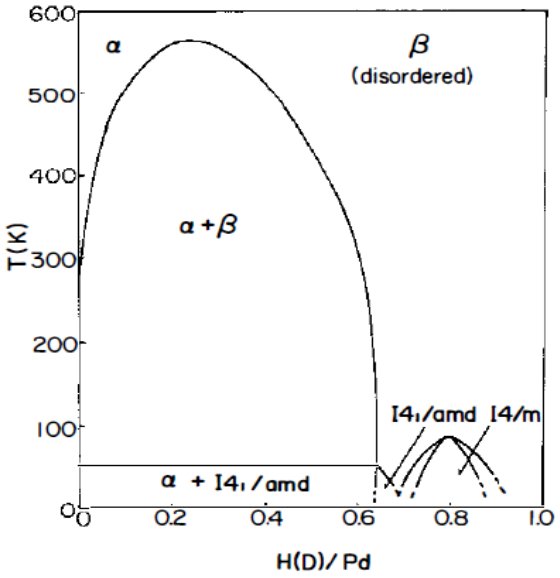

FIGURE 2.5: Phase diagram of Pd-H(D) showing the miscibility gap $\alpha + \beta$ and the low temperature ordered phase [35].

hydrogen absorbed in the Pd films will lead to a physical change such as swelling or heating during the hydride formation and subsequent mechanical stress of the film. Generally, the stresses that are produced by thin Pd films are more than result from bulk material.

Fig. 2.6 gives the information of the Pd-coated cantilever hydrogen sensor which behaves excellent in the α phase. From Sievert's law, hydrogen absorption and concentration within the metal varies in proportion to the square root of the hydrogen pressure. This figure shows that the change in the kinetic of the deflection are reversible and ultimately demonstrates that the volume recovers since the hydrogen was removed in 1000 seconds. Fig. 2.7 illustrates cantilever deflection Δ Z versus $\sqrt{P}$. In this phase a sensitivity of nearly $3.5mm/\sqrt{bar}$ is calculated from the slope of $\Delta/\sqrt{p}$ as shown in the figure. A thickness for Pd film from 10nm to 40nm is suitable for monitoring the phase change.

2.7.2 Resistive Pd-film Sensors

The electrical characteristic of Pd hydride system has been studied by incorporating hydrogen into the Pd film electro catalytically via solution as well as via a gas phase [39]. The resistance of the Pd hydride depends on its phase at the time of measurement and therefore on the hydrogen concentration in the Pd lattice. The resistance of the film increases linearly withe increasing hydrogen content throughout the α and α+β phase with a higher rate of increase in the α phase

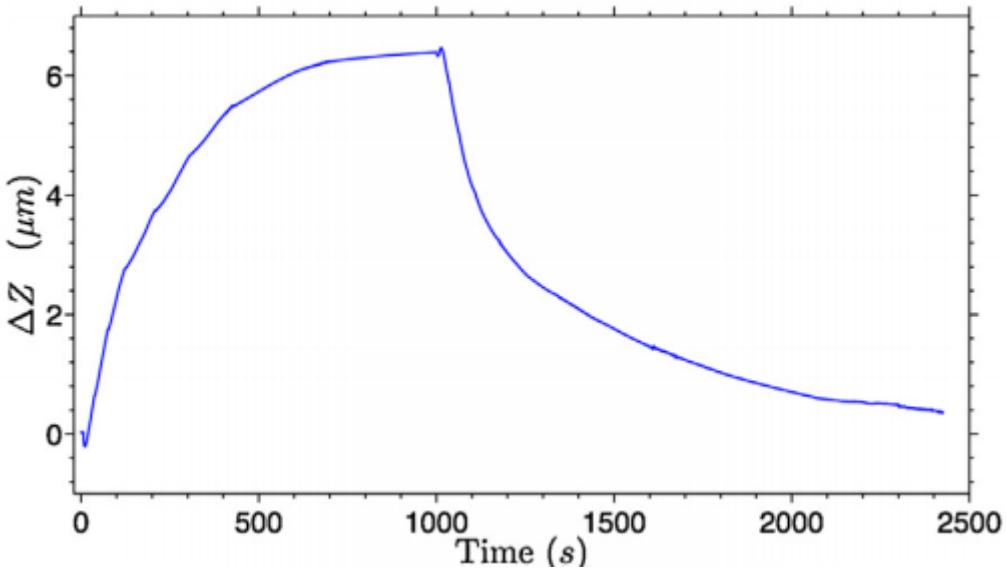

FIGURE 2.6: Kinetic of the deflection Δ Z induced by hydrogen absorption from 0 to 1000 seconds with hydrogen pressure varying from 10^{-7} to 10^{-5} bar. From 1000 to 2500 seconds the hydrogen was removed by vacuum pumping down. Reproduced from [38].

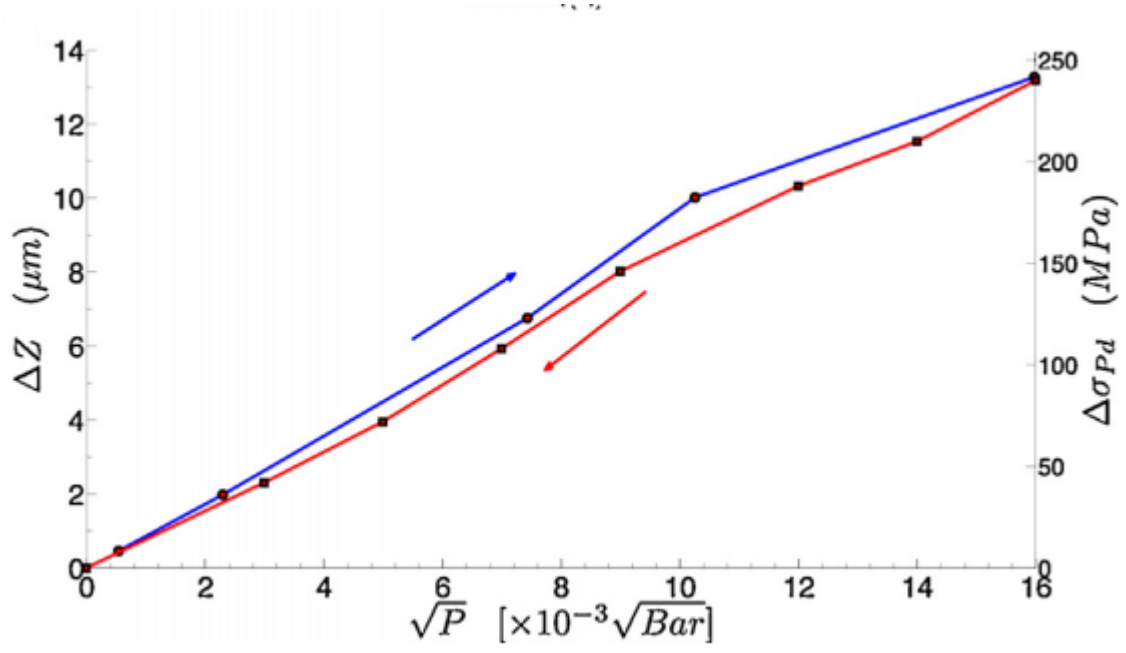

FIGURE 2.7: The successive steady state deflections by gradual pressure increments both for absorption and desorption of H_2 in palladium [38].

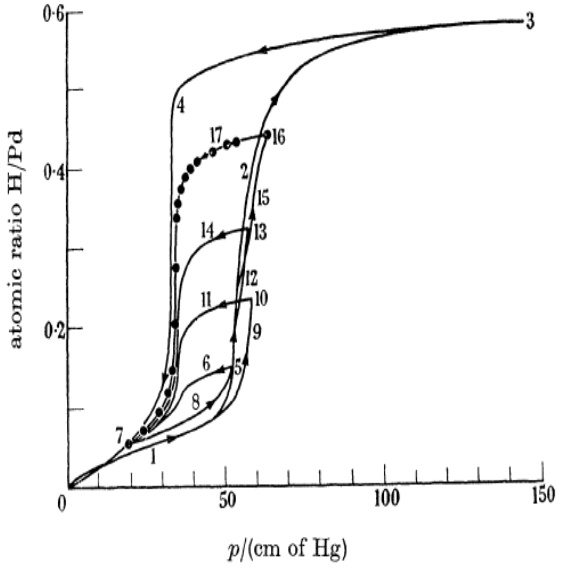

FIGURE 2.8: Atomic ratio H/Pd as function of hydrogen pressure[40].

concentration range compared to the $\alpha + \beta$ phase. When the β-phase of the hydride is reached, the rate of change decreases further and for some samples, a decrease of resistance is observed with increasing hydrogen concentration at this point. The hysteretic variation of hydrogen content with hydrogen pressure as shown in Fig. 2.8 results in the resistance characteristics also showing hysteresis as the hydrogen desorbs from the Pd film. This hysteresis in the electrical characteristic is due to large volume changes in the α-PdH to β-PdH phase change which leads to film embrittlement and restricts the pressure range in which pure Pd sensors can function.

shows how Pd changes with the introduction of hydrogen [35].

2.7.3 Pd Alloy Films

The utilization of alloys of Pd with metals, such as silver or nickel can resolve the limitation of limited reversibility by stabilising the α-PdH phase. Alloy metals have specific effects on the Pd lattice due to their different atomic sizes and electronic configurations. Elements like silver and lead possesses larger atomic sizes compared to Pd, which causes the Pd lattice to expand and particularly the size of the octahedral interstices. All of the alloys have greater terminal hydrogen solubility than does pure Pd. For instance, the hydrogen solubility at which the hydride phase first forms at a given temperature, is shifted to higher concentration. Elements like Nickel have smaller atomic sizes compared to Pd, and cause a

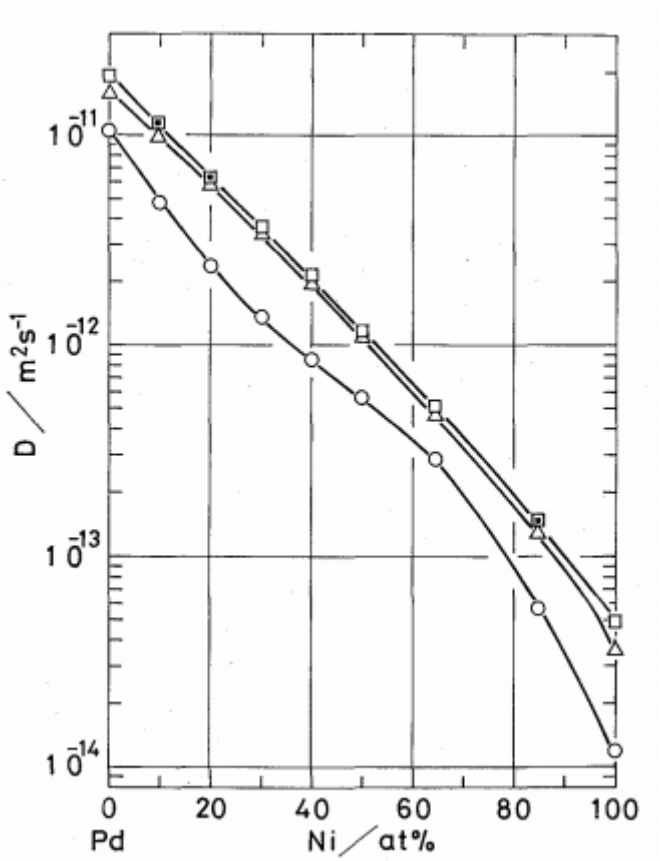

FIGURE 2.9: Diffusion coefficient of hydrogen at 298K vs. Ni content in Pd-Ni alloys. circle: as cold rolled, triangle: annealed at 773K for 3.6ks, square: annealed at 1123k for 7.2ks [41].

contraction of the lattice which favours lower solubility at low hydrogen content and higher solubility at higher hydrogen content compared to pure Pd.

The hydrogen diffusivity vs. Ni content at room temperature is illustrated in Fig. 2.9. Sakamoto *et al.* have used an electrochemical permeation method to determine the variation of the diffusivity of hydrogen through annealed and cold rolled PdNi membranes in the temperature range of 279 to 335K and of Ni composition from $1-100\%$ [41]. The diffusivity in the annealed Pd-Ni alloys decreases in an almost logarithmic fashion with the increasing Ni content. Atomic diffusion process is a totally random thermally activated movement of atoms in a solid resulting in the net transport of atoms. For a single atom in a defect free crystal the movement can be described by random walk model; if the diffusion coefficient is given by D and time is given by t, the average distance of the atom from its initial position l is proportional to the square root of Dt, as Eq. 2.9 shows.

$$l = \sqrt{Dt} \tag{2.9}$$

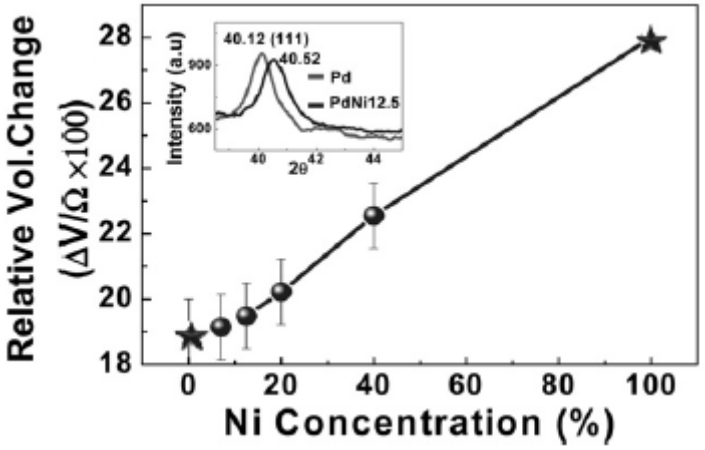

FIGURE 2.10: Relative volume change vs Ni concentration [42].

Based on Eq. 2.9 the time of hydrogen atoms diffusion through a 50nm PdNi alloy can be calculated. The diffusion time, for example, for the hydrogen atoms diffusion through a 50nm pure Pd film is 0.25ms. The diffusion time for a 50nm pure Ni film is 0.25s. As most sensors have response time of at least multiple seconds and often more, these two diffusion time indicate that the atomic diffusion time through the film is not a limiting factor in PdNi-Si Schottky barrier hydrogen sensors. The rate limiting steps are how fast the hydrogen atom can dissociate at the Pd/air interface and can be trapped at the Metal/Semiconductor interface.

With an increase of Ni content, the diffusivity in the PdNi alloys decreases in an almost logarithmic fashion. Nitrogen inclusion also affects the relative volume change, the ratio of volume expanded by hydrogen absorption to the initial volume. Fig. 2.10 displays the relative volume change as a function of Ni concentration [42]. It is well known that hydrogen atoms occupy interstitial sites in metal and produce an expansion of the surrounding lattice.

In this context, increased concentration of Ni leads to the corresponding increase in the relative volume change. The increased $\Delta V/\Omega$ value allows the alloy film to expand further when absorbing the same amount of hydrogen atoms. Lee *et al.* demonstrated a Pd-Ni alloy thin film hydrogen gas sensor, which shows an almost linear relationship between the sensitivity and hydrogen concentration. The sensor was able to detect low concentration down to 0.01% [43]. The sensitivities of pure Pd film and $Pd_{0.93}Ni_{0.07}$ films were 5.1% and 3.1% for 1% hydrogen, respectively. The response time for the sensors was defined as the time for the electric resistance change to reach 36.8% of the total change, with the resulting numbers being 49 and 5 seconds of Pd and PdNi, respectively.

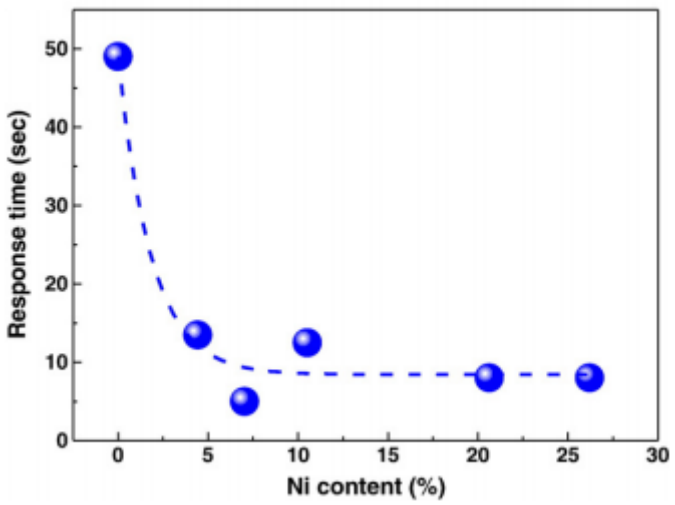

FIGURE 2.11: Time response to 1% H_2 versus the Ni content in PdNi alloy films [43].

Fig. 2.11 illustrates the time response for various Pd-Ni alloys under exposure to 1% hydrogen gas. With increasing Ni concentration, the response time decreases significantly to 7 seconds.

Fig. 2.12 shows the sensitivity changes for pure Pd and PdNi alloy sensors versus the H_2 concentration. For pure Pd film, when the hydrogen concentration reaches 2% a hysteresis mechanism was observed: the phase transition was from α phase to β phase and return to the α phase. In the alloy films no hysteresis behaviour happens during the absorption and desorption process up to 2% hydrogen. In the aspect of the sensitivity, PdNi alloys show a linear increase below the 2% concentration hydrogen.

2.8 Metal Oxide Semiconductor Sensor

Hydrogen sensors based on a metal-oxide-semiconductor (MOS) layout has been investigated for several decades since the first report was published in 1975 [44]. Since then, enormous amount of literature related to this subject has been published. Over these years, different MOS sensors with catalytic metal gates have been fabricated and measured. Generally, MOS type of hydrogen sensors can be divided into two categories: metal oxide semiconductor field effect transistor (MOSFET), metal oxide semiconductor capacitor, as well as MOS Schottky diode.

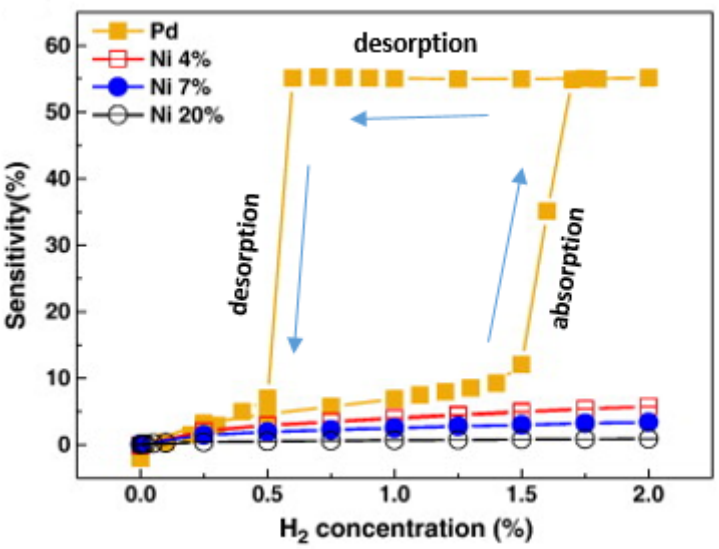

FIGURE 2.12: Hysteresis curve of various PdNi alloys sensitivity during the absorption and desorption as a function of hydrogen concentration [43].

2.8.1 Metal-Oxide-Semiconductor Field Effect Transistor

A MOSFET type hydrogen sensor is a specific form of a chemically sensitive field effect transistor in which the gate metal has been replaced with Pd. Fig. 2.13 illustrates the basic schematic of MOSFET transistor sensor. Normally, in a MOSFET transistor, the conductivity between the source and drain is manipulated by the voltage from the gate. When the MOSFET hydrogen sensor is working under a hydrogen-mixture ambient, the hydrogen molecules will be adsorbed on the Pd-gate surface and dissociate into hydrogen atoms. Then hydrogen atoms will continue to diffuse through the gate and reach the Pd-SiO_2 interface. The hydrogen atoms at the metal insulator interface are polarized and form a dipole layer that change the work function of the metal resulting in a threshold voltage change of the transistor. The threshold voltage drift signal measured by the sensor corresponds to the hydrogen concentration [45] according to the langmuir isotherm in Eq. 2.10:

$$\Delta V = \Delta V_{max} \frac{C\sqrt{P_{H2}/P_{O_2}}}{1 + C\sqrt{P_{H_2}/P_{O_2}}} \tag{2.10}$$

Δ V_{max} is the maximum observable voltage shift, C is a constant, P_{H_2} and P_{O_2} are the partial pressure of hydrogen and oxygen respectively [46]. Hydrogen sensors based on the MOSFET structures have been developed in a variety of directions. Kim *et al.* have developed a dual-MOSFET device which can operate at an ele-

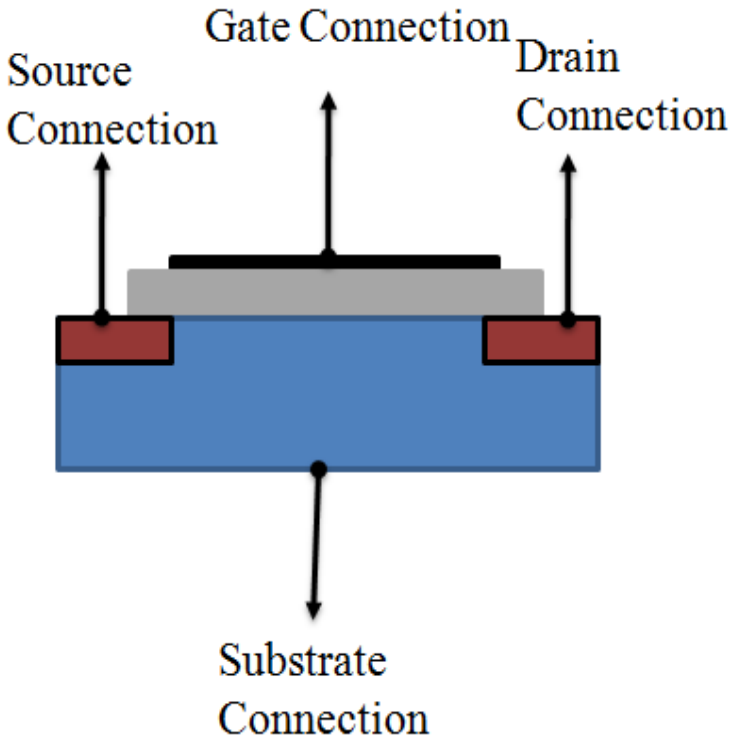

FIGURE 2.13: Cross section view of a basic MOSFET hydrogen sensor, a dipole layer formed as the hydrogen atoms accumulated at the metal/oxide interface creates a work function change.

vated temperature of 150^{o}C with 18s response and recovery time for 5000ppm [47]. A MOSFET sensor with a unique gate structure which has Ti and oxygen accumulated region surrounding Pt grains has been presented by Usagawa *et al.* [48]. The hydrogen concentration that can be detected in this structure ranges from 100ppm to 1%. MOSFET hydrogen sensor not only exhibits a good selectivity compared to other sensing techniques, they also demonstrate cross-sensitivity to only a few hydrogen compounds such as NH_3 and H_2S. Nevertheless the main flaws of MOS sensors are their instability which leads to issues such as hydrogen-induced drift, and their slow response after been stored for a long time.

2.8.2 Metal-Insulator-Semiconductor Capacitor

The metal-oxide-semiconductor capacitor hydrogen sensor is considered as the simplest MOS device [49]. Typically, the structure consists of a thin oxide layer in the middle of a metal layer and silicon substrate. A charge accumulation layer forms on both sides of oxide layer. MOS capacitor hydrogen sensor use Pd or other noble metals as the top metal electrode as shown in Fig. 2.14(a). The hydrogen

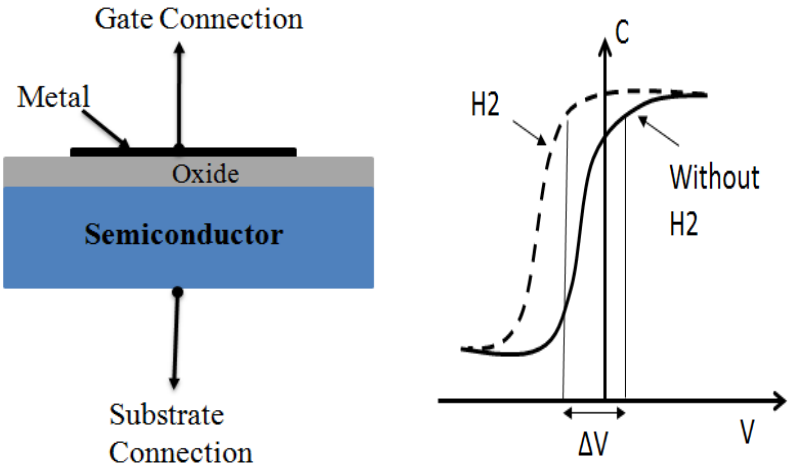

FIGURE 2.14: (a)Cross-section view of a basic MOS-capacitor sensor. (b) C-V curves explicit the effects of the hydrogen dipole layer: a negative flat band voltage shift [53].

sensitivity arises primarily though the hydrogen dipole layer at the interface between the Pd and oxide. This dipole layer leads to a flat band voltage shift, which is a measure corresponding to the hydrogen concentration on the surface of Pd electrode [50].

The first MOS capacitor using a thin Pd film as the metal electrode was developed by Steele *et al.* [51]. They observed a flat band shift of up to 1V in the capacitance-voltage (C-V) curves when 4% hydrogen was introduced at room temperature with a 50 ppm detect limit. The sensor has a 10s and 60s response and recovery time, respectively. Recently, several novel metals have been developed as a catalytic metal for gate electrode in MOS capacitor. A Ni-SiO_2-Si capacitor can operate at 140^oC to detect hydrogen between 50 ppm and 1000 ppm in nitrogen with a response time of 20-50s. Lu *et al.* fabricated a MOS capacitor hydrogen sensor with a Ni-SiO_2-Si structures with only a 2.4 nm Si oxide [52].

At 150^oC this sensor illustrates fast time response (4 s for 1% hydrogen) compared with the other thick oxide MOS capacitor sensor. A 30nm Pd layer was deposited on the gate by a Nd:YAG (Nd:$Y_3Al_5O_{12}$) high power pulsed layer for a MOS capacitor [54]. This device can detect hydrogen concentrations down to 24 ppm with 3 orders of sensitivity. It was reported that Pd is an ideal material for the catalytic electrode in a MOS capacitor hydrogen sensor, which can detect less than 1% hydrogen in the air ambient. Pt-MOS capacitor hydrogen sensor can operate at a higher hydrogen concentration where the Pd-MOS capacitor sensor meets the

saturation point.

2.9 Schottky Barrier Hydrogen Sensor

Schottky barriers function as a diode which is made of a metal contact with a semiconducting material. The basic Schottky barrier hydrogen sensor sensing mechanism is again hydrogen dissociation to H^+ by the noble metal such as Pd, which will continuously diffusing to the metal-semiconductor interface. The ions will be trapped on the interface and form a dipole layer which decreases the Schottky barrier height and lead to larger electron flow across the barrier. The Schottky diode structure was chosen for our thesis and the specific mechanism will be discussed in Chapter 3 (see fig. 3.18).

Recently, Pd and Pt was extensively used in Schottky barrier based hydrogen sensor [55, 4, 56]. For semiconducting material, Si, GaN are the most popular materials to fabricate the Schottky barrier [57]. The reason to choose GaN as the semiconducting material is due to its wide bandgap (3.4 eV), high electron saturation velocity, good thermal and chemical stability, so it could work at higher temperature for hydrogen sensing [58]. Karl *et al.* fabricated a hydrogen sensor which is based on a Pd/nanowire Schottky barrier and contact with SiO_2/Si substrate [59]. This sensor demonstrates a detecting range of hydrogen concentration from 3 ppm to 5000 ppm and a sensitivity of 6.9% at 100 ppm.

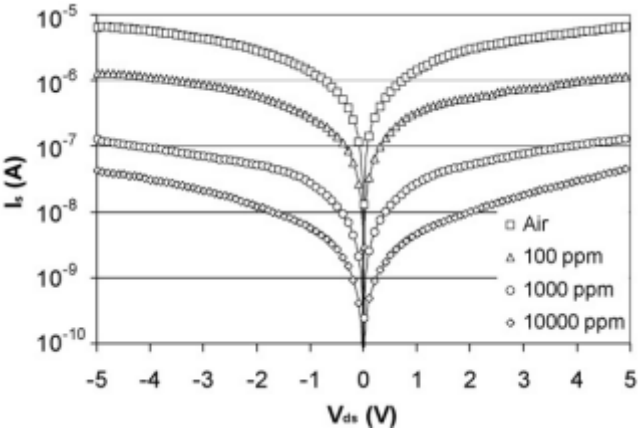

FIGURE 2.15: I-V characteristic of Pd/nanowire Schottky barrier hydrogen sensor at various of hydrogen concentration [59].

Fig. 2.15 reveals the current-voltage (I-V) characteristic of the nanowire sensor for various hydrogen concentrations.The time response is 60 minutes at lower concentrations, and at the higher concentration (10,000) ppm the response time is less

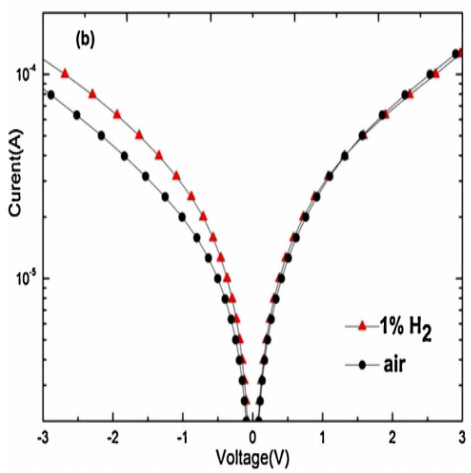

FIGURE 2.16: I-V curves of a Pd/GaN Schottky barrier in air and 1% H_2[60].

than 1 minute. Zhong *et al.* developed a Schottky barrier hydrogen sensor on a porous planar GaN film with the GaN film epitaxially grown on a Si substrate [60]. At room temperature, the detecting range of this sensor was from 320 to 10000 ppm. The response time for this sensor is 60 seconds. The I-V curve of this sensor in air and hydrogen is illustrated in Fig. 2.16.

Kiziroglou *et al.* compared the transport characteristics of evaporated Ni-Si Schottky barriers with that of the electrodeposited Ni/Si Schottky barriers of the same structure [61]. They have observed that the electrodeposited Ni/Si Schottky barriers exhibit better rectifying behaviour than the evaporated one. The poor rectifying of the evaporated Schottky barrier was caused by the formation of an interfacial layer at the Ni-Si interface due to the intermixing of the high energy Ni atoms with Si during evaporation. The interfacial layer will lower the Schottky barrier height leading to an increase of the reverse current density. This, in turn, will lead to a significantly reduced sensitivity to hydrogen.

2.10 Conclusion and Comparison

A market survey related to hydrogen sensor has been performed to identify the commercially available options [3]. The number of commercial sensors manufacturers marketing is increasing every year. A total of 53 different models from 21 different manufactures were found. The different working principles and the number of models of each individual type are summarized in Table 2.1.

Typical characteristics of different sensor types are summarized in Table 2.2. Each

TABLE 2.1: The number of each type of commercial hydrogen sensor surveyed and the manufacturers for each type [3].

Working principle	models	manufacturers
Catalytic	9	6
Thermal conductivity	4	3
Optical	2	1
Electrochemical	19	9
MOS Capacitor and MOSFET	1	1
Semiconducting metal oxide	11	6
Total	53	21

of the technologies discussed in this chapter is a good sensor platform with strong performance in at least one aspect of operation, and many of them are commercially successful. However, none if these type of sensors is ideally suited for every application. Customers therefore must compromise and choose the most appropriate technology that will best meet their application requirement. A summary of the ability of each type of technology to meet these performances is given in table 2.3.

In table 2.2, the requirement in specific areas is highlighted for further research and development. The upper limit of the hydrogen sensor working temperature is primarily based on the location of the sensor, and the limit of 125^{o}C is used in some application areas, for example nearby an engine [3]. Vacuum operation would be advantageous as well. Both the response and recovery time need to be reduced for all different type of sensing technology.

In comparison with other hydrogen sensing technologies, metal-semiconductor Schottky barrier devices based on hydrogen sensitive Pd films have advantages such as high sensitivity and selectivity as well as low cost. MOS and semiconducting metal-oxide can be deployed to detect hydrogen during a catalytic reaction on the sensor's surface. They can also measure low surface concentration compared with other conventional sensitive techniques.

The particular aim of this thesis is to produce a low cost, small size, and low power consumption hydrogen sensor. Considering the above, electrodeposition technology to produce metal semiconductor Schottky barrier hydrogen sensor is a very promising approach when the slow time response can be addressed. Therefore, the following research will focus on fabricating and improving the response time of the Schottky barrier hydrogen sensor to reach a level of less than 1 minute. Work is carried out to find the best PdNi alloy composition, which has lead to

TABLE 2.2: Characteristics of hydrogen sensor, modified from [15].

Sensor type	Advantages	Disadvantages
Catalytic	Linear signal result Stable Wide operation range Simple circuit design	High power consumption Not hydrogen selective limited sensitivity Room temperature operation
Thermal conduction	Wide measuring range Long term stability Low cost	Higher/lower detection limit Cross-sensitive to He Slow time response
Optical	No source of ignition in safety Unaffected by Magnetic Interference Wide area monitoring	Interference with Light
Acoustic	High sensitivity Suitable for Multi-sensor array	Interference from humidity Unable at higher temperature
Electrochemical	Low power consumption Resistant to poisoning	Narrow temperature range Using some electrolytes Restricted lifetime
MOS Capacitor	High sensitivity and selectivity Rapid response, Low power consumption	Dependence on temperature initial insensitivity to hydrogen
MOSFET	High sensitivity and selectivity Small size Mass production possible	Susceptible drift Sluggish response after storage in air
Metal Oxide	High sensitivity Fast response Low cost	Poor selectivity Limited detection range

a sensor with the fastest time response reported so far, as well as extremely low power consumption.

TABLE 2.3: Characteristics of hydrogen sensor, data from [15] [28] [52],[62, 63, 64, 65].

Sensor type	Performance			
	Measuring range(%)	Response time(s)	Power (mW)	Sensitivity
Pellistor	0-4	< 30	1000	>50mV/1%
Thermal conductivity	0-100	< 10	< 500	1.3 mV/K
Electrochemical	0.02- 25	< 90	2-700	$\leq \pm$ 2% of measured value
Semiconducting Metal-oxide	0-2	< 20	< 800	4.5%/10ppm
MOS field effect transistor	0-4.4	< 2	700	0.112mA/5000ppm
Optical	0.1-100	< 60	1000	26%/4% H_2 for micro-mirror 14 pm for FBG
Schottky Diode	0.025-0.5	> 1000	$<10^{-3}$	6.9%/ppm for Pd/nanowire 16%/1% H_2 for PdNi

Chapter 3

Electrodeposition of PdNi-Si Schottky Barrier

3.1 Introduction

In this chapter, we will introduce the basic theory behind the two key chosen processes applied in this thesis.

- The co-electrodeposition of metals onto semiconductors
- The modification of the Schottky barrier under the influence of interface states

We will illustrate the Schottky barrier theory with results on basic Pd-Si or Ni-Si electrodeposited Schottky contacts. Electrodeposition is a very simple, quick and cost effective method which does not require any vacuum chamber unlike the conventional material deposition techniques such as evaporation and sputtering. It only deposits on exposed regions of the device and does not waste any material in the process. It is hence very suitable for the deposition of expensive materials such as Pd and Au. Electrodeposition requires a conductive cathode and is usually associated with deposition on semiconductors. However, Kiziroglou *et al.* [61] showed that even relatively lowly doped Si is sufficiently conductive to act as cathode. The formation of the Schottky barrier upon metal deposition will limit the conduction through the barrier. It will be shown though in the next sections that on an n-type substrate the Schottky barrier is forward biased during elec-

trodeposition and that the electrodeposition process can be carried out with good control.

3.2 Theory of Electrodeposition

3.2.1 Introduction

The fundamentals of electrochemical deposition are described in detail in Ref. [66]. The most important aspects are highlighted in the next few sections. The basic process during electrodeposition is the reduction of a metal ion to metallic solid on the cathode material as represented by Eq. 3.1. Eq. 3.1 can describe different processes. Electrodeposition and electroless deposition constitute the electrochemical deposition. The first situation is an electrodeposition process in which Z electrons are provided by an external power supply. Secondly, electroless deposition process in which reducing agent in the solution is the electron source. In most situations the electrodeposition process dominates the electrochemical deposition. Fig. 3.1 shows that the metal salt MA dissociates in the solution into positively charged metal cations M^{n+} and negatively charged anions A^{n-}. The cathode electrode, which is negatively charged will attract the positively charged M^{n+} cations and is used for the plating. Meanwhile the negatively charged A^{n-} anions migrate to the anode electrode, which is positively charged. There is an external circuitry used to complete the loop which reduces the M^{n+} cations to the metallic form M while the electrons which are removed from the metal M form the current through the circuit. Since the number of ions in the solution that contains the metal salt MA is constant, it follows that the anode slowly dissolves. If there is no external circuit connected, then the speed of the two reactions may not be the same.

$$M^{z+}_{solution} + Z_e \rightarrow M_{lattice} \tag{3.1}$$

The potential difference cannot be directly measured as it requires two terminals. In order to measure the potential difference of an interface, a connection should be made to another interface to form an electrochemical cell as shown in Fig. 3.1. The cell reaction can only happen naturally if the free energy change ΔG is negative. Free energy change as a function of concentration of the reactants is given by:

$$\Delta G = \Delta G^0 + RT \ln Q \tag{3.2}$$

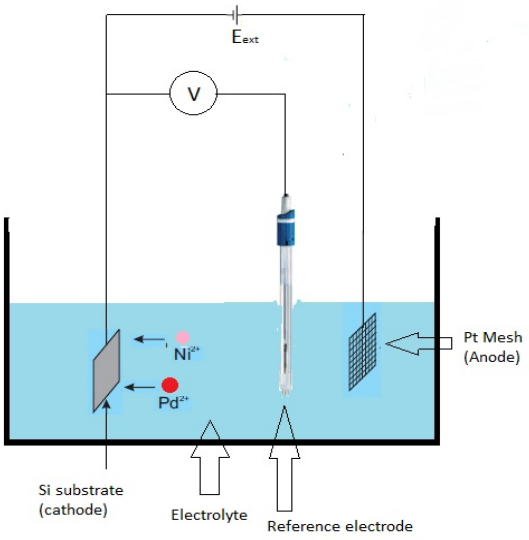

FIGURE 3.1: Schematic of a typical set up for electrodeposition of Ni and/or Pd, with an external potential driving the metal ions to the cathode, where they are deposited as thin metallic films.

Where R is the gas constant, T is the absolute temperature, Q is the ratio of concentrations of product and reactant. For standard states, when activities of the reactants and products equal 1, the standard free energy change Δ G^0 is equal to ΔG. The free energy is proportional to the potential E between the two interfaces. As long as the concentration of solution is below around 0.01 mole per liter, activity is equal to concentration, and Eq. 3.2 converts into the well known Nernst Eq. 3.3.

$$E = E^0 - \frac{0.0592}{n} \log[M^{n+}] \tag{3.3}$$

3.2.2 Thickness Control

A specific thickness of thin metal film can be deposited by electrodeposition. The thickness is controlled in real time straightforwardly by the total current. The total charge transferred in the process can be calculated by

$$Q = \int I dt = n * q * a \tag{3.4}$$

Where n is the number of electrons involved in electrodepositing, q is the electrical charge per electron and a is the number of atoms deposited. This atom number a is related to the deposited film thickness t. The mass of the metal film deposited is

TABLE 3.1: PdNi electrodeposition rates.

Substances	Deposition rate (nm/mC/cm^2)
Ni	0.34
Pd	0.41
$Ni_{0.5}Pd_{0.5}$	0.38

$$m = m_w * \frac{a}{N_a} = \rho * A * t \tag{3.5}$$

m_w is the atomic weight of species M, N_a is Avogadro's constant number, A is the contact area for electrodeposition and ρ is the density of metal. Thus the relation between thickness and charge is now established by combining those equations to

$$t = \frac{m_w Q}{nA\rho q N_a} \tag{3.6}$$

Using Eq. 3.6, the deposition rates can also be calculated. Table 3.3 lists electrodeposition rates for pure Nickel, Palladium and $Pd_{0.5}Ni_{0.5}$ in nm per mC per cm^2. Normally the rate of electrolysis is considered to depend on the kinetic of the two electrode reactions. Therefore, an expression for overpotential is introduced. As a non-equilibrium electrochemical cell, the potential difference η between the electrode as a result of current flowing E(I) and the equilibrium potential of this same electrode E_e is defined as overpotential 3.7.

$$\eta = E(I) - E_e \tag{3.7}$$

This overpotential is used as the power source to drive the overall electrode reaction. A basic current-overpotential relationship for the electrodeposition is described by the Butler-Volmer Eq. 3.8 in which j_0 is the exchange current density (when η=0) and α is the transfer coefficient.

$$J = j_0[exp(\frac{(1-\alpha)n\eta}{V_T}) - exp(\frac{(-\alpha)n\eta}{V_T})] \tag{3.8}$$

When the overpotential is small, the current density varies linearly with the overpotential, and behaves as in Eq. 3.9

$$J = j_0 \frac{n\eta}{V_T} \tag{3.9}$$

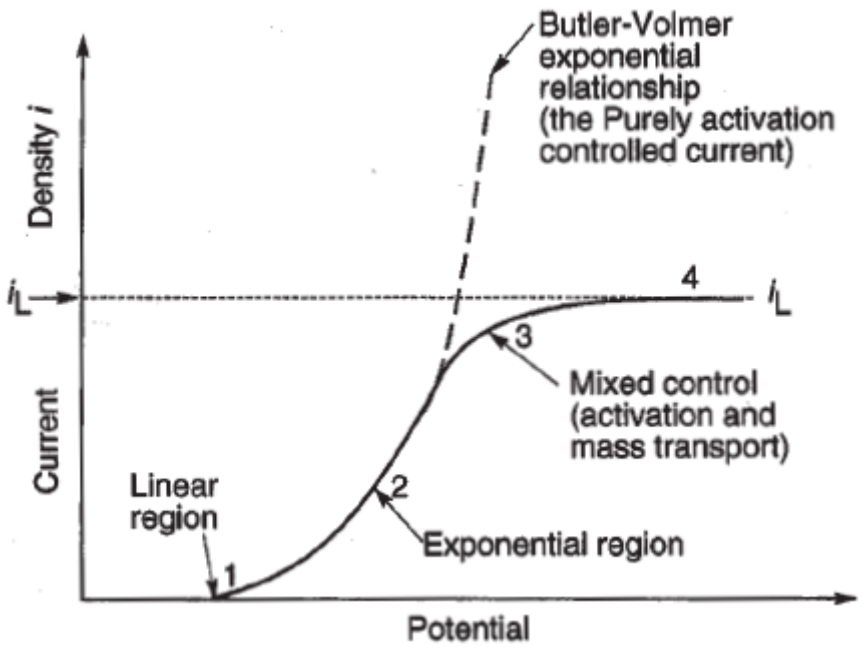

FIGURE 3.2: Four regions of basic current-potential relationship of electrodeposition [67].

With the overpotential increasing the cathodic current density is dominant if η is negative and the current density is given by:

$$J = -j_0 e^{-\alpha n \eta / V_T} \tag{3.10}$$

If the potential is very high, mass transport will restrict the current to a maximum value and the value is given by Eq. 3.11.

$$i_L = \frac{nV_T D}{\delta RT} C_b \tag{3.11}$$

in which D is the diffusion coefficent for M^{n+}, δ is the diffusion layer thickness and C_b the bulk concentration of M^{n+} in the solution.

3.2.3 Cyclic and direct current (DC) Voltammetry

There are two different types of transient techniques to explain the electrodeposition behaviour. In the first one, an instantaneous variation of the electrode potential or current is applied and the system is monitored when it approaches its new steady state. Chronoamperometry or chronopotentiometry is dependent on

whether potential or current is perturbed respectively. The second type is when a periodically variation of current or potential is offered to the system, the response is measured as a function of the frequency of the variation. This method is called cyclic or ac voltammetry.

Cyclic voltammetry is one of the most popular electrochemical technique when researching a system for the first time. Several electrode kinetic and electrodeposition processes can be studied in detail from the analysis of cyclic voltammograms recorded as the rate of mass transport varies with time. The cell current is recorded as a function of the applied potential. The working electrode potential is ramped as a linear function versus time at a fixed scan rate. The applied potential is varied as a triangular waveform between two switching values, as shown in Fig. 3.3.

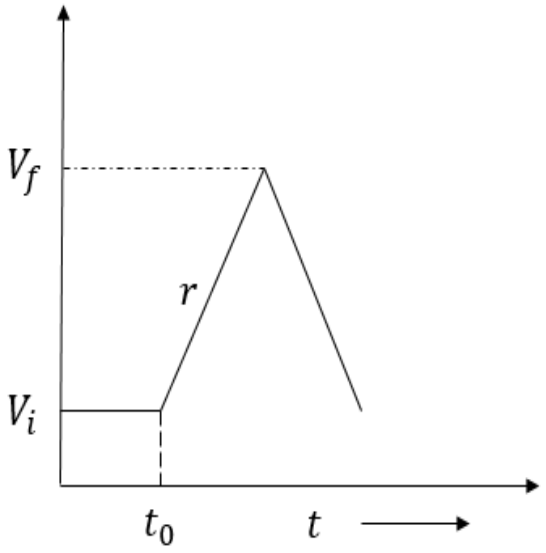

FIGURE 3.3: Variation of applied potential with time during cyclic voltammetry. The switching potentials V_i and V_f, the rate of the potential change r and the start time of the ramp t_0 are process parameters [68].

This has the advantage that the product of the electron transfer reaction that happened in the forward scan can be probed again in the reverse scan. The dependence of current on applied potential during cyclic voltammetry is shown in Fig. 3.4 for a 50nm $Pd_{0.7}Ni_{0.3}$ Schottky barrier hydrogen sensor.

The cathodic and anodic peaks are formed due to imbalances between the consumption and replenishment of ions near the cathode and anode respectively. The locations and magnitudes of the anode and cathodic peaks can be used to characterize the electrical system. In the beginning of the redox reaction, only the oxidized species M^{n+} exist, presumably. Therefore, for the first half cycle, a negative potential is applied chosen resulting in a cathodic current. During this scan

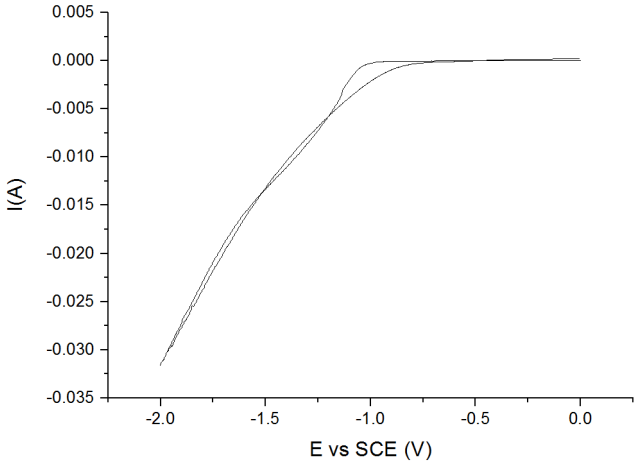

FIGURE 3.4: Variation of current with applied potential during cyclic voltammetry for a 50nm $Pd_{0.7}Ni_{0.3}$ Schottky barrier hydrogen sensor.

the product is generated on the surface of the electrode. The reverse scan results in an anodic current and dissolution.

In my work, cyclic voltammetry is only used to obtain the potentials at which Nickel and Palladium deposition starts to allow the determination of the deposition potential where the desired current density is achieved. To ensure good nucleation, it is advisable to start the process with a few high potential and short duration pretreatment pulses. The critical number of atoms require to form a cluster while depositing is inversely dependent on the overpotential [66]. A high negative pulse potential was therefore chosen to facilitate formation of a large number of small clusters on the electrode surface while the short duration of the pulses ensures the clusters do not grow and form a continuous film. DC amperometry is the final step to deposit the film, which involves the application of a constant deposition potential to the cell. The deposited charge is measured in real time via the deposition current and the amperometry will be stopped when it reaches the required charge.

3.2.4 Electrochemical Deposition Equipment Setup

The basic setup of the electrodeposition experiment is shown in Fig. 3.5. This three-electrode electrodeposition Autolab PGSTAT12 system with potentiostat controls the equilibrium electrode potentials by using a saturated calomel reference electrode (SCE, Radiometer analytical model). The anode consists of large area

platinum gauze, which connects to the positive pole of the potentiostat. This anode functions as a counter electrode and the silicon wafer as the cathode connects to the negative pole of the potentiostat. There is a laptop connected to the potentiostat to monitor the electrodeposition process with a potentiostat current-time transient curve.

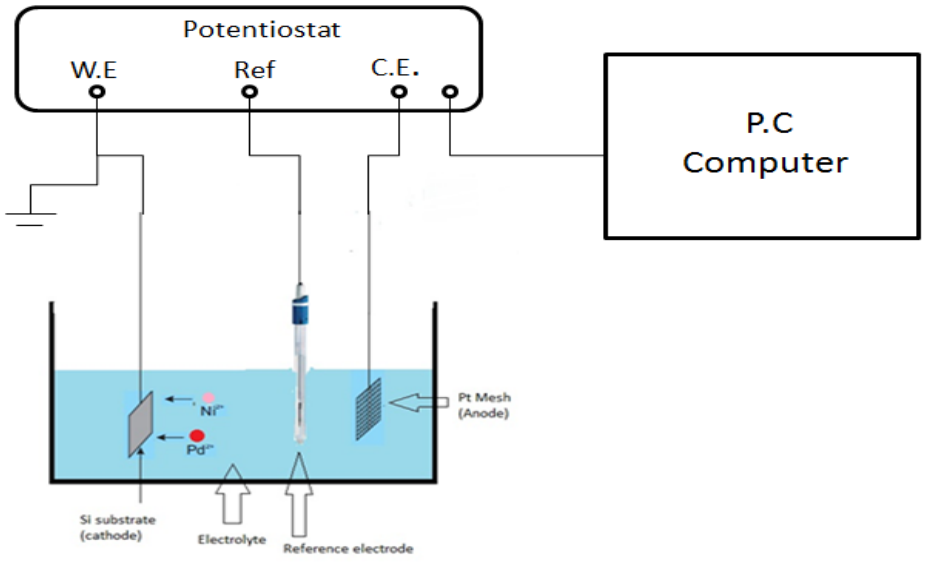

FIGURE 3.5: Schematic of experimental setup for PdNi electrodeposition on Si,and the system was controlled and monitored by a PC computer.

Fig. 3.6 shows a SCE which contains calomel, a mercury chloride solution: Hg—Hg_2Cl_2—Cl^-; The overall electrode reaction in the calomel electrode is Hg—Hg_2Cl_2+2e$\Leftrightarrow$ Hg+2Cl^-, and the electrode potential is as displayed in Eq. 3.12 [66],

$$E = E^0 - \frac{RT}{2qN_a} \ln[Cl^-] \tag{3.12}$$

where R is the gas constant, T is the absolute temperature, and Cl^- is the concentration of Cl anion in mol/L. The most frequently used calomel electrode is the saturated calomel electrode, in which the concentration of KCl is at saturation. The potential of the SCE, at 25^{o}C is 0.242V versus normal hydrogen electrode. SCE has a large temperature coefficient [66], making it inappropriate in some applications.

$$E[V] = 0.242 - 7.6 \times 10^{-4}(T - 298) \tag{3.13}$$

According to the literature [69] we found a recipe for the electrochemical PdNi bath used in our work, shown in Table 3.2. Removing either the palladium and

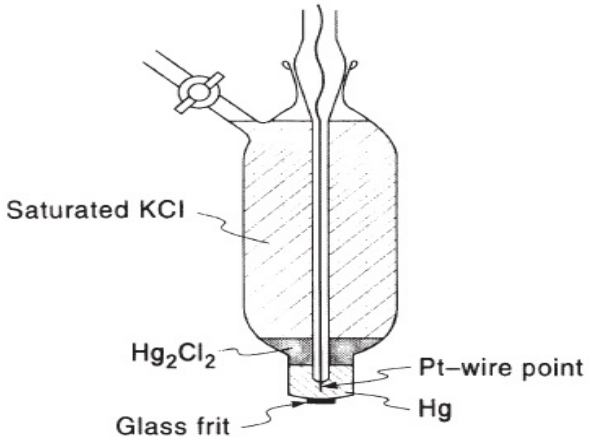

FIGURE 3.6: Saturated calomel electrode [66].

TABLE 3.2: PdNi electrodeposition constituents.

Chemical	Pd Bath (g/L)	Ni Bath(g/L)	PdNi Bath(g/L)
$PdCl_2$	16.7	0	16.7
$NiSO_4$	0	33.3	33.3
$(NH_4)_2SO_4$	16.7	16.7	16.7
NH_3 (35%)	45ml/L	45ml/L	45ml/L

nickel salts in the PdNi bath will obtain the pure nickel and pure palladium bath, respectively. Nickel sulphate ($NiSO_4$) and palladium ethylenediamine dichloride ($PdCl_2$) are prepared as the Nickel and Palladium ion sources. The role of ammonia in the solution gives homogeneity and brightness (as in the case with Cl^2) which decreases the anodic corrosion by avoiding the oxidation [70]. DI water was chose as the solvent and the pH value of the solution was adjusted between 7 and 7.5 by using sulfuric acid and ammonia.

3.3 Electrodeposition of Pd-Ni Alloys

In order to deposit an alloy on the wafer instead of a single metal, the electrochemical solution must contain salts of all metals to be alloyed. The potentials differences caused by the applied overpotential will affect the alloy deposited at clearly different rates. Fig. 3.7 depicts typical polarization curves, with the deposition potential as a function of current density for two metals separately. From these curves, it is inferred that a deposition bath that contains both metal ions

will co-deposit the two metals A and B in the ratio J_3/J_4 at a potential of V_2.

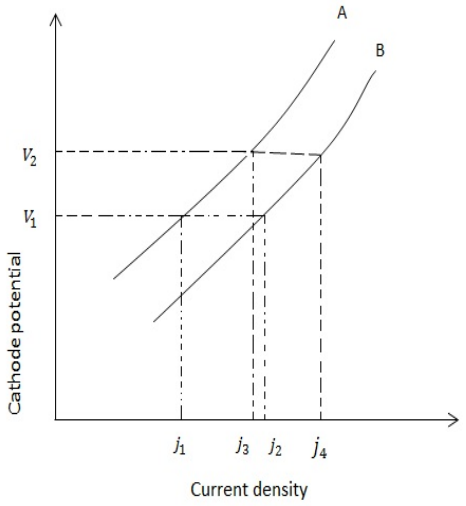

FIGURE 3.7: Polarization curves for the deposition of alloys [66].

In case of a deposited alloy, the density and effective atomic weight need to follow the rules on the fractions of the constituent metals. Therefore, the effective density and atomic weight of the alloy can be expressed by assuming the mass and volume of the individual elements are conserved in the alloying process. The equations for the alloy density and atomic weight are Eq. 3.14 and Eq. 3.15.

$$\frac{1}{\rho_{Alloy}} = \frac{x_{Ni}}{\rho_{Ni}} + \frac{x_{Pd}}{\rho_{Pd}} \tag{3.14}$$

$$\frac{1}{M_{Alloy}} = \frac{x_{Ni}}{M_{Ni}} + \frac{x_{Pd}}{M_{Pd}} \tag{3.15}$$

3.3.1 Energy Dispersive X-Ray

Energy dispersive X-Ray (EDX) spectroscopy is an analytical technique used to study the chemical composition of a material. It is usually used in conjunction with scanning electron microscopy and therefore allows elemental analysis with resolution on the nanoscale. During the EDX analysis, the sample is bombarded with a collimated, high energy electron beam, which excites some of the inner shell electrons in the atoms of the material. The vacancies left behind in the inner shells are ultimately filled by outer shell electrons. The energy lost by the outer shell electrons in this transition is released as X-Ray which is collected by a detector

and transformed into a voltage proportional to the X-Ray energy. These energies are dependent on the energy difference between the atomic orbitals and provide a unique signature for each element. The number and energy of the X-Ray emitted from a specimen can be measured by an energy-dispersive spectrometer.

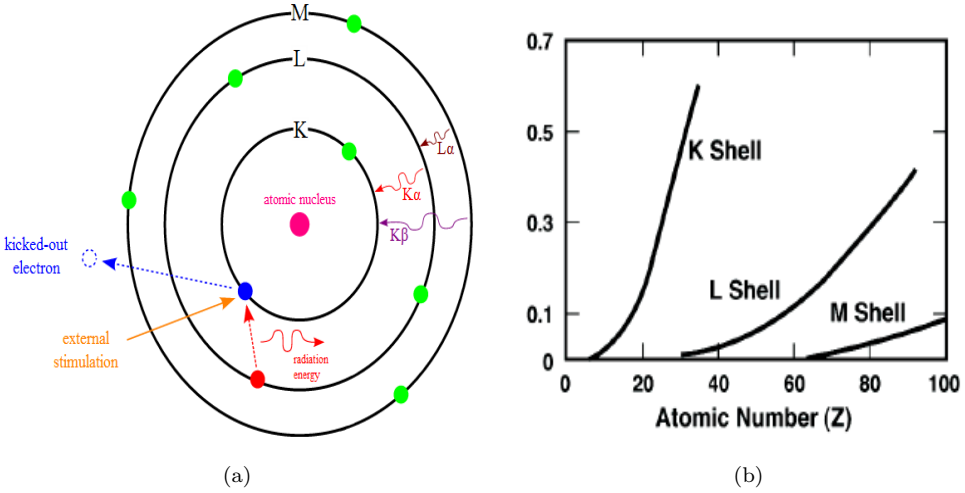

(a) (b)

FIGURE 3.8: (a)Principle of EDX. (b) Dependence of the fraction of ionization events that produce characteristic X-Rays [71].

By studying the number of emitted X-Rays of each energy, it is possible to find the relative proportions of the elements present in the material. The electronic transitions between different energy levels in the atom after bombardment by an electron beam is shown in Fig. 3.8(a). The L, M, and N orbitals are in fact composed of sub shells with finer energy separations. The large number of possible transitions give rise to a number of line series, which are classified on the basis of the energy orbital the electron is moving to [72]. Fig. 3.8(b) shows that the low atomic number element predominantly emit X-rays in the K series while elements with higher atomic numbers emit lines in the L and M series [71]. Electronic transitions to the K orbitals also produce the highest percentage of characteristic X- Rays compared to the L and M series. The rest of electrons emitted are called Auger electrons. Fig. 3.9 gives the EDX spectrum for the standard PdNi-Si Schottky barrier hydrogen sensor. This type of Pd-Ni alloy composition was achieved by electrodeposition at a potential of -0.8V. The EDX result for this film shows the material of the film to be simply Pd and Ni with a large Si peak due to the substrate. Discarding the Si, the atomic concentrations for Ni and Pd are 31% and 69%, respectively.

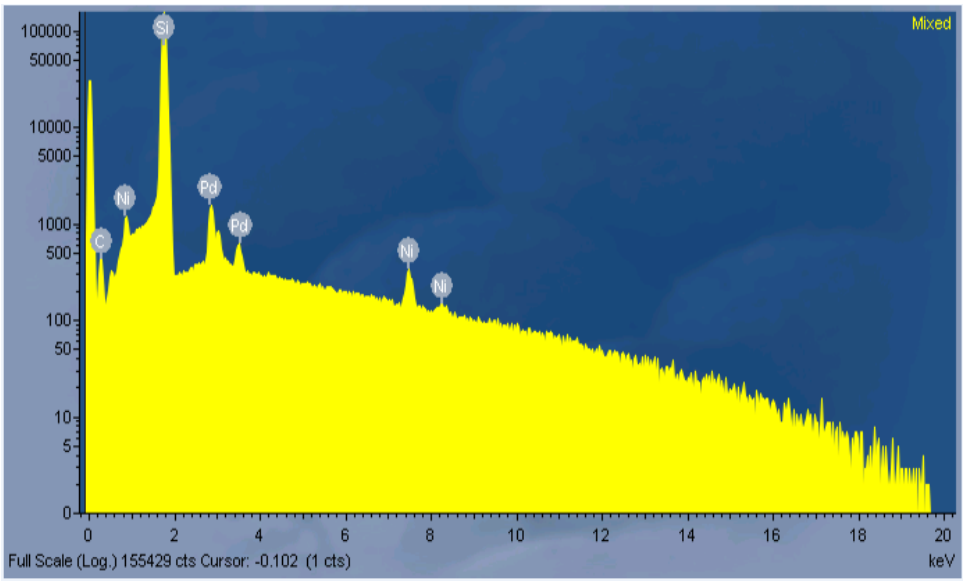

FIGURE 3.9: EDX spectrum for the PdNi film electrodeposited at a potential of -0.8V

3.3.2 Deposition of Uniform PdNi Alloys

Based upon the explanation of Fig. 3.7, different compositions of PdNi alloys can be fabricated by electrodeposition through variation of the potential. The results are given in Fig. 3.10 and Table 3.3. These data show that by varying the electrodeposition potential, one can reproducible achieve alloy compositions ranging from 100% Pd at -0.2V to 30% Pd at -2.0V. Further increase of the (negative) potential might lead to even larger Ni concentrations in the alloy, but this process would also lead to hydrogen evolution (reduction of hydrogen ions to hydrogen gas in the reversed process of Eq. 2.4) resulting in non-homogeneous films. Furthermore, for our application such a high Ni concentration is not beneficial.

The relation between the concentration of the individual elements in the $Pd_{1-x}Ni_x$ alloy at the electrodeposition potential is approximate linear over the entire range and can be fitted with the phenomenological Eq. 3.16. The large range of validity of this relation is surprising and shows that the Pd-Ni system is extremely suitable for the electrodepostion of alloys.

$$x = a(V_0 - V) \quad V_0 = 0.03V \;\; and \; a = 0.36/V \tag{3.16}$$

Fig. 3.10 shows that a wide range of Ni concentrations can be achieved from a PdNi solution simply by varying the deposition potentials. The concentration ratios of the elements are determined by the electrodeposition potential with larger negative

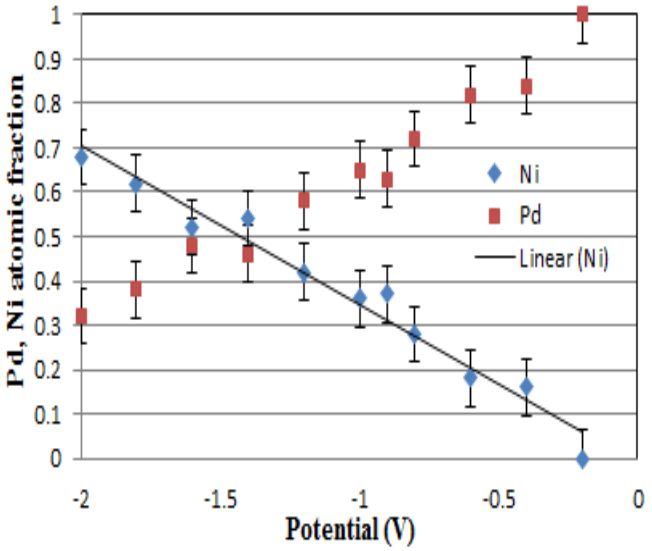

FIGURE 3.10: EDX analysis of Pd, Ni atomic fraction in films deposited at different potentials from a PdNi solution.

TABLE 3.3: EDX result for PdNi alloy composition from different deposition potentials.

Potential	Ni (At%)	Pd (At%)
-2.0	68	32
-1.8	62	38
-1.6	52	48
-1.4	55	46
-1.2	42	58
-1.0	36	65
-0.9	37	63
- 0.8	30	70
-0.6	19	8
-0.4	14	86
-0.2	2	98

voltages leading to high Pd concentration. The linear fit for the Ni content in the co-alloy deposition is also shows in Fig. 3.10. When a voltage of -0.8V is applied the alloy film contains nearly 30% Ni (as table 3.3 shows as well). The higher negative deposition potential is applied the higher the Ni concentration is achieved, and vice versa.

There have been previous occasions in which the effect of potential or current on the composition of the alloy has been studied. Xiao *et al.* [73] developed a Pd-Ni alloy nanowire on highly oriented pyrolytic graphite surface by electrodeposition, the EDX results displayed Ni content in the nanowire increases when the growth

The effect of growth parameters on Ni content of alloy

Samples	E_{grow} (V_{SCE}), t_{grow} (min)	Ni content in alloy (wt.%)
A	−0.3, 120	10.65
B	−0.4, 60	12.4
C	−0.45, 40	15.5
D	−0.5, 30	18.3

FIGURE 3.11: The Ni fraction in PdNi films deposited at different potentials from Xiao *et al.* [73].

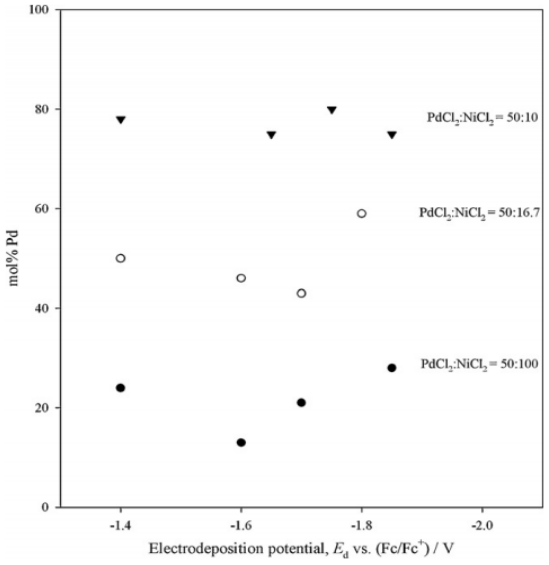

FIGURE 3.12: The dependence of Pd atomic content in the PdNi alloy on the electrodeposition potential [74].

potential is more negatively as Fig. 3.11 shows. Our data in table 3.3 are in agreement with this trend. However, the increase in Ni concentration in the Pd-Ni alloy can be extended massively by further increasing the negative potential.

Huang *et al.* has studied a co-deposited PdNi alloy based on $PdCl_2$ and $NiCl_2$ by using electrodeposition [74]. Fig. 3.12 depicts the Pd atomic concentration in the PdNi alloys in a range of -1.4 to -2 V. The ratio of $PdCl_2$ and $NiCl_2$ of 1:2 is identical to our Ni-Pd ratio in the solution (see table 3.2) but our substitution of $NiCl_2$ by $NiSO_4$ allows us to vary the composition in a controlled way, in contrast to those authors do not see much dependency of alloy composition on deposition potential.

Apart from the PdNi alloy electrodeposition, other co-metal electrodeposition techniques including Co, Fe, Ni, Au, Zn have been developed in recent years [76, 75, 77, 78]. Dolati *et al.* have reported a electrodeposition of the Au-Ni alloy from cyanide-citrate electrolytes with the composition of the alloy shown in

Potential (V)	Ni (%)	Potential (V)	Ni (%)	Potential (V)	Ni (%)
−0.45	0.65	−0.70	0.24	−0.95	0.14
−0.50	0.63	−0.75	0.21	−1.00	0.14
−0.55	0.53	−0.80	0.20	−1.05	0.11
−0.60	0.42	−0.85	0.17	−1.10	0.11
−0.65	0.30	−0.90	0.14		

FIGURE 3.13: Au-Ni composition as a function of potential [75].

Fig. 3.13 [75]. With the potential range from -0.45V to -1.10V the Ni content in the alloy can be varied from 65% down to 11%. Lu *et al.* demonstrated that with the variation of deposition potentials from -0.5 to 0.3 V the fraction of Au in the alloy of Au-Fe, Au-Co can be tuned in the range of 75% to 97% [77].

3.3.3 Deposition of Composition-Modulated PdNi Alloys

By changing the potential or deposition current during the deposition it is possible to vary the alloy concentration during the electrodeposition. Such techniques for electrodeposition of composition-modulated alloys in single-bath plating has been described in detail by Leisner [79]. Single bath composition-modulated electrodeposition have been described in materials term by numerous authors [80, 81, 82]. An example is the composition modulated Fe_xPd_{1-x} nanowire by Jeon *et al.* [81]. The Fe content in the alloy is varied by pulsed electrodeposition as is shown in Fig. 3.14. As far as aware, no-one has every used the method of composition-modulation to improve functional electrical properties of sensors or devices.

The excellent control of the alloy composition with potential allows us the grow Pd-Ni alloys with gradual or step-wise change of the alloy composition in a single bath electrodeposition run. By changing the potential during the electrodeposition, the relative rates of Pd and Ni electrodeposition can be changed as well. If change the potential continuously a concentration gradient will be established and if the potential was changed step-wise, a number of layers of PdNi with different concentration will grow as illustrated in Fig. 3.15. By controlling the total amount of charge that passes through the system, the thickness of each layer is exactly determined in Eq. 3.6. In the example given in Fig. 3.15, the total deposition process was divided into three steps for a total PdNi film thickness of 50nm. Initially, the electrodeposition potential was set to -1.2V to create a 40% Ni concentration at the Schottky barrier interface with the Si. To create the appropriate thickness

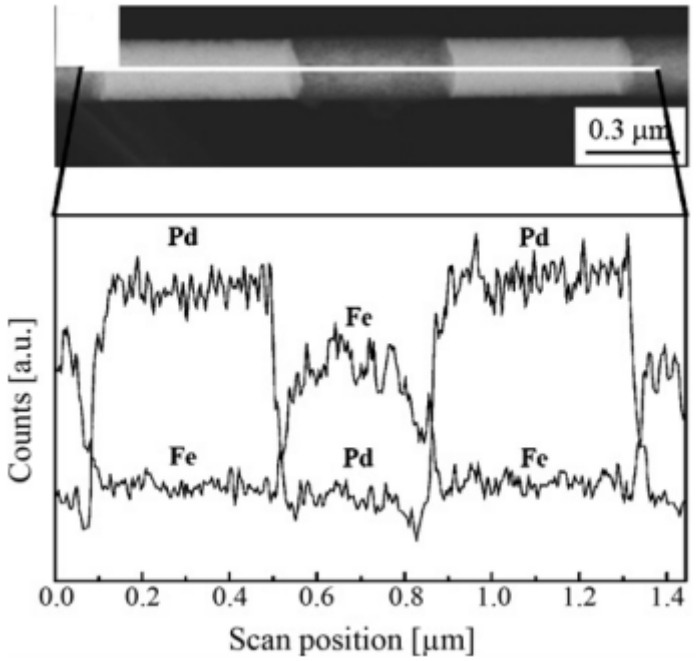

FIGURE 3.14: The Fe content in the Fe_xPd_{1-x} alloy corresponding EDS result [81].

of 17nm, the total charge during the deposition process should be equal to 20mC. This charge was reached after 7 seconds for this barrier layer at this potential. The potential was then reduced to -0.8V for the 30% Ni on the middle "bulk layer film. At this lower potential, the current flow is significantly lower and the time to reach an additional 20mC is increased. To create the surface layer, the potential is further decreased to -0.5V for 10% Ni in the surface layer of the film. The final process ends when the total charge reaches 60mC, which means the thickness of the PdNi film is 50nm. Structures similar to above will be used in the PdNi hydrogen sensors as will be detailed in Chapter 6.

3.4 Operation of Schottky Barrier

The Schottky barrier height is one of the most characteristic properties of a metal/semiconductor interface. The Schottky barrier height reflects the energy level mismatch since the majority carriers flow through the metal-semiconductor interface. The Schottky barrier height hence controls the electronic properties across metal-semiconductor interface and plays a vital role in the successful operation of a metal-semiconductor device [83].

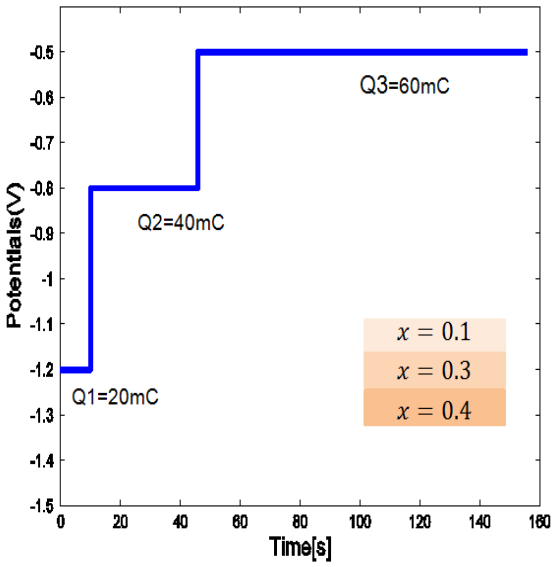

FIGURE 3.15: The potential variation during the electro-deposition with three steps. Each step corresponds to 20mC of charge. The corner schematic correspond to the steps of electrodeposition.

3.4.1 Schottky Barrier Height

Metals and semiconductors have different work function and when the metal contacts an n-type semiconductor, the Fermi levels in these two materials must be equal at thermal equilibrium under the continuous vacuum level condition. The flat-band diagram is not at thermal equilibrium if the Fermi energy in the metal is lower than in the semiconductor. When the metal and semiconductor are physically connected, electrons will diffuse from the semiconductor, leaving behind positively charged ionized donor atoms, forming the depletion region. The charge creates a negative field which lowers the band edges of the semiconductor. Electrons flow into the metal until equilibrium is reached between the diffusion of the electrons from the semiconductor into the metal and the drift due to the electric field. The band diagram is shown in Fig. 3.16 and the equilibrium is characterized by a constant Fermi energy throughout the structure. The barrier height ϕ_B is equal to the difference between the metal work function ϕ_m and the semiconductor electron affinity χ is. The built-in potential V_{bi} is the difference of the barrier height ϕ_B and the distance between the bottom of the conduction band and the Fermi level V_{bi} as shown in Eq. 3.17.

$$V_{bi} = \phi_m - \chi - \frac{E_C - E_F}{q} = \phi_B - \chi - \frac{E_C - E_F}{q} \tag{3.17}$$

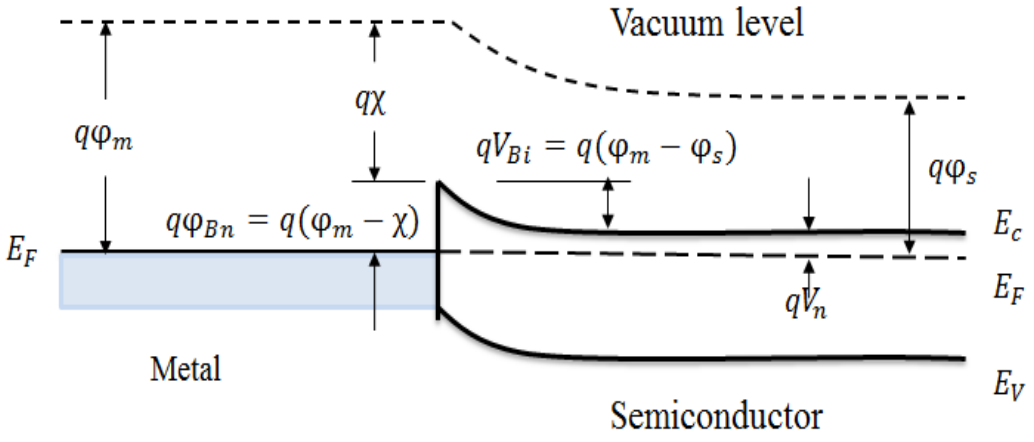

FIGURE 3.16: Energy band diagram of a metal-semiconductor contact in thermal equilibrium [84].

3.4.2 Current-Voltage Characteristics of Schottky Barrier

A Schottky barrier works similar to a one side abrupt p-n junction. However, the vital difference is that the majority carriers induce the current transport in a Schottky barrier while the minority carriers induce the current transport in a p-n junction. Schottky barrier have four basic transport processes under forward bias [85], as shown in Fig. 3.17.

1. Diffusion and thermionic emission current: Electrons cross the potential barrier and escape from the semiconductor into the metal.
2. Tunnelling current: Electrons tunnel through the barrier.
3. Minority carriers are injected from the metal into the semiconductor.
4. Carriers recombine in the space charge region

Diffusion current and thermionic emission current are described by very similar equations. For Si with relatively high doping concentration of more than 10^{17}cm^{-3}, such as in our devices, the thermionic emission current is dominant and the current flow will be explained using this theory as illustrated in Fig. 3.18. In equilibrium (Fig. 3.18(a), the current is zero and the electron flow from the semiconductor into the metal is equal to the electron flow from the metal into semiconductor. When the device is under forward bias condition (Fig. 3.18(b)), a positive bias is applied to the metal. The Semiconductor remains at the same potential, but the metal Fermi-level shifts to lower energies because of the applied voltage. This change

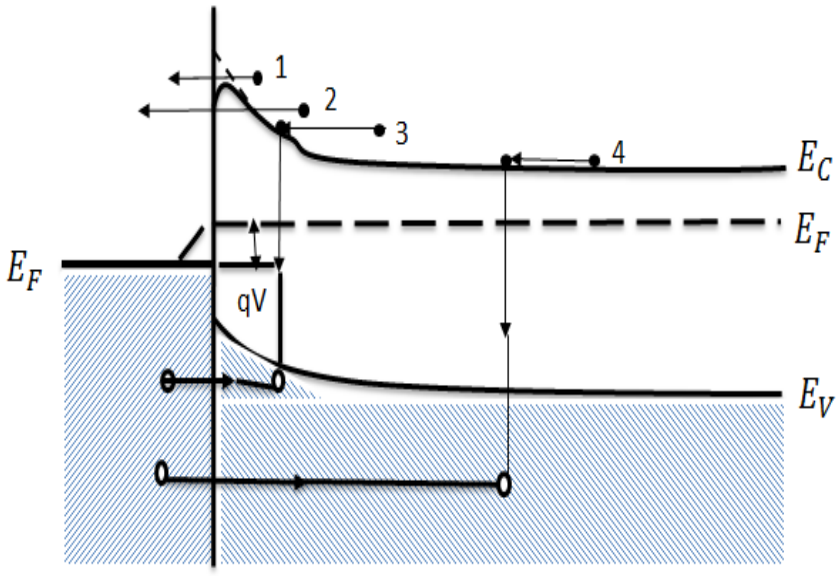

FIGURE 3.17: Four basic transport process under forward bias [84].

will lead to a decrease in the barrier potential. Therefore, the current density J^+ from the semiconductor to the metal will increase significantly. Meanwhile, the electron current density J^- from the metal to the semiconductor will still be very low due to a high and constant barrier between the metal and the semiconductor. When negative bias is applied on the metal, the device will be under reverse bias condition (Fig. 3.18(c)). The current density J^+ is low because of the large barrier potential. The reverse bias current remains very low, resulting in a rectifying behaviour.

The current density of a homogeneous Schottky barrier is given by [85, 86],

$$J(V) = J_S(e^{\frac{qV}{\eta kT}} - 1) \tag{3.18}$$

,where the saturation current density J_S is defined as

$$J_S = A^*T^2(e^{-\frac{q\phi_B}{kT}}) \tag{3.19}$$

In this equation, V is the applied voltage, q the electron charge, k the Boltzman constant, T the absolute temperature, η the ideality factor and ϕ_B the electron Schottky barrier height. A^* is the Richardson constant, which is expressed as

$$A^* = 4\pi m^* q k^2/h^3 \tag{3.20}$$

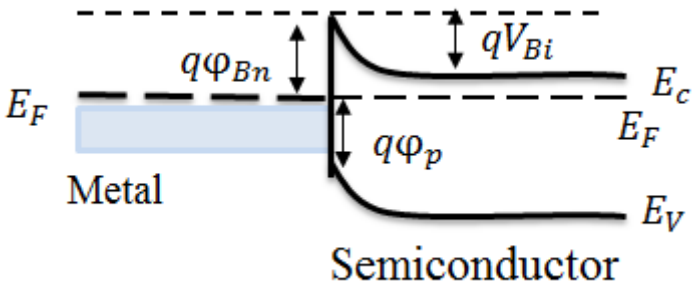

(a)

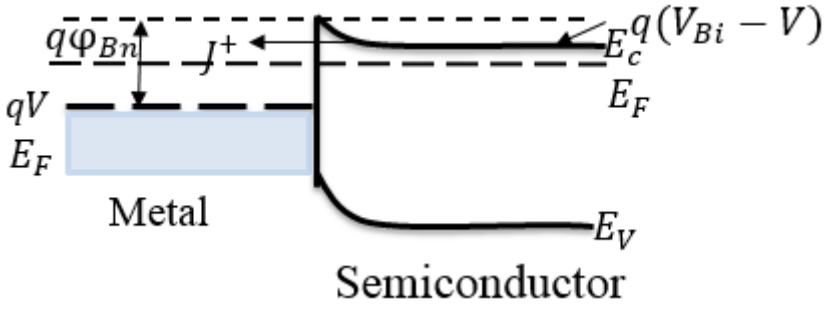

(b)

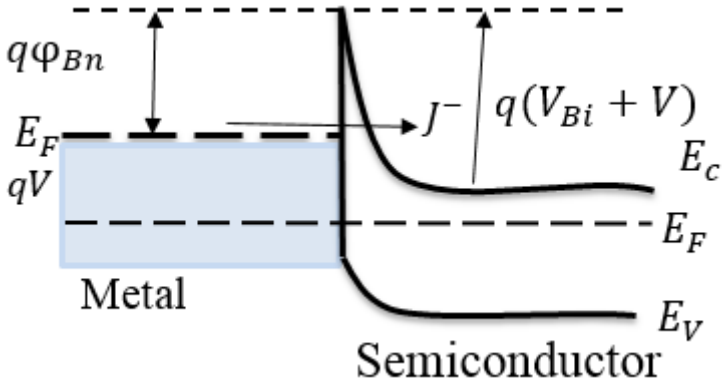

(c)

FIGURE 3.18: Current transport by the thermionic emission process. (a) Equilibrium band diagram without bias. (b) Band diagram of a forward biased Schottky barrier when the positive bias V is applied to the metal. J^+ is the current density from the semiconductor to the metal. (c) Band diagram of a reverse biased Schottky barrier when a negative bias V is applied to the metal and J^- is the current density from the metal to the semiconductor. Modified from [84].

TABLE 3.4: The I-V characteristic parameters of $Pd_{1-x}Ni_x$-Si Schottky barrier.

x	J_S (A/cm^2)	ϕ_{Bn} (V)	η
0	5.12×10^{-5}	0.725	1.71
0.3	7.12×10^{-7}	0.74	1.39
0.55	3.91×10^{-8}	0.74	1.21
1	1.39×10^{-7}	0.65	1.07

where h is the Plank constant (6.63×10^{-34}J·s), and m* is the semiconductor effective mass. When the applied bias V is much greater than $\frac{3kT}{q}$, the exponential part of Eq. 3.18 dominates and the equation can be expressed as

$$J = J_S e^{\frac{qV}{\eta kT}} \tag{3.21}$$

The intercept of the straight line equation gives the value of $\ln J_S$ when $\ln J$ is plotted on log axis as a function of V as shown in Eq. 3.22. Therefore, the ideality factor η can be calculated from the slope (Eq. 3.23) and the barrier height from the intercept (Eq. 3.24)

$$\ln J = \ln J_S + \frac{q}{\eta kT} \tag{3.22}$$

$$\eta = \frac{q}{kT}\frac{dV}{d(\ln I)}V \tag{3.23}$$

$$\phi_B = -\frac{\ln(J_S/A^*T^2)kT}{q} \tag{3.24}$$

The variation of current with applied potential for $Pd_{1-x}Ni_x$-Si Schottky barrier is shown in the Fig. 3.19. In this figure it is obviously that the PdNi-Si device exhibits Schottky barrier behaviour with a very low reverse bias current and high on and off current ratios with the forward bias current at least four orders of magnitude higher than the reverse bias current. The reverse bias current of the Schottky barriers are in the range of 0.1-10 nA and there is no breakdown observed until the negative bias reaches -2V.

Table 3.4 shows the I-V characteristic parameters of $Pd_{1-x}Ni_x$ Schottky barrier hydrogen sensors which extracted from Fig. 3.19. The ideality factor value in the thermionic emission theory is between 1 and 2. Since the value is close to 1, that indicates a good fit of the I-V data to the thermionic emission model. Therefore the thermionic emission is the dominant current conduction mechanism

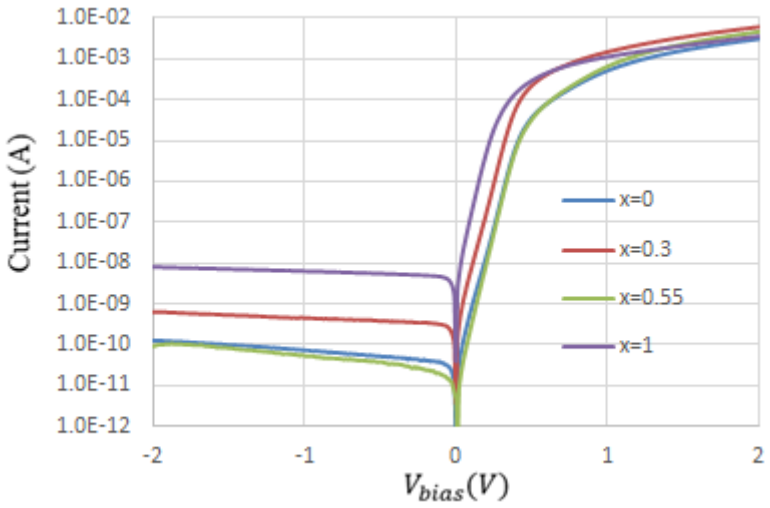

FIGURE 3.19: I-V characteristics of electrodeposited $Pd_{1-x}Ni_x$-Si Schottky barrier.

in the Schottky barrier. The Schottky barrier height for both the Ni-Si and Pd-Si barriers are in line with previous experimental results [61, 87]. Kiziroglou *et al.* have had fabricated a Ni-Si Schottky barrier by electrodeposition, the J-V curves was showed in the Fig. 4.5 and a SBH of ϕ_B=0.78V is obtained. A palladium on porous silicon Schottky barrier was fabricated by sputtering from Rahim *et al.* [87], compare with the conventional Pd-Ni Schottky barrier with a SBH ϕ_B=0.75V, the Pd/Si is equal to 0.88V. With the comparison of Ni-Si, Pd-Si and table 3.4 the Schottky barrier height does not show a strong correlation with Ni content in the PdNi alloy film. Ni (5.15eV) [88] and Pd (5.12eV) [89] possess similar workfunctions, which means that the SBH could not change significantly with the variation of film composition. Difference in Fermi level pinning might explain the lower barrier and higher current for the pure Pd film.

3.4.3 Capacitance-Voltage Characteristics of Schottky Barriers

C-V measurement are employed to determine important diode parameters, such as Schottky barrier height, substrate resistivity, and doping concentration. The depletion region of a Schottky barrier behaves in some respects like a parallel -plate capacitor. When a small AC voltage is superimposed upon a DC bias, charges of one sign are induced on the metal surface and charges of the opposite sign in the semiconductor. The theoretical analysis of C-V curves as illustrated by the ideal curve in Fig. 3.20 will be described below.

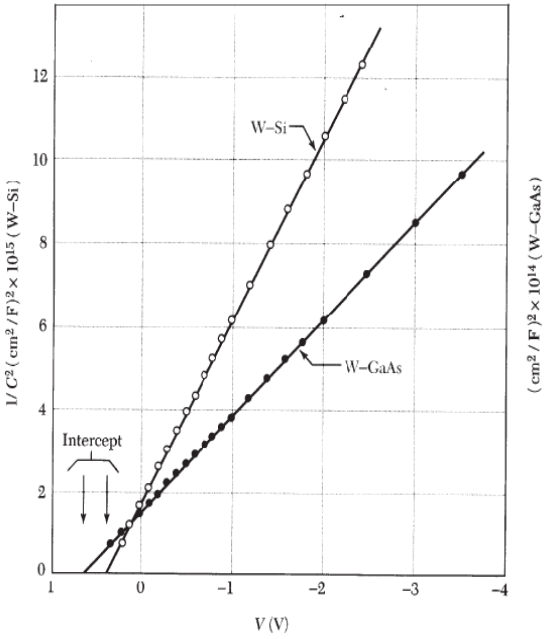

FIGURE 3.20: Ideal C-V characteristic of Schottky barrier [84].

Neglecting the minority carriers, the capacitance C of a Schottky barrier formed by a metal and an n-type semiconductor is given by the derivative of the positive charge due to the uncompensated donors in the depletion region Q_d with respect to applied voltage V_r, where Q_d is the positive charge caused by the a compensated donors in depletion region. Therefore the Eq. 3.25 can be expressed as Eq. 3.27 Plotting C^{-2} as a function of V_r allows extraction of both the donor doping concentration which is given by the slope of the curve, as well as Schottky barrier height ϕ_B from the intercept V_i which is equal to $V_{bi} - \frac{kT}{q}$.

$$C = \frac{\delta Q_d}{V_r} \tag{3.25}$$

$$Q_d = (2q\epsilon_s N_d)^{1/2}(V_{bi} - \frac{kT}{q} + V_r)^{-1/2} \tag{3.26}$$

$$C = \frac{\delta Q_d}{\delta V_r} = (\frac{q\epsilon_s N_d}{2})^{1/2}(V_{bi} + V_r - \frac{kT}{q})^{-1/2} \tag{3.27}$$

$$N_d = \frac{2}{q\epsilon_s}\left[\frac{1}{d(1/C^2)/dV_r}\right] \tag{3.28}$$

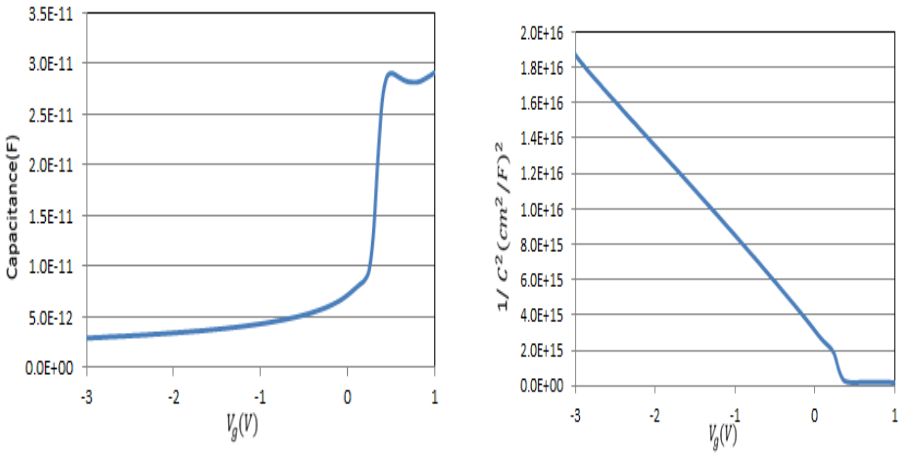

(a) (b)

FIGURE 3.21: (a)Room temperature C-V characteristic of the $Pd_{0.7}Ni_{0.3}$-Si Schottky diode. (b)$1/C^2$-V characteristic of the same device.

$$\phi_B = V_{bi} + V_n = V_i + \frac{kT}{q} + V_n \tag{3.29}$$

V_n is the distance of the Fermi energy below the conduction band given by

$$V_n = \frac{kT}{q} \ln\left(\frac{N_c}{N_d}\right) \tag{3.30}$$

Fig. 3.21 illustrates C–V curve and the dependence of $1/C^2$ on applied voltage of Schottky contacts made on the medium resistivity (1-2 Ω-cm) silicon wafer by PdNi electrodeposition. The graph shows the predicted linear behaviour in the $1/C^2$ -V curve as described in this section. Based on the slope and intercept, the various parameters are extracted. Table 3.5 lists the doping concentration of the silicon substrates and the barrier heights of Schottky barrier based on the C-V measurement results (more results were listed in Chapter 5).

TABLE 3.5: The C-V characteristic parameters of Schottky barrier, the Schottky contacts were made in the medium resistivity silicon wafer.

Structure	Side (cm)	Area (cm^2)	N_d (cm^{-3})	V_n (V)	V_i (V)	V_{do} (V)	ϕ_B (V)	ρ (Ω.cm)
$Pd_{0.7}Ni_{0.3}$	0.04	1.6×10^{-3}	3.30×10^{15}	0.234	0.70	0.72	0.93	1.24

As explained in Eq. 3.28, the slope of the $1/C^2$-V curves in Fig. 3.21(b) is proportional to the doping concentration in the semiconductor. The extracted doping

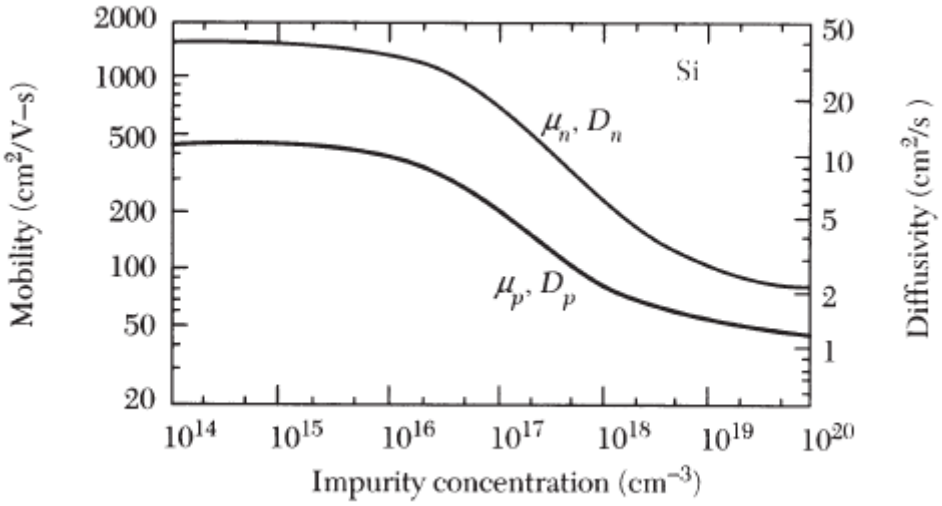

FIGURE 3.22: Mobility and diffusivity in Si at 300K as a function of impurity concentration [90].

concentration of n is $(3\pm\ 0.2)\times\ 10^{15}\text{cm}^3$. As the resistivity of n-type silicon is determined by electrons solely, the resistivity ρ can be expressed as

$$\rho = \frac{1}{qN_d\mu_n} \tag{3.31}$$

Where N_d is the electron concentration and μ_n is the electron mobility. The bulk mobility of silicon is retained from the Fig. 3.22 [90]. At the same dopant concentration, impurity scattering does not reduce mobility. Therefore the electron mobility μ_n can be chosen as its bulk value of 1405 cm^2/V.s. The extracted doping concentration hence corresponds to a resistivity of 1.24 Ω-cm which fits within the range of the nominal specification of 1-2 Ω-cm. Those results indicate that the fabricated devices and analysis are of a good standard, and it also shows that C-V measurements is a method for determining doping concentration or resistivity which can compete with the four point probe method [90]. The extracted Schottky barrier height will be analysed and discussed in more detail in the following chapters.

3.5 Conclusion

In this Chapter the working principle of electrodeposition was introduced as the key step to form the metal alloy-semiconductor interface in the Schottky barrier

hydrogen sensor. It is shown that with the right choice of solution, by properly adjusting the electro-deposition potential, it is possible to create PdNi alloys with the ratio of Pd to Ni spanning almost the entire range. Based on this possibility we present in the next chapter a new technique of composition-modulated PdNi films, in which each part of the PdNi film is separately optimized within a single electro-deposition process for use in a Schottky barrier hydrogen sensor. The rectifying properties of the electrodeposited PdNi-Si Schottky barriers are analysed and compared with the theory of thermionic emission. These C-V and I-V measurement results reveals that the electrodeposited PdNi-Si Schottky barrier possesses excellent rectifying characteristics with high Schottky barrier height, low ideality factor, and most importantly, low reversed bias leakage which makes them extremely suitable for low power sensors.

Chapter 4

Design and Fabrication of Hydrogen Sensor

4.1 Introduction

In this chapter, the device design will be explained together with the fabrication steps that are necessary to realize a functional hydrogen sensor. The Schottky barrier hydrogen sensor consists of a pair of back to back PdNi-Si Schottky diodes as fig. 4.1 shows. The reason we choose the back to back structure is because it restricts the current consumption during a two terminal measurement to low values by always maintaining one of the Schottky diode in reverse bias. The benefit of the electrodeposition technology for PdNi Schottky barrier has been confirmed with extremely low reverse bias current, that provide low power consumption in the idle state. The equipment that is used to measure the response in hydrogen and in other gases is explained. Finally, the fabrication of sensors for aqueous measurements is described together with its test measurements.

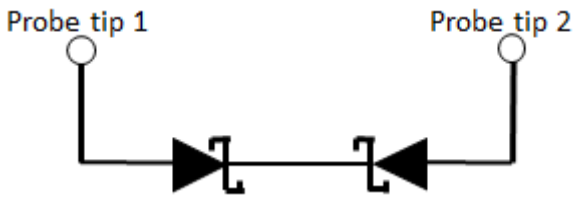

FIGURE 4.1: Block diagram of back to back Schottky barrier.

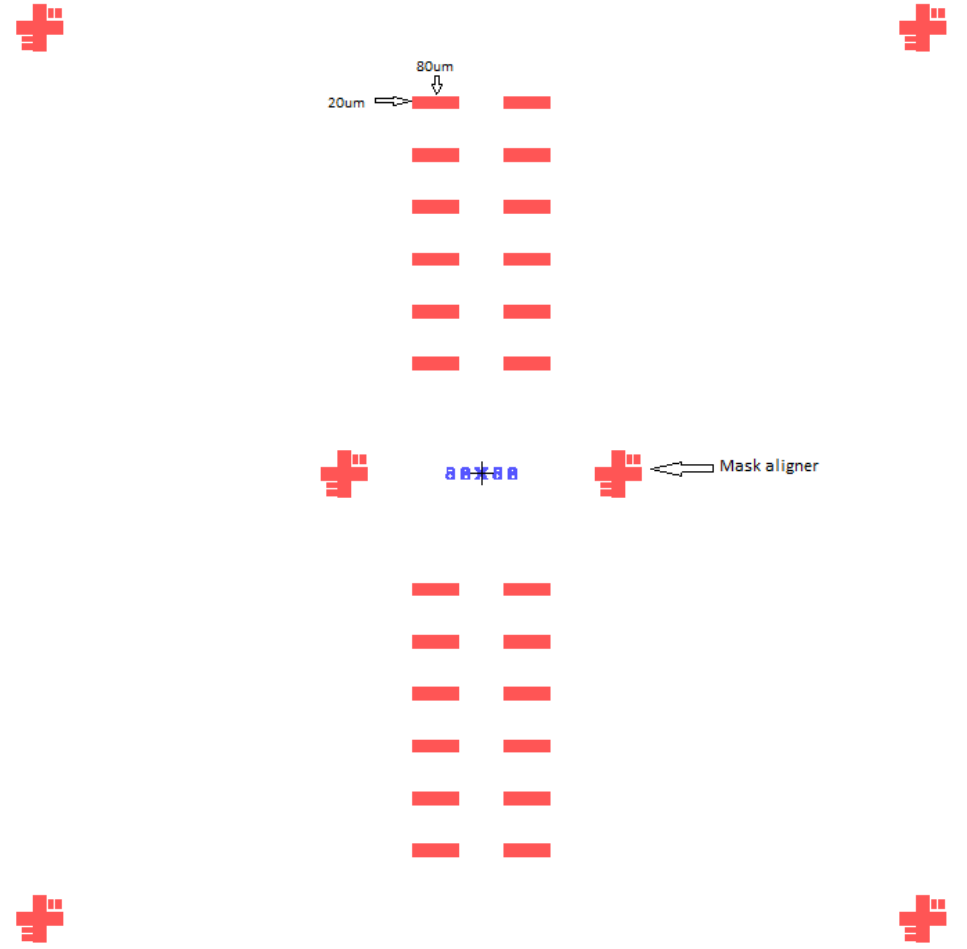

FIGURE 4.2: The first mask for forming the PdNi film.

4.2 Mask Design

The fabrication of all devices is done using photolithography and the mask design is the key important step for this. The sensor is fabricated using a two step process allowing for relatively cheap fabrication. The basic unit sample size of each of our hydrogen sensors is a $1.7mm \times 1.7mm$ which is patterned with windows for PdNi growth and Al contact pads. The first photolithograhy step is used to define the electrodeposition area (PdNi) , the first mask design is shown in Fig. 4.2.

A single PdNi area is $20 \times 80 \mu m^2$ and the separation between the PdNi electrodes is $80 \mu m$. The orange coloured crosses in the Fig 4.2 are the alignment marks, which are used to align the sample to the mask during the photolithography process. The structure of the PdNi film area is used to form back to back Schottky barrier sensors with the Si substrate acting as a key component. The back-to-back set-up restricts the current consumption during a two terminal measurement to low values by always maintaining one of the Schottky diode in reverse bias. The Fig

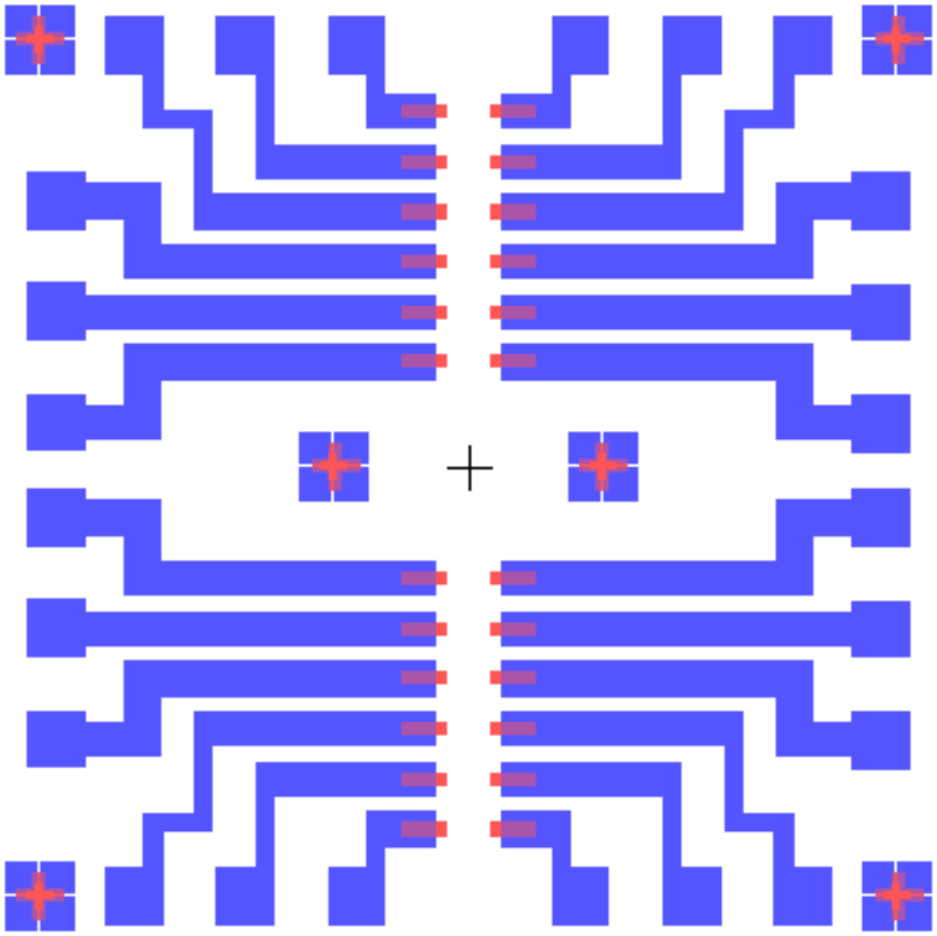

FIGURE 4.3: Layout of the structure for hydrogen sensor unit. The blue line and blue square is covered by Al.

4.3 shows both the first masks for the PdNi (red) and the second mask for the Al evaporation contact pads (blue), which form an integrated hydrogen sensor unit. The Al pad sizes are 100 μm $\times$ 100 μm with the Al lines connecting the pads to the PdNi. The total area of the structures on the basic sample are roughly equal to a 2-inch wafer. A typical wafer contains 224 hydrogen sensor units allowing for efficient fabrication. The mask is designed for use with a positive resist.

4.3 Fabrication Process

In the following subsections, the key fabrication processes are discussed and the design considerations are explained. A schematic of the fabrication process is give in Fig. 4.4.

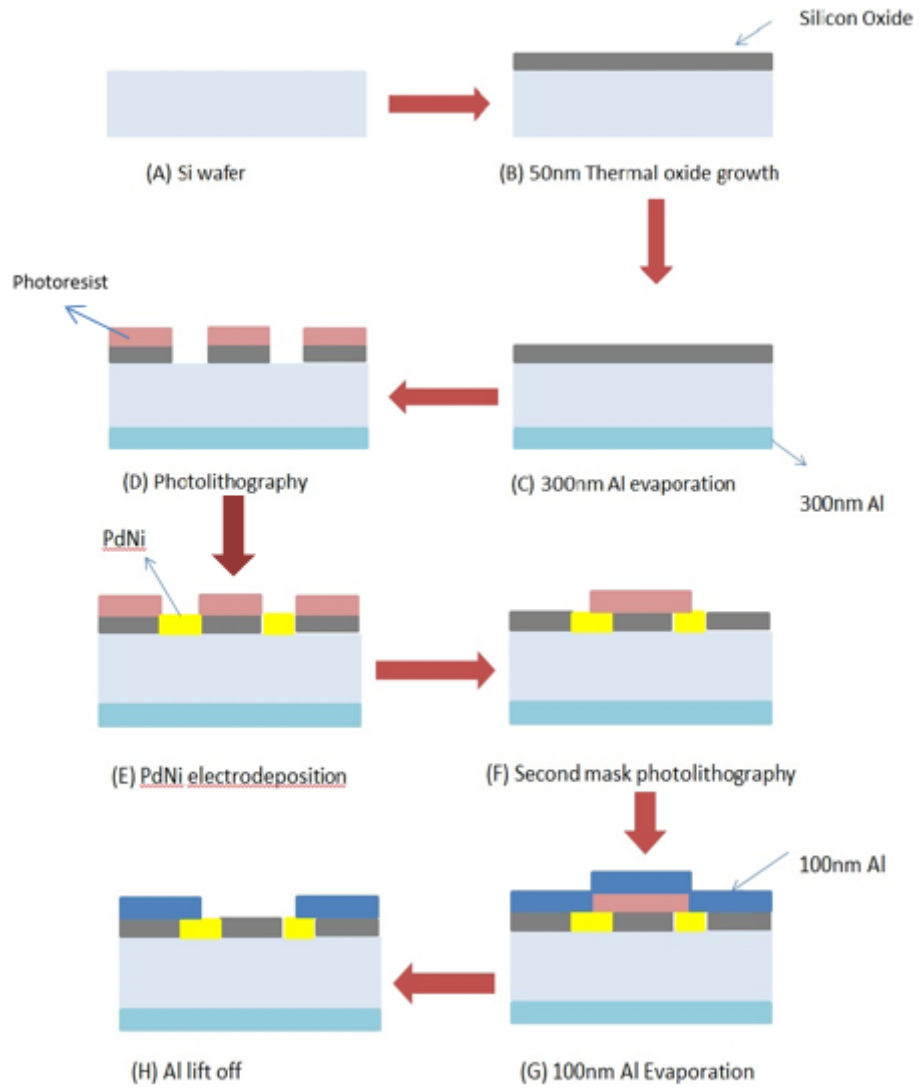

FIGURE 4.4: The fabrication process of PdNi Schottky barrier hydrogen sensor.

4.3.1 Si Wafer and Thermal Oxide Growth

The Silicon wafer used to fabricate the Schottky diode pairs is 6-inch, n-type, $1-2\Omega.cm$ with $<100>$ orientation. Low resistivity of the wafer is beneficial for the electrodeposition process of PdNi films as otherwise part of the electrodeposition potential will drop over the Si wafer. However, low Si resistivity gives a high reverse bias as Fig. 4.5 shows, because it leads to the electrons tunnelling through the Schottky barrier (thermionic field emission). This process does not depend strongly on the barrier height and is hence not sensitive to hydrogen gas. Moreover, the large reverse bias current also leads to a massive increase in power consumption. A compromise between these conflicting requirements is needed. It turns out that a resistivity of a few $\Omega.cm$ is sufficient resistive to prevent tunneling

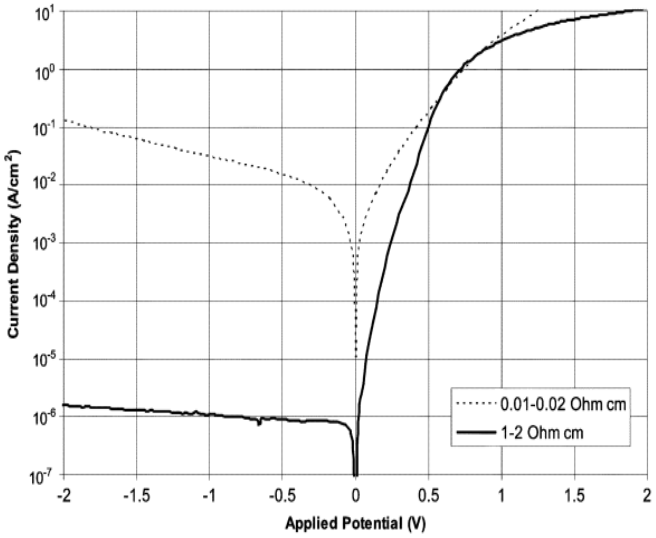

FIGURE 4.5: J-V curves of electrodeposited Ni-Si contacts for Si resistivity of 1-2Ohm.cm and 0.01-0.02 Ohm.cm [91].

and sufficiently conductive to prevent the ohmic voltage drop over the Si from the literature[91].

As illustrated in Fig 4.4, the first step is to clean the new wafers with fuming nitride acid for 15 minutes and with 20:1 HF for 1 minute, and store them in an uncontaminated single wafer holder. If the surface of wafer is insufficient cleaned by the preparation step, the result of thermal oxidation will result in the appearance of some black dots on the wafer surface. Then we use the Furnace "A1 507 DRYOX" option and update the WetOX work time to 56min 30s for a 50nm silicon thermal oxide on the Silicon surface. After the thermal oxide growth process is finished, the thickness of thermal oxide is measured by the ellipsometer to ensure the correct thickness. As wet oxide thickness growth is not linearly with time, we required several experiments to determine the appropriate time.

4.3.2 Thin Film Al Evaporation

The Al thin film is deposited by evaporation, for which we choose the BAK600 evaporator. Some of factors which will influence the uniformity of metal film are soak power, time, vacuum level, as well as material settings. Soak power and soak time controls the melting point of the Al material. The vacuum pressure for the evaporator has to be as high as possible. With small features, any impurity could lead to an influence on both the strength of the film and the electrical behaviour. The Fig 4.4(C) is the evaporation of Al on the backside of the silicon

Table 4.1: Photolithograpgy process

Procedures	Steps
Mask Lithography for electrodeposition and Al wiring	wafer dehydration for 2 hours
	Put S1813 at room temperature for 30 minutes
	Spinning 5000rpm 1.2μm
	Hot plate 95^oC for 2min
	Exposure 620TB 2.2s
	Developer MF 319 30-32s
	Water rinse 30s

wafer. This layer will not be used as electrode in the final hydrogen sensor but is a necessity for the subsequent electrodeposition to reduce the series resistance. It also allows measurements of individual Schottky barriers. In order to deposit Al on the backside of wafer, first use fuming nitride acid to clean the wafer; secondly spin coat photoresist on the front side of wafer to avoid the Al deposit to contaminate the front side and to ensure the integrity of the thermal oxide during the next cleaning step; Thirdly, the wafer back side is etched in a 20:1 HF solution for 40s to 60s; Then, the wafer is rinsed and moved quickly into the evaporation chamber, which is rapidly evacuated. Once, the vacuum pressure is sufficiently low, we evaporate 300nm Al. The thickness of the film is calibrated using a quartz crystal. Afterwards, the resist on the front side is stripped away by acetone.

4.3.3 Photolithography for Electrodeposition

Photolithography is an important step in Si technology, and is used to remove a certain pattern of the resist of the wafer for the following fabrication process. There are two types of photoresist used for photolithography, positive and negative photoresist. Each of photoresist requires different masks, exposure time, developing time and the result of features with different characteristics. In our work, positive resist was chosen for both photolithography steps. In case of a positive resist, the exposed areas are removed during development; in case of a negative resist the exposed areas are crosslinked and difficult to removed during the development. Therefore, the unexposed areas will be developed easily. The exposed positive resist is removed by the the developer. The process is outlined in Fig. 4.6 and table. 4.1. Fig. 4.4(D) shows the positive photoresist of the lithography.

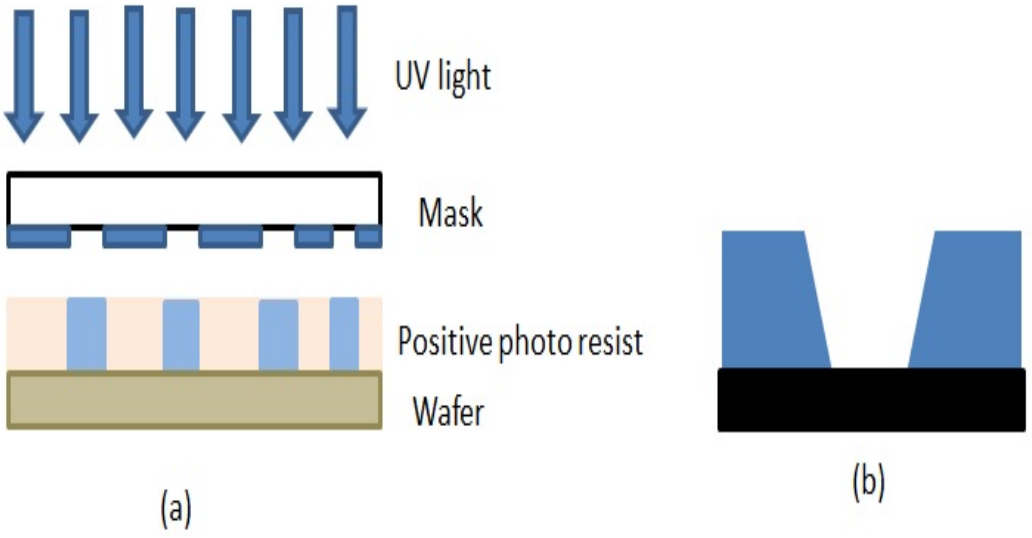

FIGURE 4.6: Photolithography of positive photoresist.

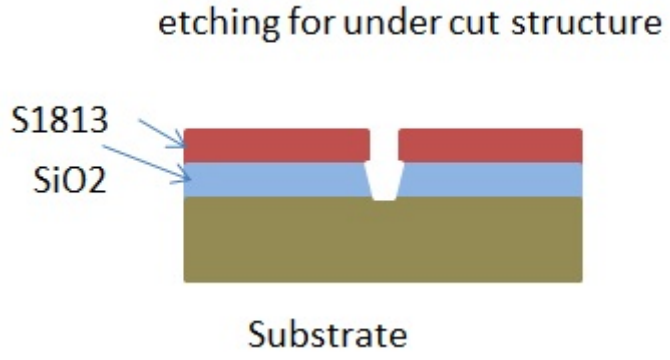

FIGURE 4.7: Wet etching for electrodeposition.

4.3.4 Wet Etch

Wet etching is a typical process used in Si technology, to isotropically remove a silicon dioxide layer (HF) or doing anisotropy etching on a silicon substrate (KOH), for example. In our work, wet etch is used to remove SiO_2 and leave the Si exposed for electrodeposition. The process of wet etch of thermal oxide is illustrated in Fig. 4.7. The thermal oxide (SiO_2) in the area which is defined by the photolithography, was etched away by a 20:1 HF as shown in the Fig. 4.4(D). Normally the 20:1 HF etches thermal oxide at a rate of 30nm, so the etch time for 50nm thermal oxide can be chosen to be 2.5min-3min.

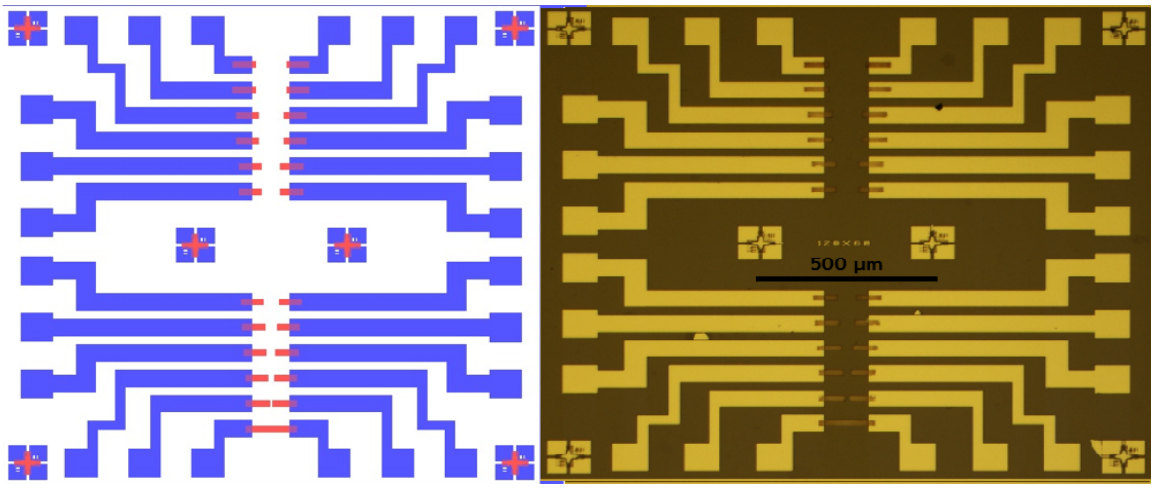

FIGURE 4.8: Mask for hydrogen sensor and final hydrogen unit by microscope, the sensor with a 2mm long and width.

4.3.5 Electrodeposition

Typically, 50nm thick PdNi films were deposited into the etched oxide patterns by electrochemical deposition, using the remaining oxide and the photoresist as a mask. There is one matter that needs attention; when electrodepositing the PdN,i the back side of wafer should be coated by photoresist to avoid the PdNi film depositing on the back side of the wafer. When the total charge reaches 60 mC, the deposition process is finished. As mentioned before, in order to control the thickness of PdNi film in electrochemical deposition, one should calculate the total deposition charge first. Eq. 3.6 demonstrates that the deposition charge is the preferred method to control the thickness, requiring the deposition area on the wafer to be calculated in advance. As is shown in Fig. 4.8, the orange part in the unit is the position where PdNi film should be deposited. Using the atomic weight of the species M, Avogadro's number N_a and the density of the metal, it is calculated that 60mC of charge corresponds to 50nm PdNi film.

$$A = 226 \times (0.13cm^2 + 0.04cm^2) + 226 \times (3.6 \times 10^{-4}cm^2 + 1.28 \times 10^{-3}cm^2) \approx 0.53cm^2 \tag{4.1}$$

The deposition potential was chosen from a range of potentials corresponding to current densities between 3 to 5 mA/cm^2. If the current density is lower, films will be growing slowly, discontinuously, and grainy. If the current density exceeds the values, the film will be powdery and brittle as shown in Fig. 4.9(b)[68].

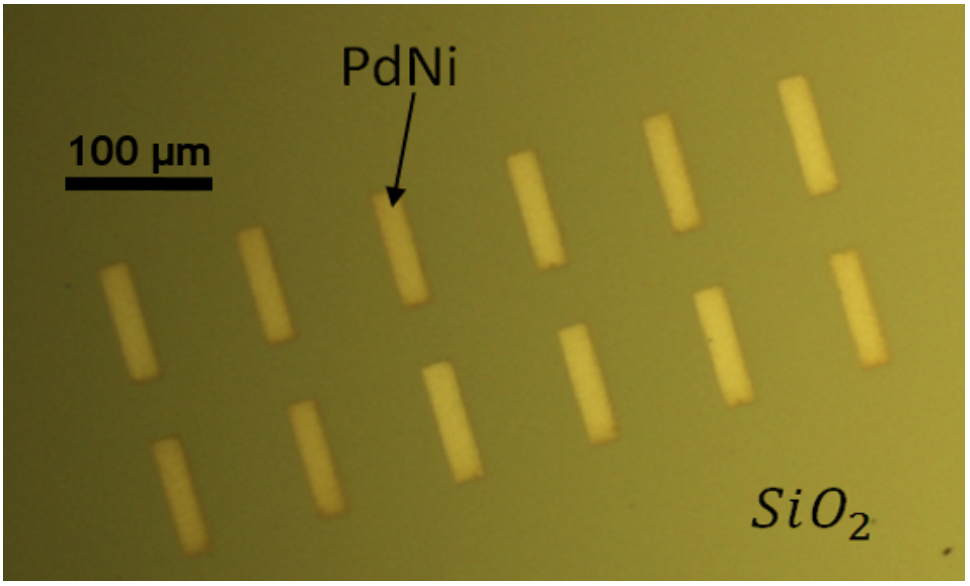

(a)

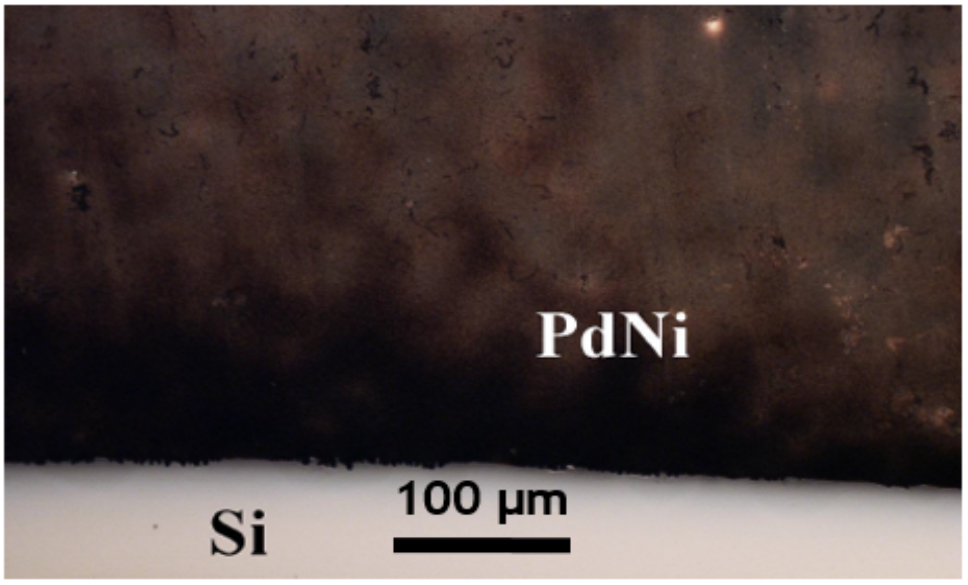

(b)

FIGURE 4.9: (a) Microscope image of Electrodeposited of PdNi films with a current density of 3-5mA/cm^2. (b) Electrodeposited of PdNi films with a current density of more than 5mA/cm^2)

.

4.3.6 Metal Lift-off

After the electrodeposition process is finished, the resist is washed away and a second photolithography step was introduced to define the Al wiring and contact pads. Before the second photolithograhy, a heating step is introduced to enhance the palladium adherence to the Si [92]. The wafer is annealed in the air at 200^oC, and this protocol always results in functional devices. A lift-off process is used to strip the layer that is covering the photoresist and give the final features of the device. The front side of the wafer is coated by 1 μm thick S1813 positive resist. After the photolithography, 100 nm Al is evaporated on the photoresist. After the evaporation, the wafer will be transferred into the acetone for 8 minutes to dissolve the resist. The areas which are not defined in the mask will be lift off by dissolved resist. The right side of Fig. 4.8 shows a microscopy image of the final hydrogen sensor.

4.4 The Characterization Equipment for Hydrogen Sensor

A Lakeshore EMTTP 4 probe station (see Fig. 4.10) is used. In order to measure the electrical characteristic of hydrogen sensor in hydrogen ambient. The cryogenic probe station has a vacuum chamber which allows for the insertion of hydrogen gas in an oxygen free atmosphere. Both nitrogen and a bottle of a mixture of 5% hydrogen in nitrogen were attached to the system.

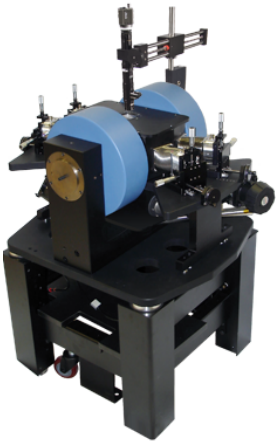

FIGURE 4.10: Picture of the EMTTP 4 probe station.

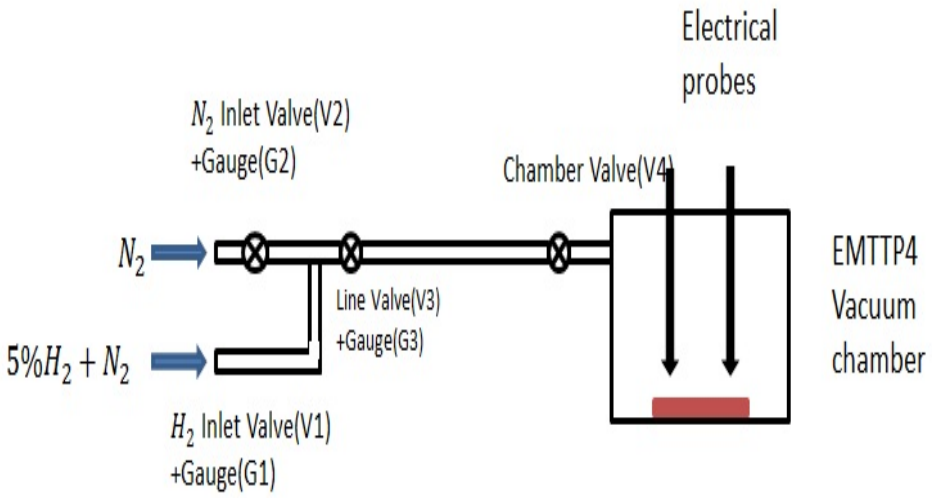

FIGURE 4.11: The Schematic of EMTTP4 system used to created hydrogen ambient in the vacuum chamber. V1-V4 are the Valves at the different points on the system.

The Fig. 4.11 shows a schematic of the probe station system. The probe station chamber can be pumped with either pure Nitrogen by opening valves V2, V3, and V4. Alternatively, the 5% hydrogen-Nitrogen mixture is pumped in the vacuum chamber by opening valves V1, V3, and V4. In this probe station, the smallest pressure increase is equivalent to the volume of one line between V3 and V4 ("tube"). For the hydrogen-nitrogen mixture this corresponds to a pressure of around 5mbar, which is equal to a hydrogen partial pressure of 250 μbar $\equiv$ 250 ppm.

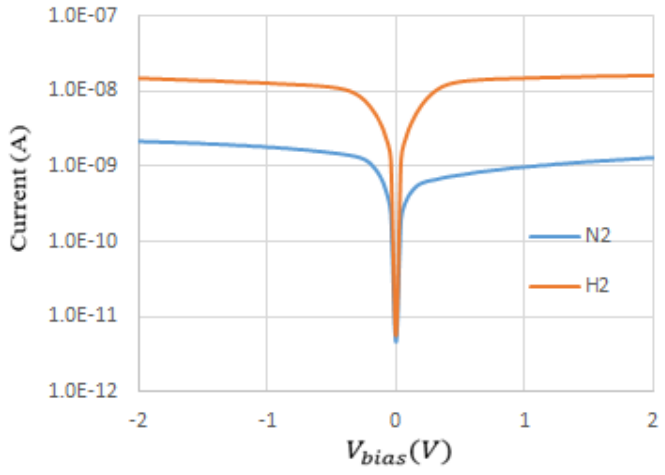

FIGURE 4.12: I-V characteristic of back to back Pd-Si Schottky barrier in both hydrogen and nitrogen ambient.

A typical approach to electrically characterize the hydrogen gas sensors is as follows: The chamber is evacuated and subsequently filled with nitrogen gas to a

pressure of 0.3 bar. Around 20 "tubes" of the hydrogen-nitrogen mixture are added to the chamber which results in an increase of the pressure to 0.4 bar with a hydrogen partial pressure of 5mbar. Once the hydrogen ambient was created, the device is contacted with the probes and electrical measurements are performed by using an Agilent B1500 parameter analyser. Typical I-V characteristic of a PdNi-Si Schottky barrier hydrogen sensor are illustrated in Fig. 4.12. Detailed analysis and explanation will follow in the subsequent chapters.

4.4.1 Measurement strategy

As Fig. 4.3 shows, the hydrogen sensor unit consists of twelve parallel back to back Schottky barrier hydrogen sensors. Initially, all twelve of the hydrogen sensors will be tested by generating the I-V characteristic in hydrogen ambient. After optimization of the fabrication process, all of sensors are generally functional and provide good reproducibility. The sensors with the most symmetric I-V curve and lowest reverse bias are chosen for the more detailed measurements, such as I-V-t, temperature dependent I-V, and various hydrogen concentration measurements, and C-V measurements.

4.5 Sensors for Aqueous Measurement

As part of the current project, we have established a collaboration with the Geosciences Environmental Institute (GET) in Toulouse, France for the performance of aqueous measurements. In this section, we show the preparation of a printed circuit board (PCB) board for aqueous measurement. As is shown in the above section and will be shown in the following chapters, the electrodeposited PdNi-Si Schottky barrier hydrogen sensor has robust sensor characteristic such as low power consumption and low cost to be considered for ubiquitous sensing. One particularly attractive application is deep sea distributive sensing. In such measurements, many sensors need to be employed to cover a large area of sea, while the sensors need to be autonomous for a significant time.

The layout of the PCB board with and without PDMS is illustrated in Fig. 4.13. The board has 3 pin holes at each side and a small square in the middle, thus the single hydrogen sensor unit (piece of Si) can be attached to the board by silver paste on the back resulting in a lay-out as shown in Fig. 4.13(a). To be able

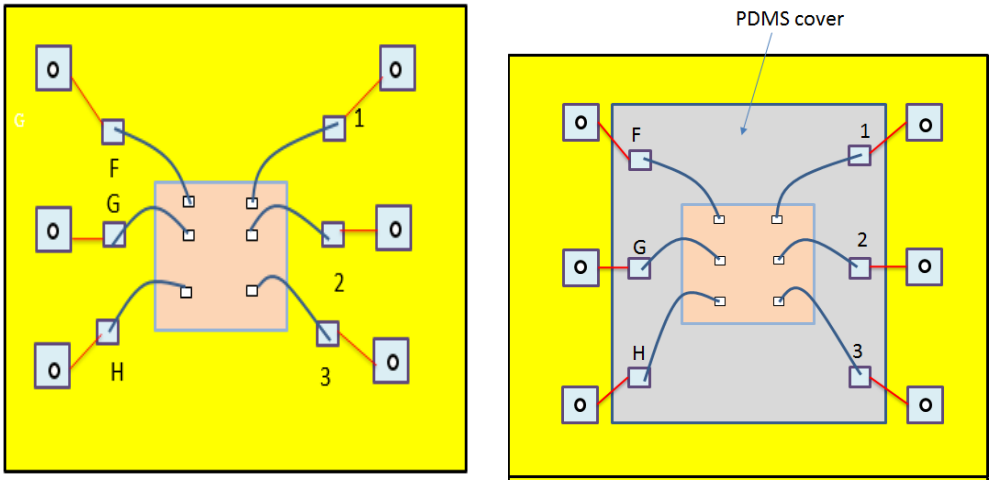

(a) (b)

FIGURE 4.13: (a) Schematic of PCB board with Si substrate with PdNi-Si hydrogen sensor. Each PCB board has three back to back sensors, being a connection between electrode F and 1 (F1), G and 2 (G2), and H and 3 (H3). (b) Schematic of PCB board with Si substrate with PdNi-Si hydrogen sensor which covered by PDMS.

to operate in an aqueous environment, the sensor needs to be waterproof as the electrodes would otherwise be shorted, but permeable to hydrogen. The solidified resist Polydimethylsiloxane (PDMS) possesses very suitable characteristics such as being hydrophobic, durable, cold tolerant, gas permeable, vapour selective [93, 94] and has been employed as a permeable barrier for gas measurement [95].

The elastomer and curing agent are mixed at a ratio of 10/1 and steered vigorously for a few minutes until filled with bubbles. The next step is to place the container of PDMS in a dessicator to degas for 5 minutes. The PDMS will be poured slowly on the surface of the device which is wired bonded at the PCB board. After the device is evenly covered by the PDMS, the device needs to be placed in an oven and be cured at 70^{o}C for 2 hours.

I-V-T measurement in both nitrogen and 5% hydrogen-nitrogen mixture ambient were taken to test the gas permeability of PDMS. Fig. 4.14 shows I-V-T (time response) of two nominally identical $Pd_{1-x}Ni_x$ x=0.3 Schottky barrier hydrogen sensors which are covered by PDMS. This figure shows that the sensors show similar sensitivity and time response as before the addition of PDMS. Once the hydrogen-nitrogen mixture gas is pumped into the chamber, the current increases almost immediately and keeps increasing with time before saturating. This confirms that the PDMS has good hydrogen permeability and the hydrogen molecules diffuse rapidly through the PDMS membrane. The future measurements in France

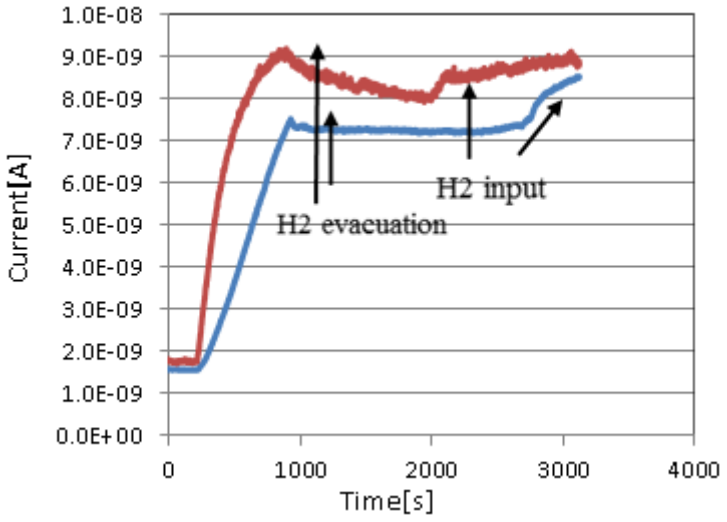

FIGURE 4.14: I-V-t (time response) of two nominally identical $Pd_{1-x}Ni_x$ x=0.3 hydrogen sensor covered by PDMS; hydrogen (0.1bar 5% hydrogen-nitrogen mixture) is added after100s,and removed at 800s by pumping down the chamber. A new hydrogen ambient was re-established after 2000s for G2 (red curve) and 2700s for F1 (blue curve) (see also Fig 4.13).

will have to show whether hydrogen ions in water will be able to diffuse (either as atomic species or molecular species) and what the sensitivity of such aqueous sensor will be.

4.6 Conclusion

Back to back PdNi-Si Schottky barrier hydrogen sensor have been fabricated according to the process and mask design outlined in this chapter in which a uniform layer of 50 nm PdNi alloy film was deposited on the Si at current density between 3-5mA/cm^2. The EMTTP4 probe station provides the controlled environment to measure the Schottky barrier hydrogen sensor in both nitrogen and hydrogen ambient. The Current-Voltage characteristic of back to back Pd-Si Schottky barrier in both hydrogen and nitrogen ambient clearly demonstrate that the back to back Schottky barrier have a good sensitivity to hydrogen. The sensors have been integrated in a printed circuit board (PCB) for aqueous measurement to create in future a ubiquitous distributed unpowered sensor network. The sensors on the PCB board have been covered by Polydimethylsiloxane (PDMS) and Current-Voltage-Time measurements in hydrogen ambient show that the PDMS provided an electrically insulating gas permeable membrane to allow aqueous operation. The aqueous measurements are currently being performed at the Geosciences En-

vironnement Toulouse laboratories in France.

Chapter 5

Effect of Uniform PdNi Alloy Composition on Sensor Sensitivity

5.1 PdNi-Si Hydrogen Sensor Mechanism

A PdNi-Si hydrogen sensor is based upon the reduction of Schottky barrier height at the Pd-Si interface. The reduction in barrier height can be measured either using capacitance-voltage (C-V) characteristics or current-voltage (I-V) characteristics. A number of key parameters have to be adjusted for the sensor to function satisfactory. The catalytic properties of the noble metal Pd are used to dissociate the hydrogen gas, which leads to formation of atomic hydrogen. The hydrogen has to be able to diffuse rapidly through the film to the metal-semiconductor interface [96]. At the metal-semiconductor interface, the Schottky barrier height (SBH) is lowered due to the formation of interface dipoles. Specifically, such model contains the following processes as shown in Fig. 5.2 and listed below.

1. Hydrogen molecules adsorb on the Pd layer and subsequently dissociate into atomic hydrogen.

2. Atomic hydrogen diffuses through the Pd layer towards the Si interface; an equilibrium atomic hydrogen concentration is established in the Pd film.

3. The positive atomic hydrogen ions lead to the formation of dipoles at the Si interface decreasing the Pd-Si Schottky barrier height.

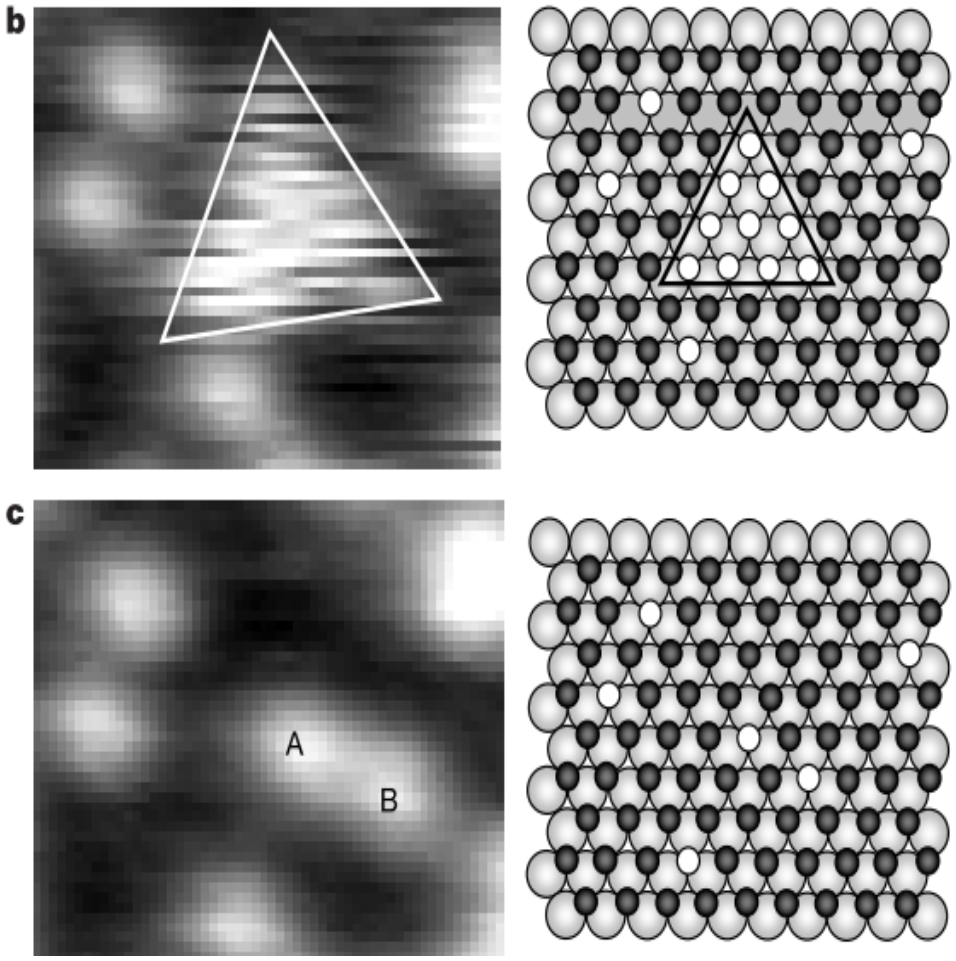

FIGURE 5.1: STM image showing the formation and annihilation of a four vacancy (4V) cluster. The bright sites are the H vacancies and the corresponding schematic diagram shows the H atoms and vacancies in the Pd substrate. The 4V cluster has been annihilated by absorption of Hydrogen, leaving two vacancies. Modified from[97]

4. Due to the Schottky barrier height reduction both reverse and forward currents increase, while the capacitance-voltage curve shifts.

The hydrogen molecule adsorption and dissociation under Pd presence is not well understood. The transient formation of active sites for the dissociative adsorption of hydrogen molecules on the Pd surface has been observed by the scanning tunnelling microscopy by Mitsui *et al.*. Fig. 5.1 illustrates this phenomenon; vacancy clusters decay via hydrogen adsorption and two of the vacancies are isolated allowing for hydrogen molecules to dissociate and to continue he adsorption process [97].

In Chapter 4, the method to develop hydrogen sensors with different PdNi composition has been described in detail. In order to improve the time response

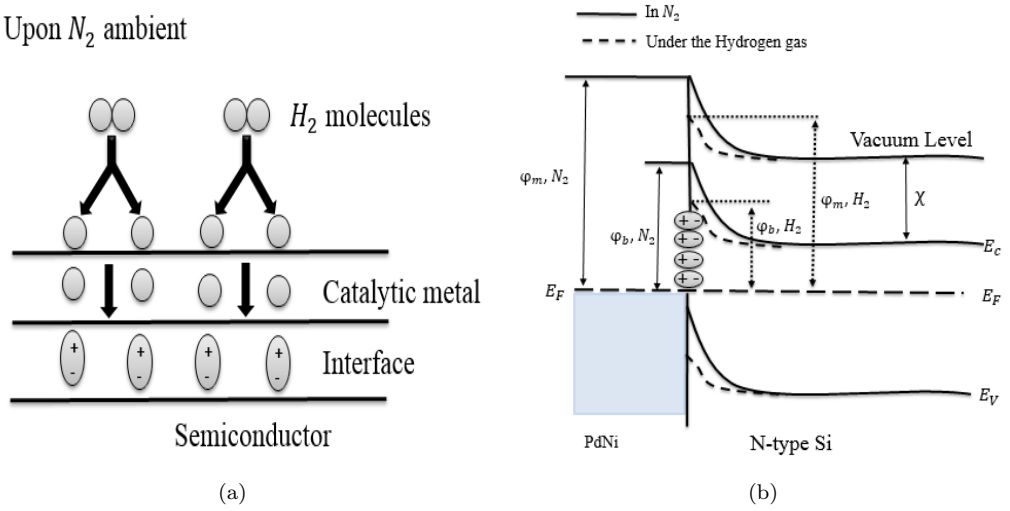

FIGURE 5.2: (a)Schematic diagram of hydrogen sensing process. (b) Corresponding schematic energy band diagram for the PdNi Schottky barrier under exposure to hydrogen gas or nitrogen.

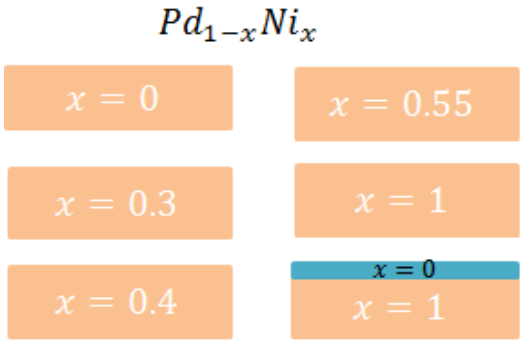

FIGURE 5.3: The different uniform 50nm $Pd_{1-x}Ni_x$ film compositions of the PdNi-Si Schottky barrier hydrogen sensor, x=0 represents a 10nm Pd cap.

of the PdNi-Si Schottky barrier hydrogen sensor, we are firstly concentrating on the variation of the Ni concentration in the PdNi alloy film. In this chapter the measurement and analysis will focus on this group of uniform $Pd_{1-x}Ni_x$ Schottky barrier hydrogen sensor to optimize the bulk structure of this thin film. In the subsequent chapter, we will introduce variations in the surface and barrier layer to optimize these components separately by the method as explained in Chapter 3. As a pure Ni surface is not expected to have any catalytic properties, an additional film is fabricated with a thin Pd layer on top of Ni film. The particular PdNi films fabricated for this purpose is listed in Fig. 5.3.

5.2 C-V Characteristics of $Pd_{1-x}Ni_x$-Si Schottky Barrier

In the previous section, the theory of how hydrogen exposure can change the SBH was briefly discussed. In order to confirm the formation of dipoles at the interface, C-V measurements were performed in 0.3bar nitrogen and 0.1 bar 5% hydrogen-nitrogen mixture gas. Steady-state C-V curves for 50nm $Pd_{1-x}Ni_x$ hydrogen sensor at 1MHz in nitrogen and 5% hydrogen-nitrogen mixture are shown in Fig. 5.4 and 5.5. The hydrogen C-V curves were measured 15 min after the introduction of the hydrogen. Before the introduction of hydrogen, a standard C-V curve for the metal-Si Schottky diode capacitor is seen. When the sensor is exposed to hydrogen, the C-V curve basically keeps the same curve shape but shifts to higher voltage. This shift is due to SBH lowering. The results hence simultaneously confirms that introduction of hydrogen causes SBH lowering without changing other electronic properties of the system such as the semiconductor doping concentration.

According to Eq. 3.28 to 3.30, the parameter extraction from C-V curves is best done from $1/C^2$ versus V graphs in which the slope is proportional to the Si carrier concentration and the intersection with the abscissa gives the Schottky barrier height. We have shown in Ch.3 that the carrier concentration derived from such C-V graphs in nitrogen is indeed equal to the nominal concentration. The addition of hydrogen does not alter the slope significantly. Parallel slope of $1/C^2$ versus voltage means the doping concentration of the Si remains constant as expected in the range of the nominal concentration of 1-10 Ω/cm. The intersection with the axis does change significantly though. Table. 5.1 lists the results of the barrier height in hydrogen and nitrogen of the Schottky barrier sensors as extracted from these curves.

It is evident that within the margin of error, the pure Ni film does not lead to a shift in barrier height while the pure Ni film with Pd cap gives a significant change. This proves that Pd is an essential component of the surface layer to provide the catalytic decomposition of the hydrogen gas into atomic hydrogen. Without Pd, the Ni film does not generate any atomic hydrogen and subsequently there is no diffusion of hydrogen to the semiconductor interface. The barrier height of the other films will be discussed later in this chapter together with the data extracted from the I-V measurements.

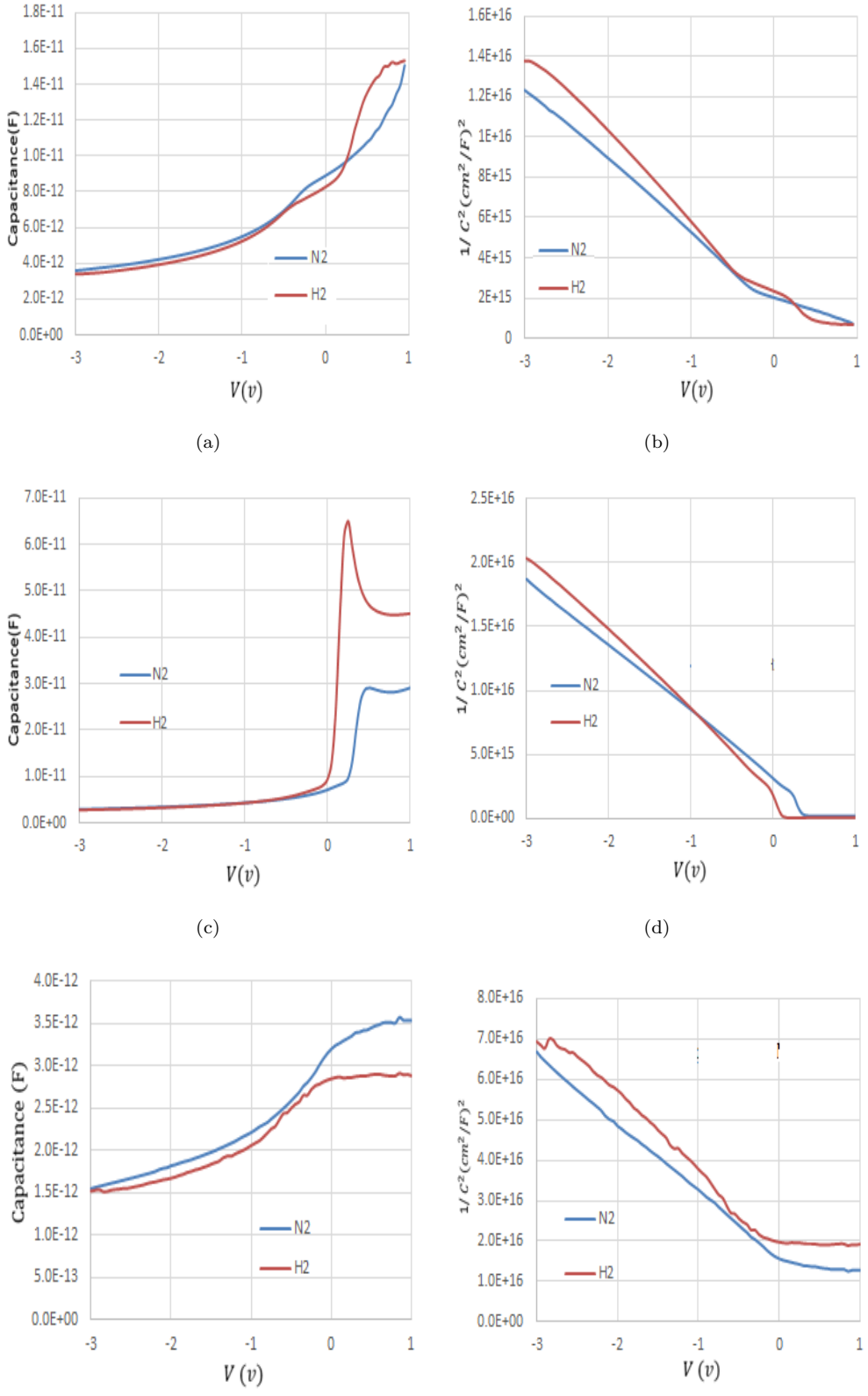

FIGURE 5.4: C-V and $1/C^2$-V characteristic of $Pd_{1-x}Ni_x$ Schottky diode of film thickness of 50nm with x=0 (a,b), x=0.3 (c,d), x=0.4 (e,f) in both nitrogen and 5% hydrogen-nitrogen mixture ambient.

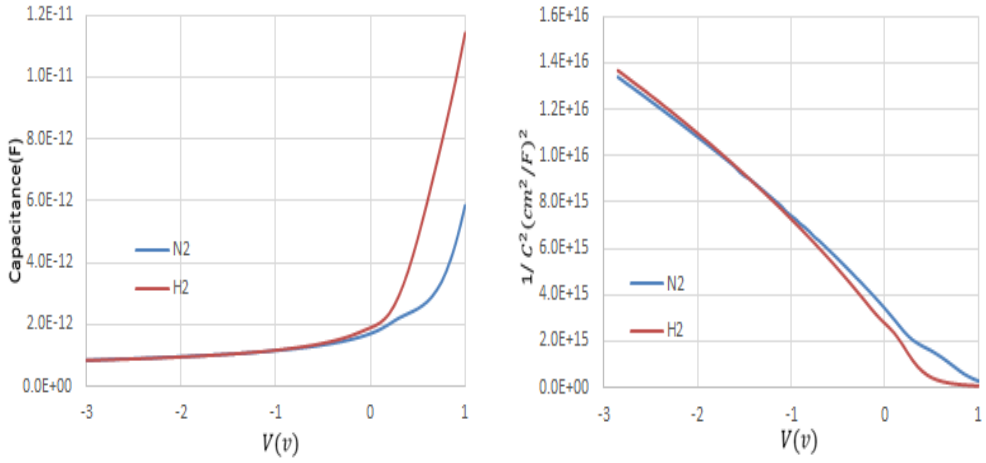

(a)

(b)

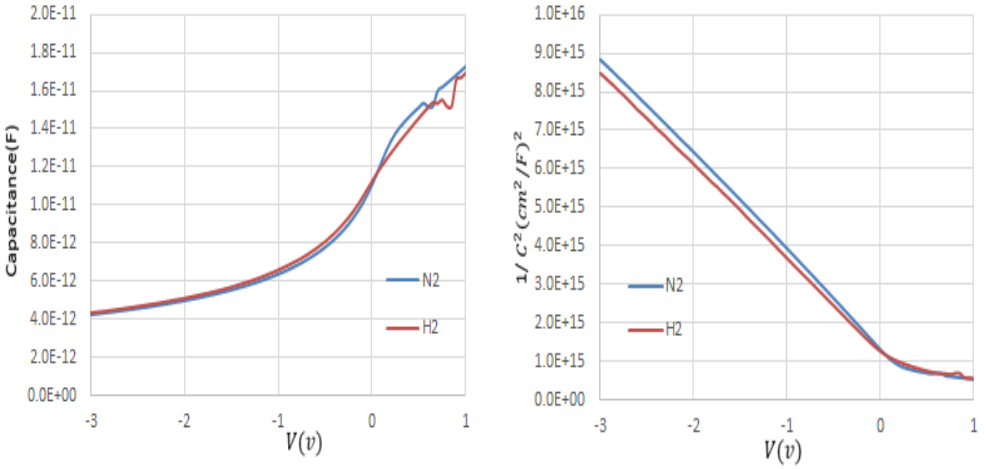

(c)

(d)

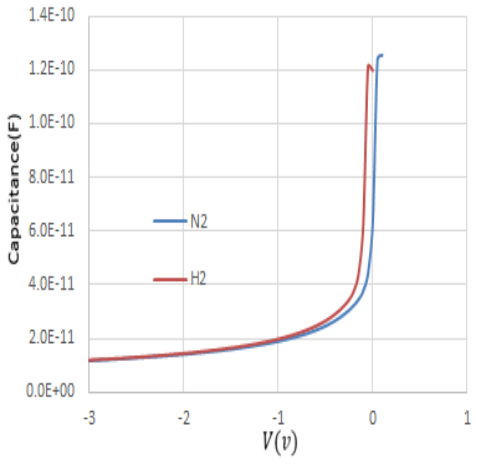

(e)

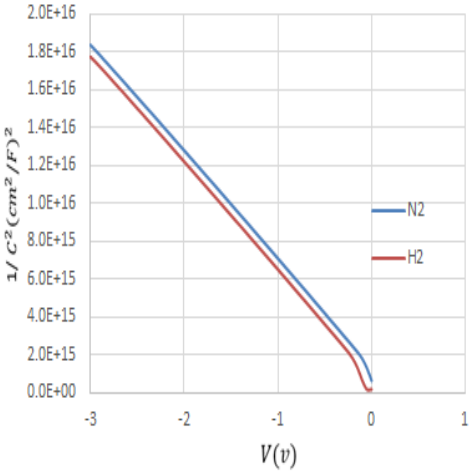

(f)

FIGURE 5.5: C-V and $1/C^2$-V characteristic of $Pd_{1-x}Ni_x$ Schottky diode of film thickness of 50nm with x=0.55 (a,b), x=0.1 (c,d), x=1 with Pd cap (e,f) in both nitrogen and 5% hydrogen-nitrogen mixture ambient.

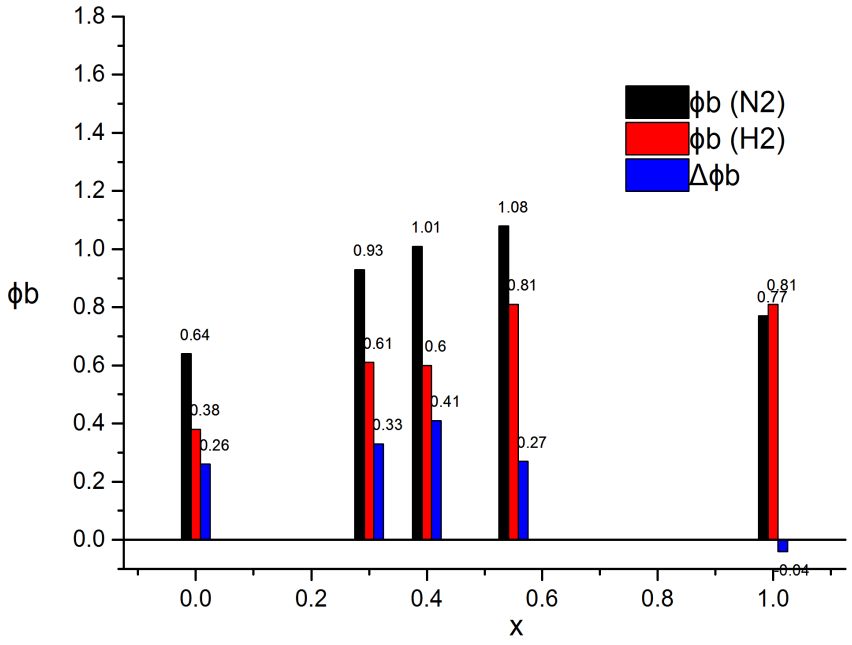

FIGURE 5.6: The Schottky barrier height ϕ_B of all uniform $Pd_{1-x}Ni_x$ structures Schottky diode in nitrogen and 5% hydrogen-nitrogen mixture ambient.

5.3 I-V Characteristics of $Pd_{1-x}Ni_x$-Si Schottky Barrier

In Chapter 3 the I-V characteristics of a PdNi Schottky barrier has been described. Using the Al back contact as electrode, I-V characteristics of individual Schottky barriers are measured and displayed in Fig. 5.7(a) to Fig. 5.7(f).

Using, the saturation current and the methods described in Chapter 3, the variation of the barrier height in nitrogen and hydrogen can be obtained. Table 5.1 lists the barrier height in nitrogen and 5% hydrogen-nitrogen mixture ambient as extracted from the I-V measurements together with the data from the C-V measurements. The I-V results for the pure Ni film show no difference between nitrogen and 5% hydrogen-nitrogen mixture due to the lack of catalytic decomposition as explained before.

Comparing the Schottky barrier height in hydrogen and nitrogen for the structures between C-V and I-V measurement except for the pure Pd, the barrier height extracted from the I-V measurement is significantly smaller than from the C-V measurements. The reason for this is the spatial variation in barrier height and

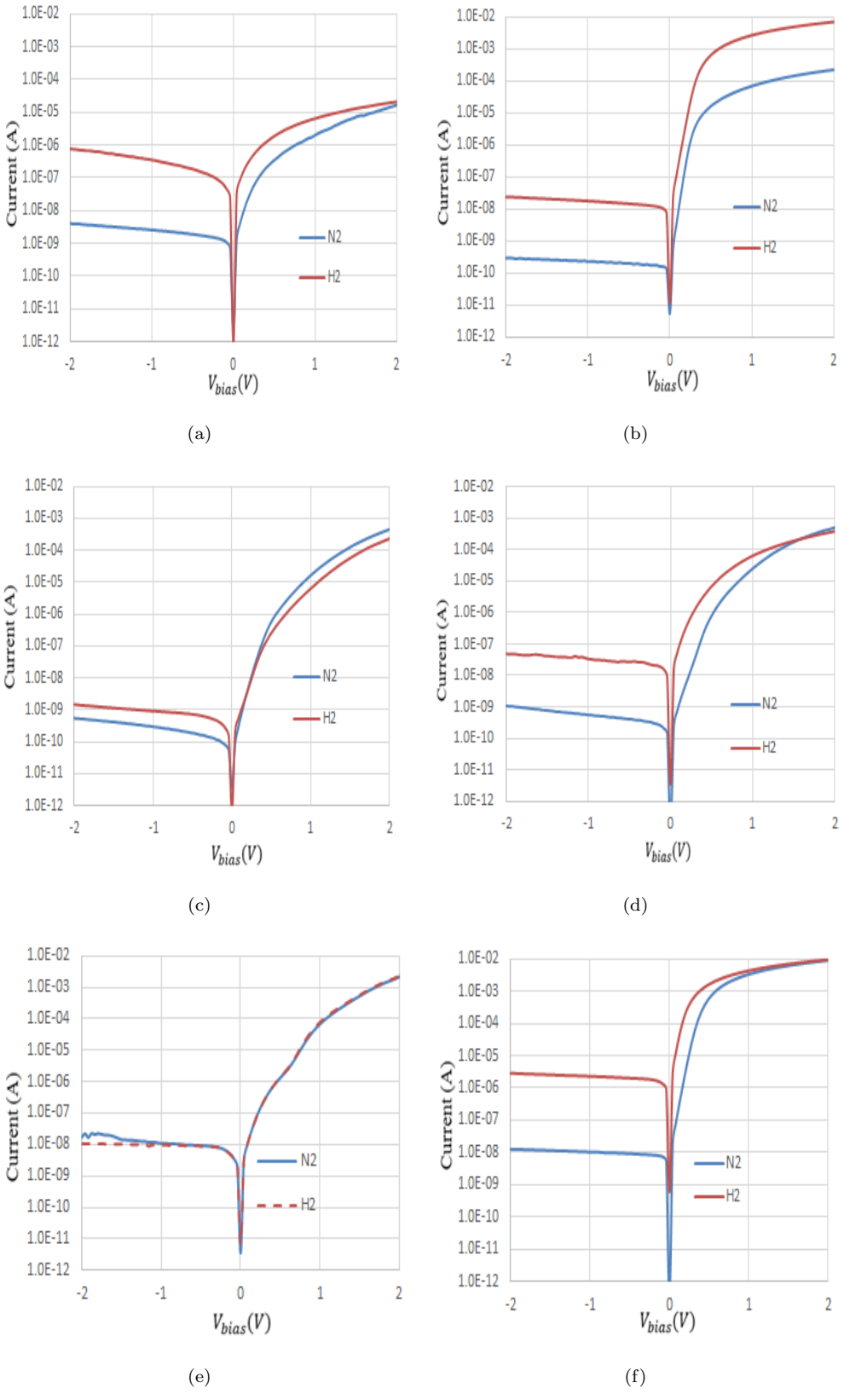

FIGURE 5.7: I-V characteristics of uniform $Pd_{1-x}Ni_x$ Schottky diodes in nitrogen (0.3bar) and 5% hydrogen-nitrogen mixture (5mbar H_2 partial pressure). (a) x=0. (b) x=0.3 (c) x=0.4 (d) x=0.55 (e) x=1, (f) x=1 with Pd cap.

TABLE 5.1: The I-V characteristic parameters of uniform $Pd_{1-x}Ni_x$-Si Schottky barrier hydrogen sensor in nitrogen and 5% hydrogen-nitrogen mixture ambient and below the I-V results shows the C-V results for comparison.

$Pd_{1-x}Ni_x$	x=0	x=0.3	x=0.4	x=0.55	x=1	x=1 (Pd)
ϕ_B (N_2)	0.73	0.71	0.81	0.74	0.65	0.71
ϕ_B (H_2)	0.63	0.62	0.78	0.67	0.66	0.57
$\Delta\phi_B$	0.09	0.09	0.03	0.07	-0.01	0.14
ϕ_B (N_2)	0.64	0.93	1.01	1.08	0.77	0.76
ϕ_B (H_2)	0.38	0.61	0.60	0.81	0.81	0.44
$\Delta\phi_B$	0.26	0.33	0.41	0.27	-0.04	0.35

the different response of capacitance and current measurement to this. Short range potential fluctuations between the interface layer and Si filtered at the edge of the space-charge region. The capacitance will hence be insensitive to potential fluctuations on a length scale which is less than the width of the space charge. Therefore, capacitance reflects the mean value of V_{bi} and ϕ_B. However, the current I across the interface layer depends exponentially on ϕ_B. Any spatial variation in the Schottky barriers lead to the current to pass through the minimum value of the barrier [98]. The exposure to hydrogen leads consistently to a decrease in Schottky barrier height in both I-V and C-V measurements for all concentrations of PdNi alloy ranging from pure Pd to pure Ni (with Pd cap). The decrease is largest in the C-V measurements for $Pd_{1-x}Ni_x$ with x=0.4 but this is the exact alloy concentration for which the barrier height is smallest. Optimization of the device structures does hence require a more systematic approach in which each component that contributes to the sensitivity is carefully separated and in which sufficient data is taken for a minimum of statistical analysis.

5.4 Back to Back $Pd_{1-x}Ni_x$-Si Schottky Barrier Hydrogen Sensors

As explained in Chapter 4, the preferential configuration for a current based hydrogen sensor is the back to back Schottky barrier configuration in which either of the diodes is in reversed bias. The consequence of such a configuration is that the current is always limited to the saturation current in reverse bias resulting in ultra-low power consumption in nitrogen. In the next chapters, the hydrogen concentration is either expresses in bar or parts per million (ppm), with 1μbar equivalent to 1 ppm.

5.4.1 Sensitivity and Selectivity

The steady state I-V characteristics of back to back uniform PdNi-Si Schottky barrier on exposure to 5mbar hydrogen partial pressure (0.1 bar 5% hydrogen-nitrogen mixture,) are illustrated in Fig. 5.8. The first thing to remark is that in nitrogen atmosphere the current is at most a few nA at any voltage. This shows that the power consumption of these sensors in the idle state is extremely low. When hydrogen is added to the system, the sensors respond with an increase in current of at least one order of magnitude. The dependency of the sensitivity on the Pd-Ni ratio is again not evident and will be analysed in more detail in the next chapter where sensitivity and time response are explicitly decoupled. Again, as in the case of the individual Schottky barriers, the sensor with only Ni does not show a response to hydrogen.

The steady state I-V characteristics of back to back uniform PdNi-Si Schottky barrier as function of hydrogen partial pressure is shown in Fig. 5.9. The sensors show a monotonous increase in current with increasing hydrogen partial pressure. The increase saturates at high values of hydrogen concentration. The theoretical dependence is discussed in more detail in the next chapter.

5.4.2 Response Time

The time response is one of the most important properties of any gas sensor. Time response of all Schottky barrier hydrogen sensors is measured in the same EMTTP4 probe station. Fig. 5.10 demonstrates the behaviour of a uniform Schottky barrier hydrogen sensor exposed to air, vacuum, nitrogen as well as hydrogen ambient. The figure shows the response firstly in air followed by subsequent evacuation, nitrogen inflow, and additional hydrogen inflow. This figure shows the current is stable and identical in vacuum, nitrogen, and air, demonstrating that the sensors are perfectly selective for hydrogen, and have also negligible response to the trace gasses in air such as CO_2. It is not before the inflow of hydrogen that the sensor responds. The current of the hydrogen sensor then keeps on increasing due to further diffusion of the hydrogen to the Schottky barrier interface until the measurement is terminated.

Fig. 5.11 shows the current as function of time upon the inflow of hydrogen for the uniform $Pd_{1-x}Ni_x$ Schottky barrier hydrogen sensors. All measurements are taken at 1V but similar conclusions would hold for other measurement voltages.

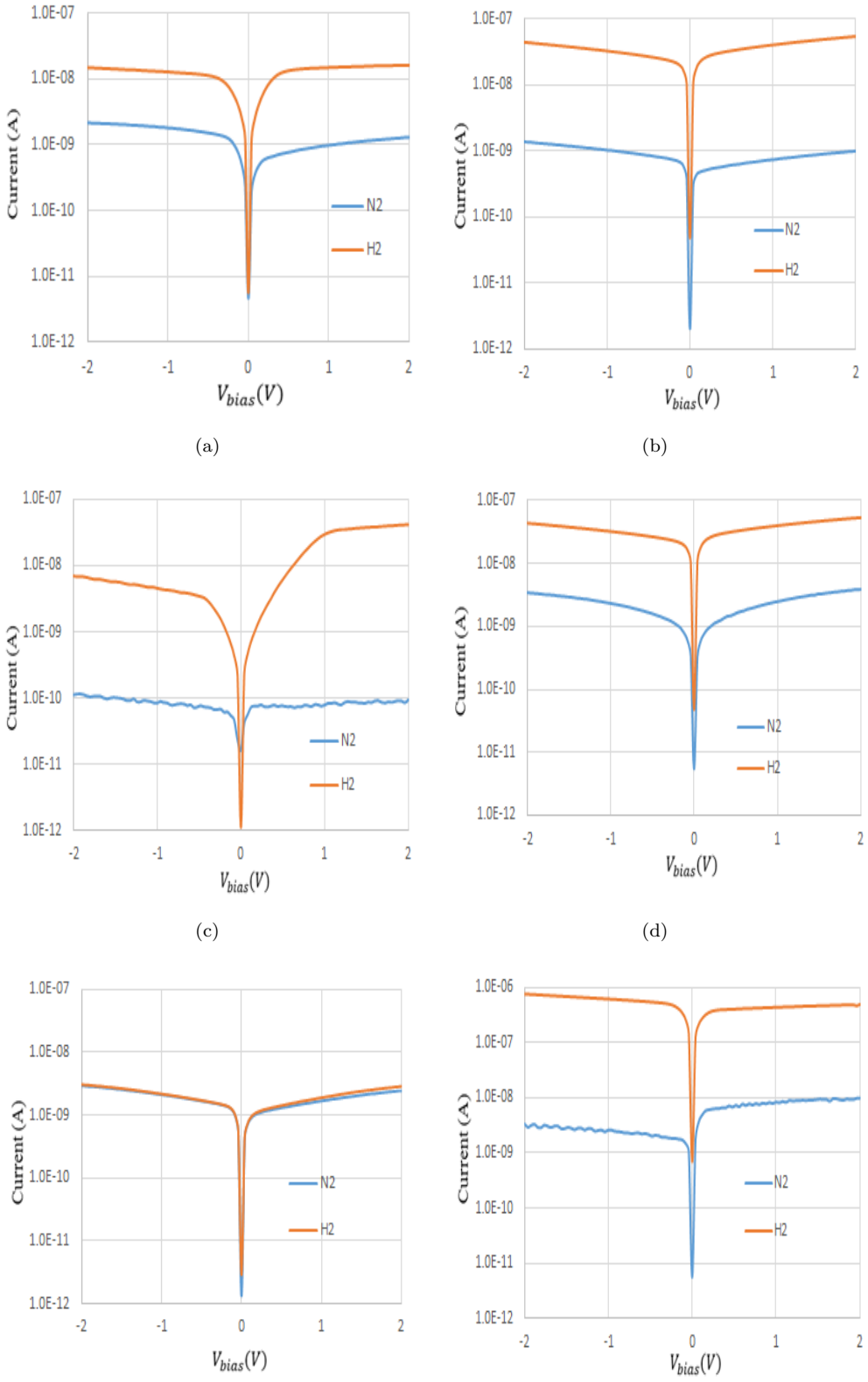

FIGURE 5.8: I-V characteristics of back to back uniform $Pd_{1-x}Ni_x$ Schottky barrier in nitrogen and 5% hydrogen-nitrogen mixture ambient (5mbar H_2 partial pressure). (a)x=0, (b) x=0.3,(c) x=0.4 ,(d) x=0.55,(e) x=1, (f) x=1 with Pd cap.

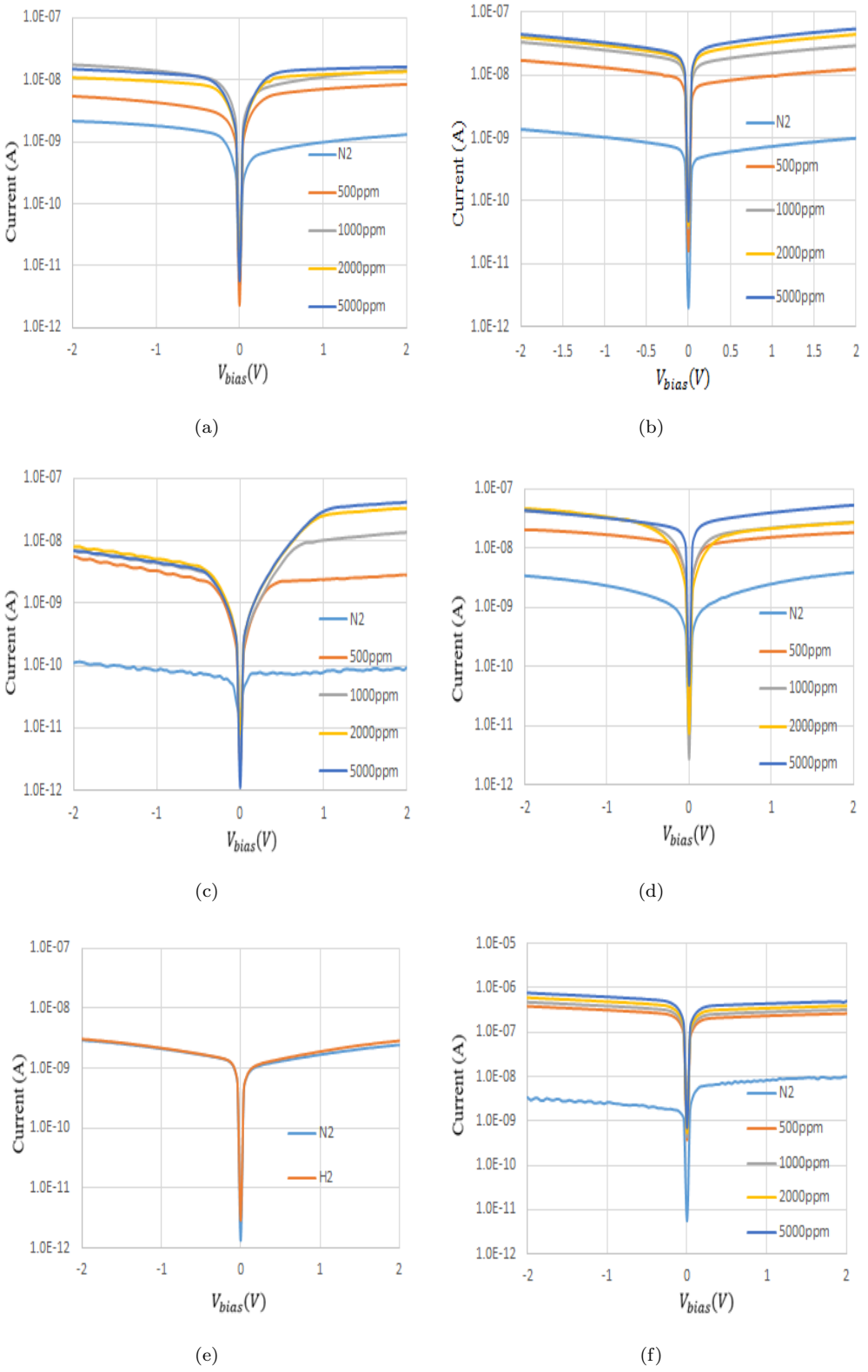

FIGURE 5.9: I-V characteristics of uniform $Pd_{1-x}Ni_x$ Schottky barrier hydrogen sensor in nitrogen and different hydrogen concentrations ranging from 0.5 mbar to 5.0 mbar hydrogen partial pressure. (a) x=0, (b) x=0.3. (c) x=0.4. (d) x=0.55. (e) x=1, (f) x=1 (Pd).

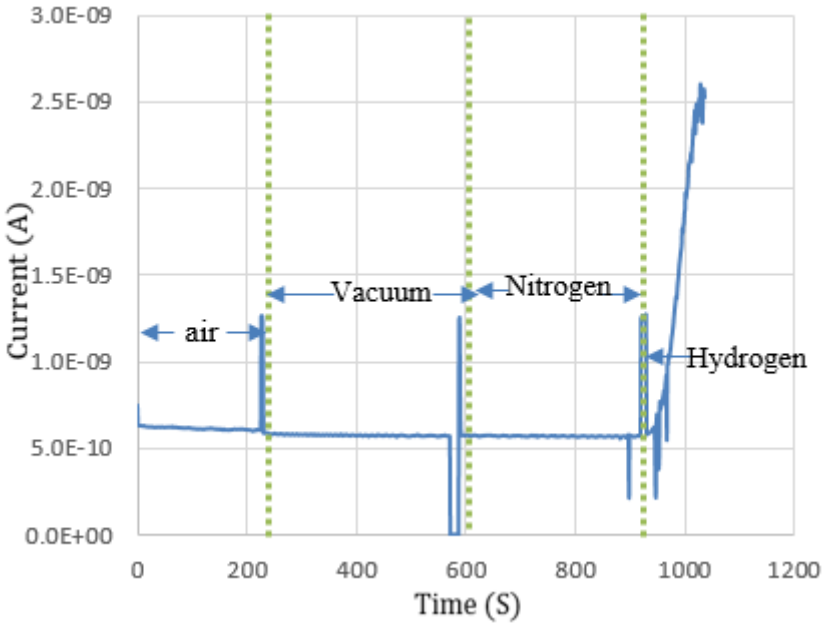

FIGURE 5.10: The current response at 0.1V for a Schottky barrier hydrogen sensor as function of time in air, vacuum,nitrogen, and 5 mbar partial pressure hydrogen. Demarcation lines correspond to the different ambients.

Similar measurements are shown in Fig. 5.12 for three typical nominal identical samples for each Pd-Ni ratio, now normalized to the current in nitrogen. For each measurement, the sensors are exposed to hydrogen after 200s and the measurement is continued for at least another 900s (15m). All sensors (excluding the pure Ni) show current increase upon exposure to hydrogen followed by further slower increase.

As explained in Chapter 2, the accepted definition of time response t_{90} is the time required to reach 90% of the difference between the current in nitrogen and the current in hydrogen in the steady state. For our faster response times, this definition works well as the samples show clear saturation. For the slower response times, the definition leads to some uncertainty but at least qualitatively correct answers. The extracted values are listed in Table 5.2 and are graphically presented in Fig. 5.13.

It can be seen that the response time increases monotonic for increasing Ni concentration in the $Pd_{1-x}Ni_x$ Schottky barrier hydrogen sensors. For x=0.4 and 0.55, the response time is of the order of an hour while even for x=0.3 the response time is a few minutes. Only the pure Pd film with a response time of 150s is close to approximating the conditions for commercial sensor operation. However, as mentioned before, pure Pd films suffer severely from a lack of cyclability due to

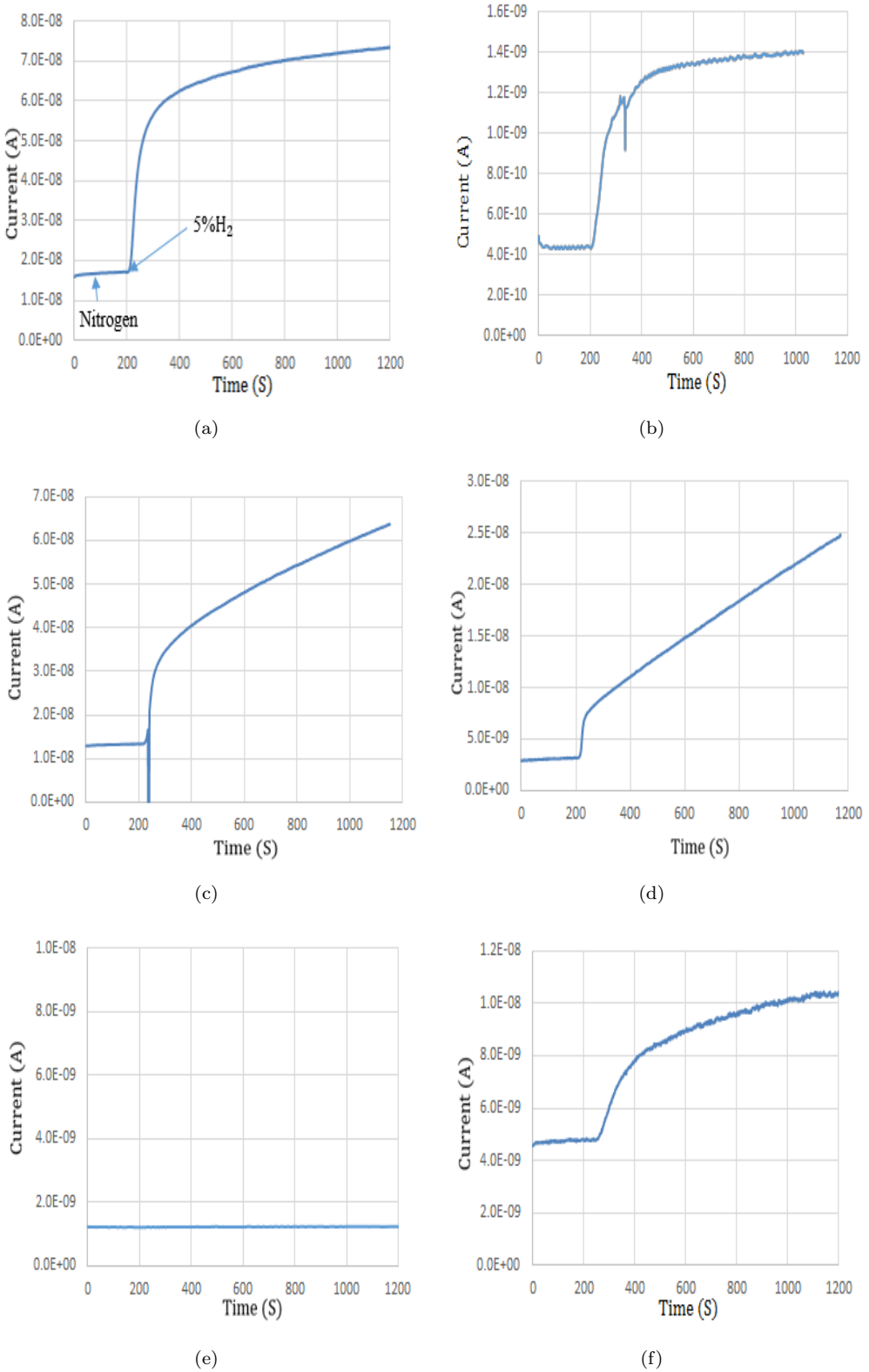

FIGURE 5.11: I-V-t measurement of uniform $Pd_{1-x}Ni_x$ Schottky barrier hydrogen sensor in nitrogen and 5% hydrogen-nitrogen mixture (5 mbar hydrogen partial pressure) at 1V with (a) x=0. (b) x=0.3 (c) x=0.4 (d) x=0.55 (e) x=1, (f) x=1 with Pd cap.

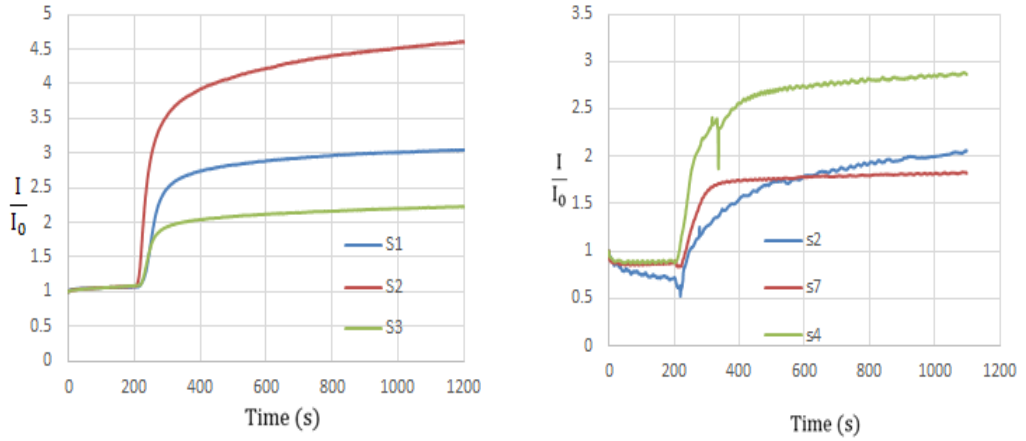

(a)

(b)

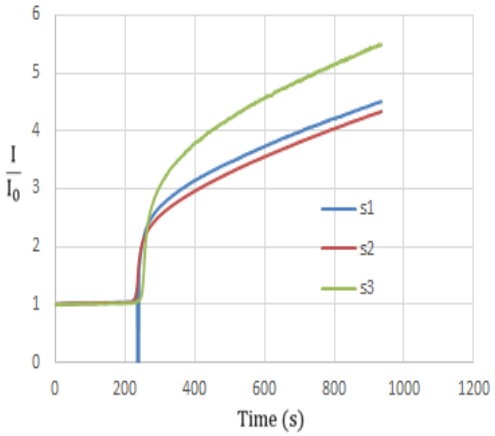

(c)

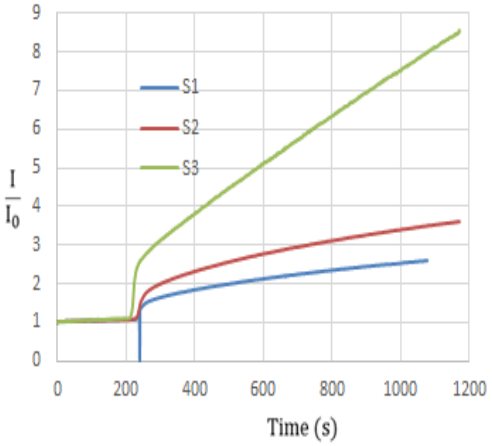

(d)

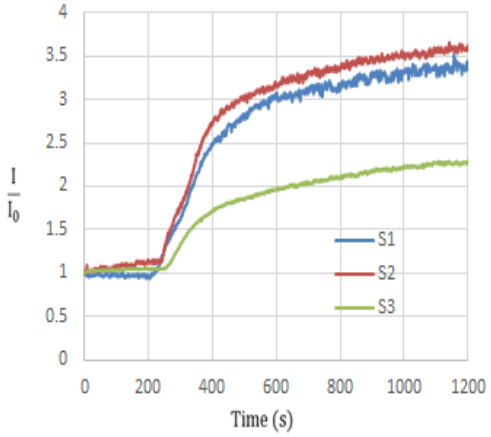

(e)

FIGURE 5.12: Normalized I-V-t measurement of uniform $Pd_{1-x}Ni_x$ Schottky barrier hydrogen sensor in nitrogen and 5% hydrogen-nitrogen mixture (5 mbar hydrogen partial pressure) at 1V with (a) x=0. (b) x=0.3 (c) x=0.4 (d) x=0.55 (e) x=1 with Pd cap. Colours reflect different sensors with identical nominal Pd-Ni ratio.

TABLE 5.2: Time response t_{90} and sensitivity of $Pd_{1-x}Ni_x$ Schottky barrier hydrogen sensor in 5 mbar partial pressure.

x	Sensitivity	t_{90} (s)
0	3.6± 0.9	150± 30
0.3	3.1± 0.5	259± 121
0.4	5.1± 0.5	3000± 1000)
0.55	5.0± 2.0	5000 ± 1000)
1	0	>10000
1 (Pd)	2.8± 0.7	450± 70

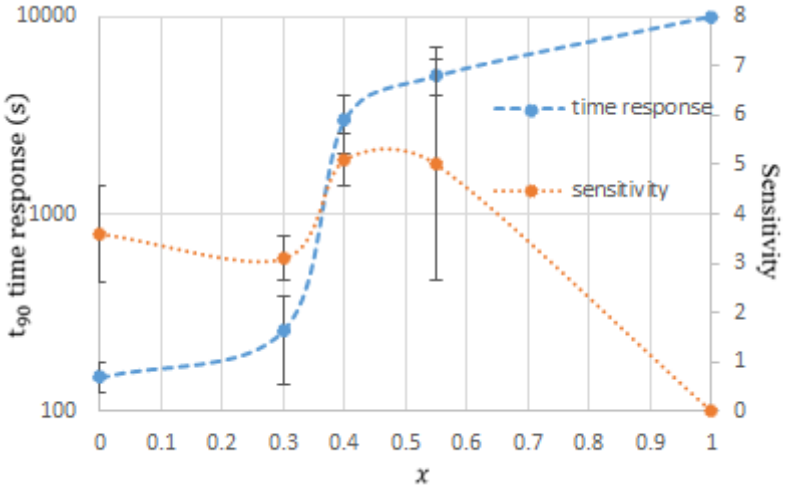

FIGURE 5.13: Time response and sensitivity of uniform $Pd_{1-x}Ni_x$ Schottky barrier hydrogen sensor as a function of x. The time response result of x=1 is a lower bound only, because pure Ni does not response to hydrogen.

the phase transition in the material upon the exposure of hydrogen which causes physical destruction of the film. It can hence be concluded that hydrogen sensors with uniform $Pd_{1-x}Ni_x$ are not suitable for commercial operation.

The response time of the of the Ni film with Pd cover, although not great in itself, does though suggest a solution to the problem. By decoupling the surface layer on which the catalytic decomposition takes place from the bulk of the sample, it should be possible to fabricate an optimized hydrogen sensor with fast catalytic decomposition and structural integrity. In next chapter we will bring this to practice by dividing the 50nm PdNi film into surface, bulk, barrier layers which will be individually optimized. With different PdNi composition in surface and barrier layers, the best response time, structural integrity and sensitivity can be achieved.

5.4.3 Temperature Dependency of Sensitivity and Response Time

Sensors would often need to work in extreme conditions with either low temperature or high temperature. Like most other sensors, our hydrogen sensor performance depends on the working temperature. To measure these properties, we used the cryogenic extension to our probe station to control the temperature. A liquid nitrogen dewar was connected through a cryo-protective pipe. Before the measurement, a hair drier was utilized to blow the chamber to ensure the aridity followed by establishment of a vacuum of 10^{-5} bar to prevent moisture or ice forming on the surface of the sensor. For temperature measurement above 292K the heating system in the probe station can be used to set the required temperature.

The temperature measurement for the uniform Schottky barrier hydrogen sensor (including 40nm Ni with 10nm Pd cover) in both hydrogen and nitrogen ambient are shown in Fig. 5.14. The current through the back to back Schottky diode increases dramatically with increasing temperature. This is expected as the current is equal to the saturation current of an individual Schottky diode which has a large temperature dependence according to Eq. 3.19. The in-depth analysis of the temperature dependence of the Schottky barrier hydrogen sensor will be presented in the next chapter. Nevertheless, it is already evident that the sensors function properly for both low temperature and high temperature with a significant sensitivity at both temperatures.

Using the saturation current equation, it is possible to extract the Schottky barrier height of uniform $Pd_{1-x}Ni_x$ Schottky barrier hydrogen sensor at the difference temperatures in both nitrogen and hydrogen ambient. The results for low temperature 252K, room temperature 292K, and high temperature 352K, are displayed in Fig. 5.15. This figure shows that with the temperature rising from 252K to 352K the Schottky barrier height decreases. When the sensor is exposed to hydrogen, the Schottky barrier height will decrease further. At high temperatures, the decrease in Schottky barrier height is roughly equal to the decrease at room temperature. At low temperatures, the Schottky barrier height lowering is smaller, possibly due to a reduction of catalytic decomposition at the surface or the diffusion which both have strong dependency on temperature.

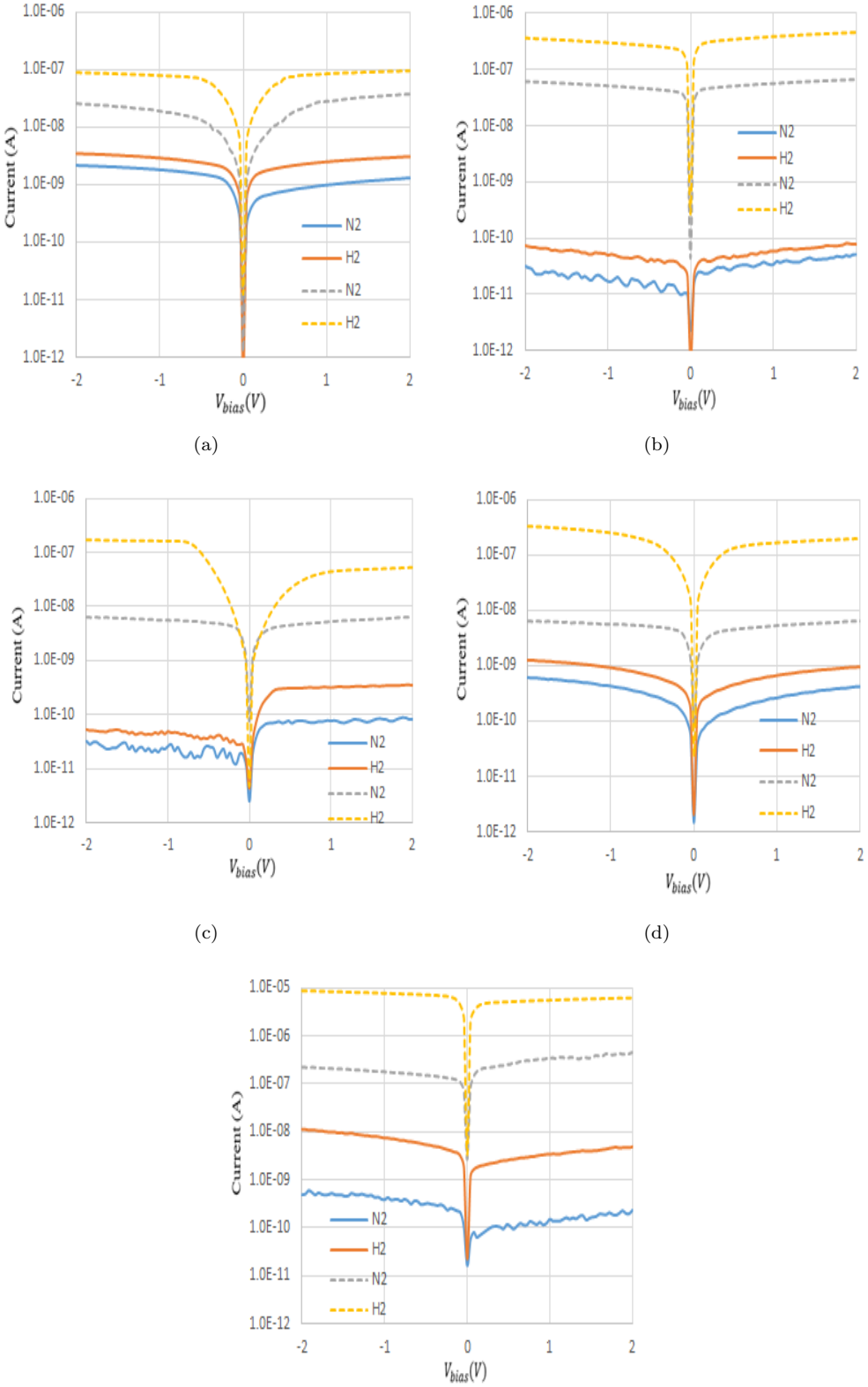

FIGURE 5.14: I-V characteristics of $Pd_{1-x}Ni_x$ Schottky barrier hydrogen sensor with in nitrogen and (5mbar partial pressure) 5% hydrogen-nitrogen mixture at cryogenic (252K solid line)and high temperature (352K dashed line). (a-e) x=0, x=0.3, x=0.4,x=0.55, x=1 (Pd).

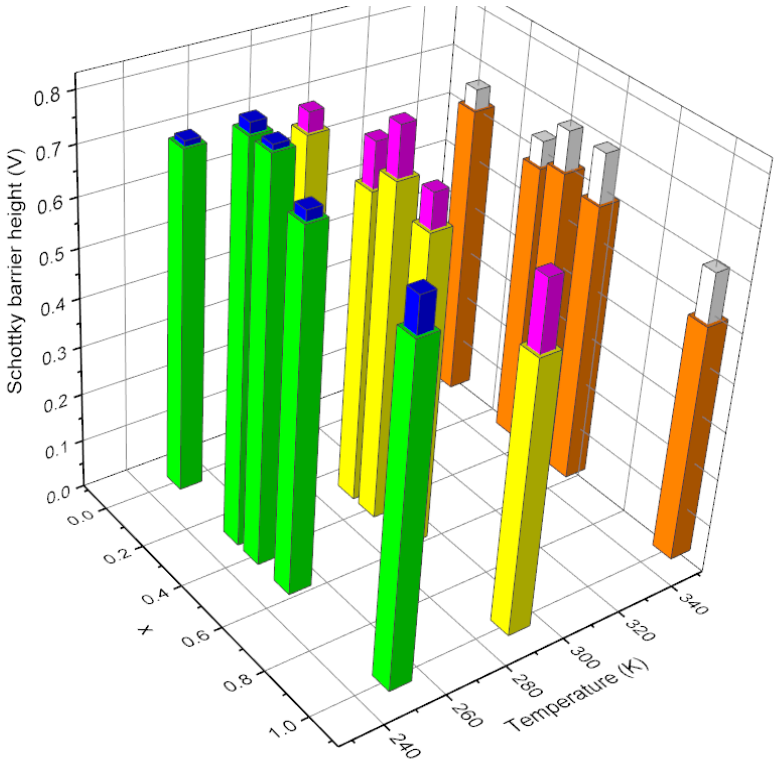

FIGURE 5.15: 3-D plot of uniform $Pd_{1-x}Ni_x$ Schottky barrier hydrogen sensor as function of temperature and Schottky barrier height in nitrogen ambient and hydrogen ambient. The narrow bar represents the Schottky barrier height in nitrogen ambient at different temperatures, wide bar represents the Schottky barrier height in hydrogen ambient.

5.5 Frequency Dependent C-V Characteristics of Uniform $Pd_{1-x}Ni_x$ Schottky Barriers

In this section the frequency dependence of capacitance-voltage characteristic of Schottky barrier hydrogen sensors are investigated. When localized interface states exist at the metal/semiconductor interface, the device behaviour is unlike the ideal case. This behaviour is primarily observed at low and intermediate frequencies. The surface states can easily follow the ac signal at low frequencies and yield an excess capacitance, which depends on the relaxation time of the surface states and the frequency of ac signal. At high frequency the charge at the surface states cannot follow an ac signal. Interface state density usually causes a bias shift and frequency dispersion of the C-V curves. Therefore, it is important to include the effect of the frequency and examine in detail the frequency dispersion of capacitance characteristic.

The frequency dependent C-V characteristic of 50nm $Pd_{1.0}Ni_{0.0}$ Schottky barrier

hydrogen sensor in air at room temperature is shown in Fig. 5.16 with the data for all other variations shown in the appendix A. Each C-V curve at a specific frequency has three regimes: accumulation, depletion, inversion which verify a typical Schottky barrier diode behaviour. The change in frequencies lead to the capacitance variation in the depletion and accumulation regions. The C-V curve shows an anomalous peak at low frequencies due to the existence of interface state density and the thickness of interfacial oxide layer and series resistance. Under low frequency operation the position of these peaks in the C-V plot shift toward the forward bias region and the value of the capacitance decreases with increasing frequency. At high frequency, trapped charges at the interface can not follow the external ac signal which means they do not give any contribution to the capacitance value.

It is also possible that the anomalous peak can be attributed to the series resistance. Werner *et al.* made a systematic measurement of Schottky barrier devices with ohmic and nonohmic back contacts. This investigation shows that devices with poor back contacts exhibit a capacitance maximum in the C-V curve. Oppositely, no peak is present for the device with ohmic back contact [99]. The absence of ohmic behaviour at the back contact resulted in a large series resistance leading to the correlation of the anomalous C-V curve with series resistance effect [100]. Based on this work, it has been illustrated that in the presence of a series resistance the C-V characteristics could exhibit a anomalous peak at the accumulation region. The peak value of capacitance can be affected by some parameters such as, doping, interface state density and the thickness of interfacial oxide layer, and the frequency of ac signal. An idealized C-V characteristic is independent of frequency and the capacitance will be increasing with increasing forward bias voltage.

It is widely accepted that a Schottky barrier diode possesses a very thin interfacial deposited or native oxide layer between metal and semiconductor, even though the semiconductor was over etched before the metal deposition. Therefore this inevitable factor may have an influence on the electrical characteristic of the diode. In order to obtain the series resistance in Schottky barrier hydrogen sensor, the method of Nicollian and Goetzberger [101] has been employed. The real series resistance of MIS structure can be subtracted from the measured capacitance and conductance in strong accumulation region at high frequency [101]. Then the admittance using the parallel RC circuit is equivalent to the total circuit admittance Y in strong accumulation as Eq. 5.1.

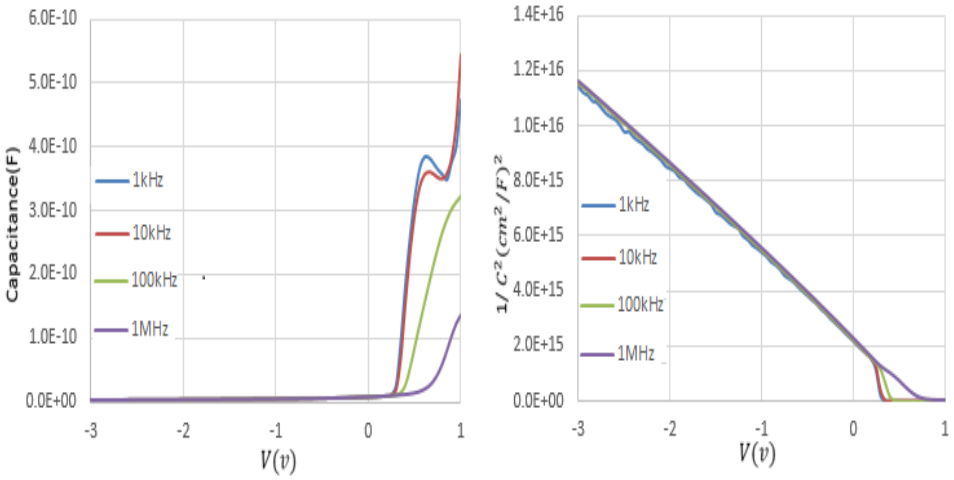

FIGURE 5.16: Frequency dependent C-V measurements of x=0 $Pd_{1-x}Ni_x$-Si Schottky barrier hydrogen sensor and $1/C^2$-V characteristic of the same device.

$$Y = 1/Z = G + j\omega C \tag{5.1}$$

Comparing the real and imaginary parts, R_s can be written as Eq. 5.2.

$$R_s = \frac{G}{G^2 + (\omega C)^2} \tag{5.2}$$

Where C and G represent measured capacitance and conductance in strong accumulation region. The capacitance of insulator layer C_{ox} is obtained by substituting R_s into the relation (Eq. 5.3):

$$C = \frac{C_{ox}}{(1 + \omega^2 R_s^2 C_{ox}^2)} \tag{5.3}$$

From this equation, the C_{ox} can expressed as Eq. 5.4.

$$C_{ox} = C[1 + (\frac{G}{\omega C})^2] = \frac{\epsilon_i \epsilon_0 A}{d_{ox}} \tag{5.4}$$

The basic frequency dependent capacitance-voltage (C-V) and conductance-voltage (G/ω-V) characteristic of 50nm $Pd_{0.7}Ni_{0.3}$ Schottky barrier hydrogen sensor in air at room temperature are illustrated in Fig. 5.17. The sensor was measured at a frequency range of 1kHz-1MHz. These two curves illustrates that both the C and G/ω varies from the inversion region to the accumulation region. The series resistance is achieved according to Eq. 5.2 and shown in Fig. 5.18 for various

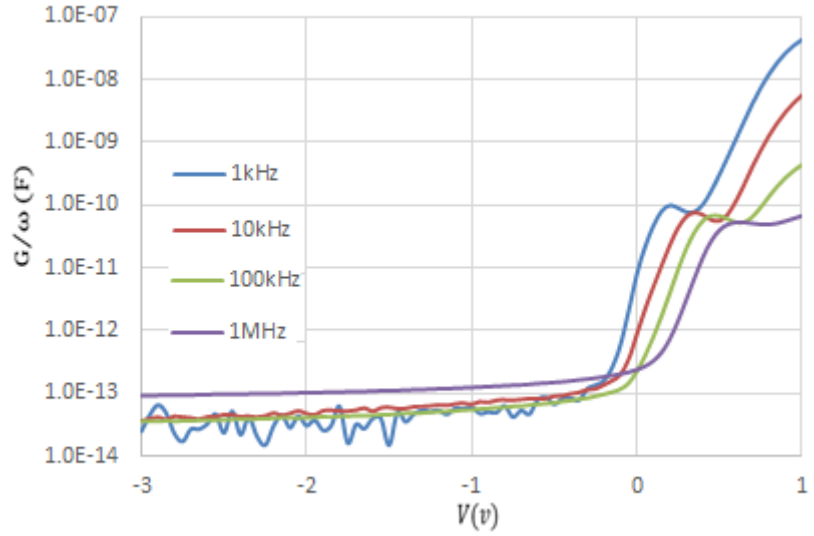

FIGURE 5.17: The frequency dependent plot of G/ω-V of 50nm $Pd_{1-x}Ni_x$ Schottky barrier hydrogen sensor (x=0.3) at room temperature and air.

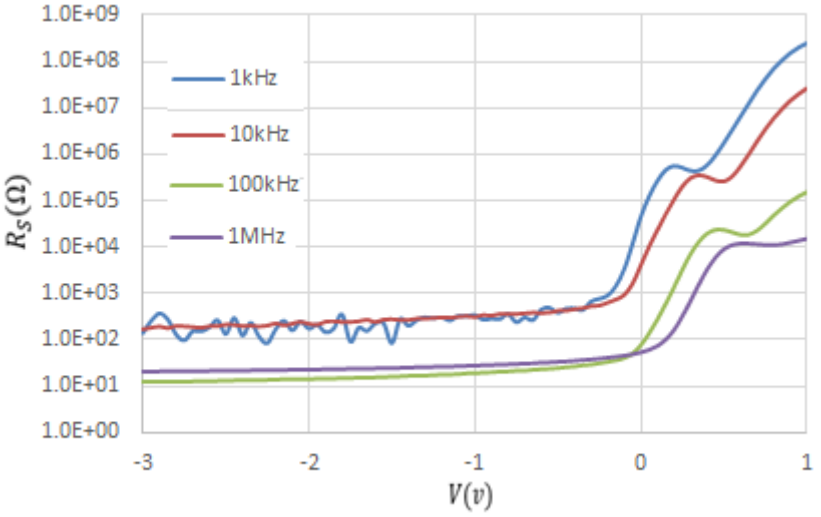

FIGURE 5.18: The variation of the series resistance of 50nm $Pd_{1-x}Ni_x$ Schottky barrier hydrogen sensor (x=0.3) as a function of bias voltage for various frequencies at air atmosphere.

frequencies. In this figure the series resistance gives two peaks, especially at low frequency which are located in the inversion and accumulation regions.

As shown in Fig 5.18 the values of R_s are independent of bias voltage at high frequency. This behaviour explains that the trap charges have enough energy to escape from the traps located at metal/semiconductor interface in the Si band gap. The surface states (N_{ss}) between Si/SiO_2 Si band gap are estimated from the combination of various frequencies C-V and G/ω-V characteristic according

TABLE 5.3: The parameters of 50nm $Pd_{1-x}Ni_x$ Schottky barrier hydrogen sensor (x=0.3) achieved from C-V and G/ω-V at various frequencies at air atmosphere.

f(kHz)	C(pF)	G/ω (10^{-9}F)	$N_{ss}(10^{12}eV^{-1}/cm^2)$	$R_s(\Omega)$
1	2.25	12.1	378	45000
10	1.77	5.65	177	4060
100	1.70	0.44	13.7	77
1000	1.49	0.06	2.11	5

TABLE 5.4: The Schottky barrier of uniform $Pd_{1-x}Ni_x$ hydrogen sensor in nitrogen and hydrogen-nitrogen ambient (5mbar partial pressure) as well as the difference of Schottky barrier height in corresponding frequency.

Hz(khz)	ϕ_B	x=0	x=0.3	x=0.4	x=0.55	x=1 (Pd)
5	ϕ_B (N_2)	0.68	0.95	1.18	1.11	0.75
50	ϕ_B (N_2)	0.62	0.95	1.32	1.10	0.73
500	ϕ_B (N_2)	0.63	0.96	1.40	1.04	0.77
5000	ϕ_B (N_2)	0.64	0.90	1.39	1.15	0.77
5	ϕ_B (H_2)	0.43	0.56	0.87	0.61	0.44
50	ϕ_B (H_2)	0.37	0.67	1.15	0.62	0.42
500	ϕ_B (H_2)	0.38	0.65	1.23	0.60	0.44
5000	ϕ_B (H_2)	0.46	0.63	1.24	0.61	0.43
5	ϕ_B (N_2-H_2)	0.25	0.39	0.31	0.50	0.31
50	ϕ_B (N_2-H_2)	0.25	0.29	0.18	0.48	0.31
500	ϕ_B (N_2-H_2)	0.25	0.31	0.17	0.44	0.32
5000	ϕ_B (N_2-H_2)	0.18	0.27	0.15	0.54	0.31

to Hill-Coleman [102] (Eq. 5.5), where A is the area of the diode, ω is the angular frequency, $((G_m/\omega)_{max})$ is measured maximum conductance in the G/ω -V plot with its corresponding measured capacitance C_m and C_{ox} is the capacitance of insulator layer. The extracted parameters for 50nm $Pd_{0.7}Ni_{0.3}$ Schottky barrier hydrogen sensor with thin interface layer achieved from C-V and G/ ω-V at various frequencies at room temperature are shown in Table 5.3.

$$N_{ss} = \frac{2}{qA} \frac{(G_m/\omega)_{max}}{((G_m/\omega)_{max}C_{ox})^2 + (1 - C_m/C_{ox})^2} \tag{5.5}$$

As can be seen in Table 5.3, when the frequency increases, the peak value of the capacitance as well as the series resistance R_s decrease. Large R_s can cause a serious error in the electrical parameters. In this table the value of the R_s is extremely small at high frequencies (500kHz, 1Mhz) justifying our approach to use these frequencies to extract C-V parameters. Furthermore, the high frequencies C and G values were corrected for the effect of R_s in the whole measured bias range to obtain the real capacitance and conductance by the Nicollian and Goetzberger's method [101]. As has been shown in Fig. 5.16, the higher values of capacitance

at low frequencies are due to excess capacitance (C_o) resulting from the surface states (N_{ss}) in equilibrium with Si. This means that the surface states can follow the ac signal and consequently contribute to the MIS capacitance.

All Schottky barrier hydrogen sensors have also been measured both in nitrogen and 5% hydrogen and nitrogen mixture ambient with variable frequencies. Table 5.4 shows all devices at various frequencies. The Schottky barrier heights have no trend with ascending or descending frequency. The Schottky barrier height in hydrogen ambient was reduced by varying amounts in the sensors. All the $\Delta\phi_B$ are basically the same and do not depend on frequency within the margin of error. For the C-V measurement 1MHz is the most reliable frequency to measure.

5.6 Conclusion

A series of uniform $Pd_{1-x}Ni_x$-Si Schottky barrier hydrogen sensors were fabricated and characterized using Capacitance-Voltage and Current-Voltage measurement. It is shown that the pure Ni films do not show evidence of response to hydrogen and that adding a thin layer of Pd on top allows those sensors to function. This clearly indicates that Ni is not a catalyst for hydrogen dissociation at room temperature, some literature have prove this phenomenon [103, 104, 105] which is in the disagreement with other literature who claim that Ni based sensor can catalyse hydrogen at high temperature [106, 107]. It is shown that for all sensors the increase in current with hydrogen can be explained by a decrease of the Schottky barrier height due to the formation of interfacial dipoles. An increase in hydrogen concentration in the gas leads to a concurrent decrease in Schottky barrier height and an monotonous increase in current. It is shown that none of the sensors response to nitrogen or air indicating excellent selectivity with respect to these gases. It is shown that sensitivity is optimum for $Pd_{1-x}Ni_x$ with x around 0.4 whereas time response is optimum for x around 0.1. This conundrum is solved by the composition-modulated technique explained in the next chapter. Temperature dependent measurements show that these sensors function properly at both slightly elevated and below zero temperature.

Chapter 6

Effect of Composition-Modulated PdNi Alloy Composition on Sensor Sensitivity and Response Time

6.1 Introduction

In Chapter 3, it was explained how we could change the Pd-Ni concentration in a single film through variation of the potential during electro-deposition. In the discussion of the operation of the hydrogen sensor in the last section, it was also made clear that the major influencing parameters of the film are the surface layer on which the decomposition of the hydrogen gas takes place, and the barrier layer which determines the sensitivity of the device. In this chapter, we will use the method introduced in Ch.3 to fabricate composition-modulated PdNi alloys with varying Pd-Ni ratio throughout the PdNi film. We will continue to fabricate 50nm PdNi alloy films which has been divided into three layers; a surface layer; a bulk layer and a barrier layer. The bulk layer is held constant, being $Pd_{1-x}Ni_x$ with x=0.3 because it is shown in table. 5.2that x=0.3 gives the fastest response time and provides good hydrogen diffusion through the bulk layer. The surface and barrier layers are varied as shown schematically in Fig. 6.2 and Fig. 6.3, We will first present the analysis the hydrogen sensors based upon Fig. 6.2 in the following section, which will justify the choice of constant surface layer in the experiment is shown in Fig. 6.3. Subsequently, the sensor with best specifications is analysed in

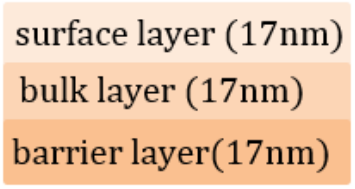

FIGURE 6.1: Schematic of three layer composition modulated Schottky barrier which include surface, bulk and barrier layer.

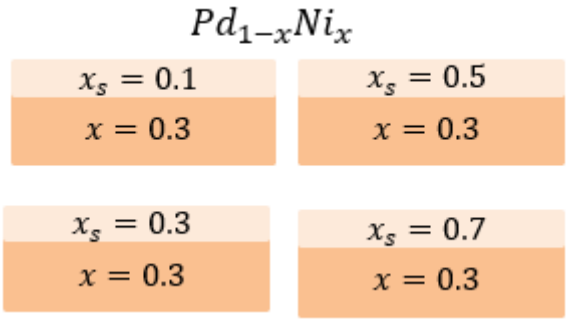

FIGURE 6.2: Schematic of $Pd_{1-x}Ni_x$ alloys with x=0.3 for the bulk layer (34nm) and the barrier layer and various concentration for the surface layer (17nm). We will refer to these sample as surface layer x_s=0.1, 0.3, 0.5, 0.7.

more detail.

6.2 Characteristics of Hydrogen Sensor with Various Surface Layer Compositions

6.2.1 Sensitivity

As discussed earlier, this series of composition-modulated composition hydrogen sensors with various Ni concentration in the surface layer with constant composition of bulk and barrier layer was designed to explore whether the dissociation speed of hydrogen atoms at the surface of PdNi film can influence the time response. Fig. 6.4 shows the back to back current-voltage characteristic of the composition-modulated alloy with various Ni concentrations in the surface layer of Schottky barrier hydrogen sensor (x_s=0.1, 0.3, 0.5, and 0.7) in both nitrogen ambient and exposure to the 0.1 bar 5% hydrogen-nitrogen mixture gas. The current-voltage characteristics in hydrogen ambient were measured 800 seconds after the 5% hydrogen-nitrogen mixture was introduced into the chamber such that the response has saturated.

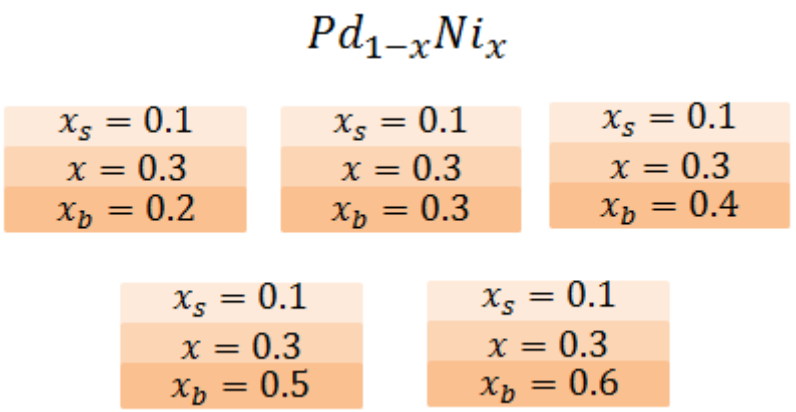

FIGURE 6.3: Schematic of $Pd_{1-x}Ni_x$ alloys with x=0.1 for the surface layer (17 nm), x=0.3 for the bulk layer (17 nm) and various concentration for the barrier layer (17 nm). We will refer to these sample as barrier layer x_b=0.2, 0.3, 0.4, 0.5, 0.6.

All of the samples with varying surface concentration exhibit the typical back to back Schottky barrier current-voltage characteristic in nitrogen ambient. All of these hydrogen sensors illustrate a good sensitivity to hydrogen ambient with a current increase of nearly one order of magnitude with 0.1 bar 5% hydrogen. A number of devices has been tested for each compositional range to prove the reproducibility of this group of hydrogen sensors.

6.2.2 Response Time

The response time was measured in a very similar way as previously shown in Ch.5. The hydrogen sensors are measured at fixed applied voltage in nitrogen and after a certain time period (200s), the hydrogen gas is added to the chamber. The current response is measured as function of time in a I-V-t measurement. A number of devices was measured for each composition and the results are shown in Fig. 6.5. The measurement is stopped after 1000s after which the curves presented in Fig. 6.4 were taken.

We have previously defined the response time t_{90} as the time it takes to get 90% of the full response to the hydrogen. If the sensor does not saturate in a reasonable amount of time (as in this measurement:1000s), the response time cannot be accurately determined. Anyway, for these samples, the response time is so slow to be not commercially relevant, and an estimate is provided for response time and sensitivity. The results are shown together with the sensitivity data in Fig. 6.6. The I-V characteristic of all devices is very similar and, as expected, no

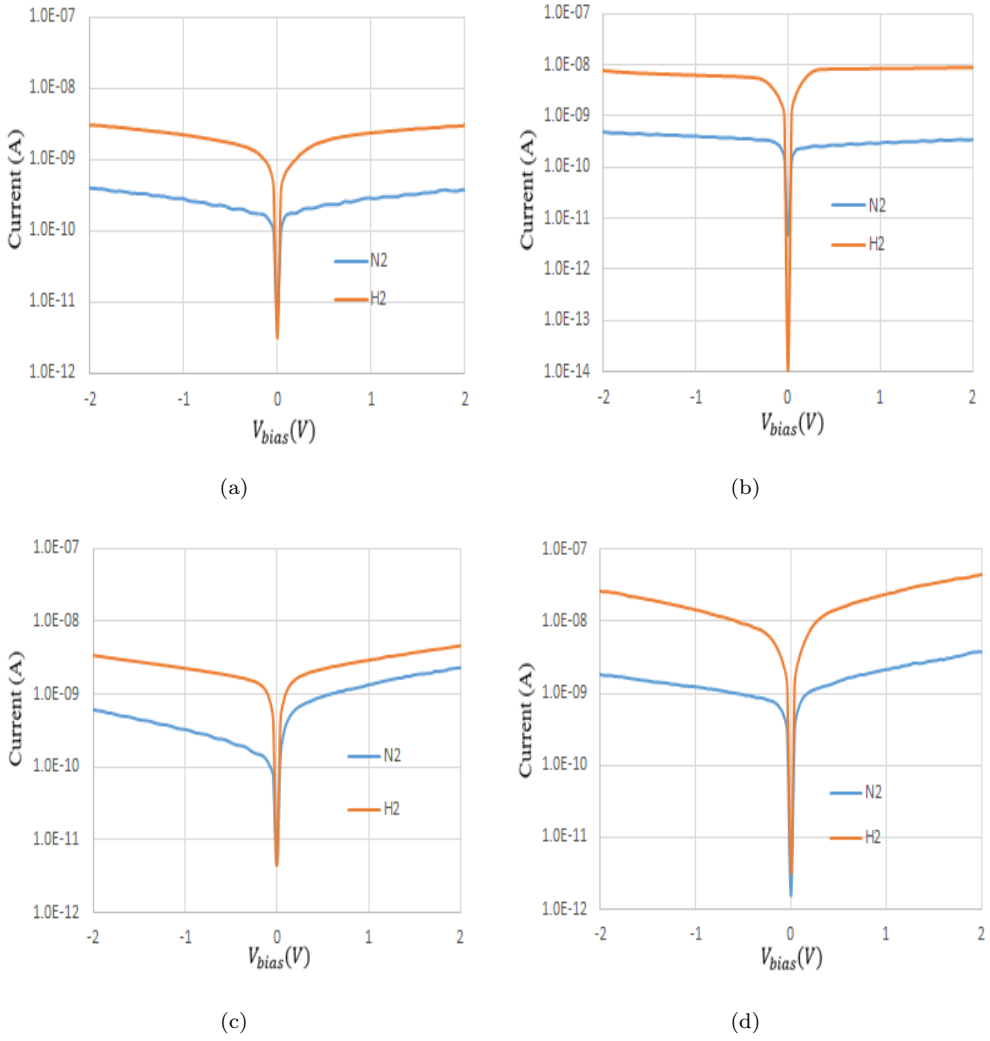

FIGURE 6.4: I-V characteristic of composition-modulated $Pd_{1-x}Ni_x$ Schottky barrier hydrogen sensor with constant bulk layer x=0.3 and various Ni concentration on surface layer at both nitrogen and 5% hydrogen-nitrogen mixture (5mbar partial pressure) ambient. (a)x_s=0.1,(b)x_s=0.3,(c)x_s=0.5,(d)x_s=0.7.

dependency of sensitivity on surface concentration was observed. A very strong dependency of the response time with Pd-Ni ratio in the surface layer is observed, though. An almost exponential behaviour is seen in which the response time improves dramatically with reduction of Ni concentration in the surface layer. The speed of hydrogen dissociation in the Pd catalytic reaction at the surface is hence strongly affected by the addition of Ni. The amount of Ni at the surface should be minimized while keeping in mind the necessity to add Ni to prevent destructive cycling to the β-Pd phase.

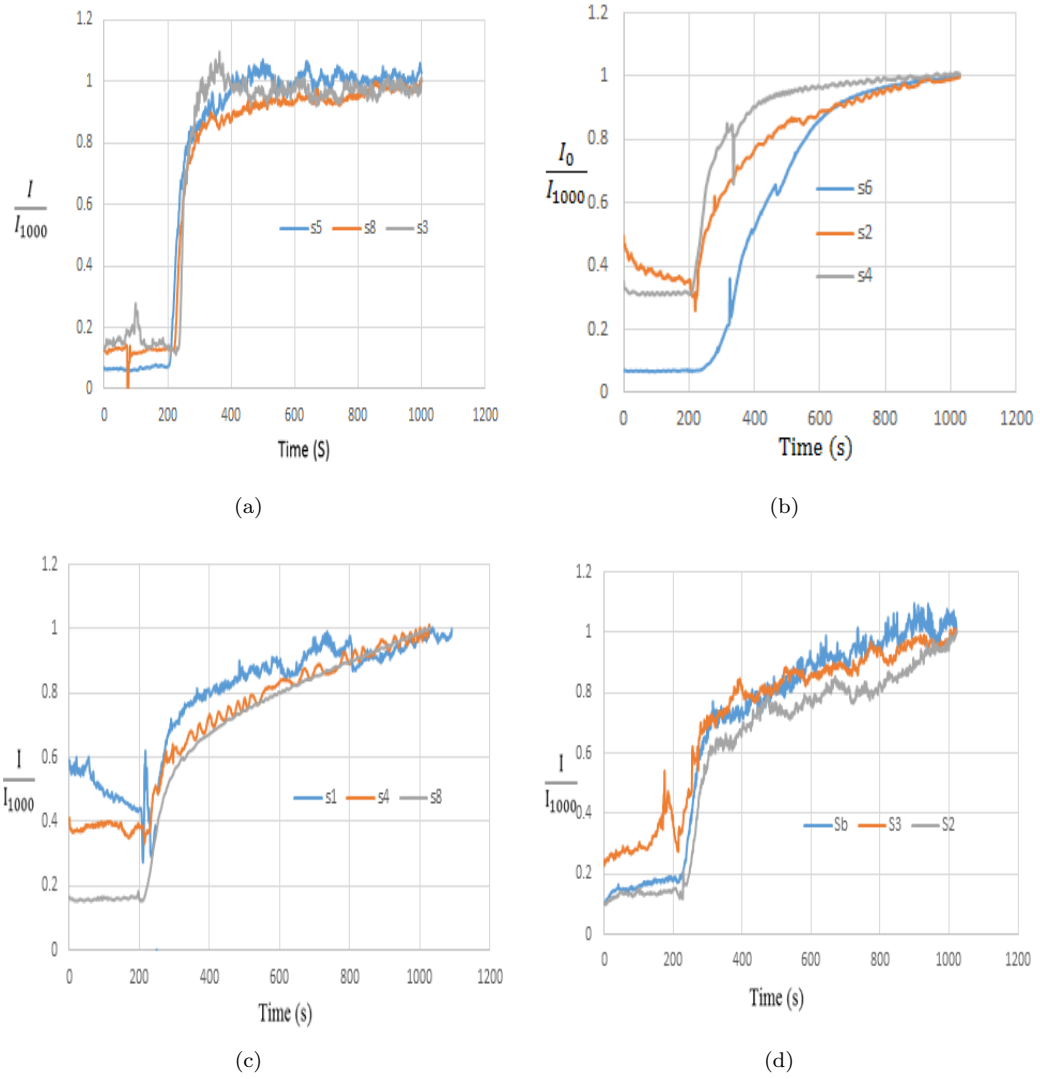

FIGURE 6.5: I-V-t characteristic of of composition-modulated $Pd_{1-x}Ni_x$ Schottky barrier hydrogen sensor in nitrogen and 5% hydrogen (5mbar partial pressure) after 200s with constant bulk layer(x=0.3) and various surface layer concentration where x_s=0.1, 0.3, 0.5, and 0.7. The labels in these figures represent the labeled devices during the measurement.

6.3 Characteristics of Hydrogen Sensor with Various Barrier Layer Compositions

6.3.1 Sensitivity

Based on the discussion on the hydrogen sensing mechanism, the performance of the Schottky barrier hydrogen sensor does not only depend on the speed of hydrogen molecule dissociation, but also on the behaviour of the hydrogen atoms at the Schottky barrier interface. Therefore, another group of composition-modulated

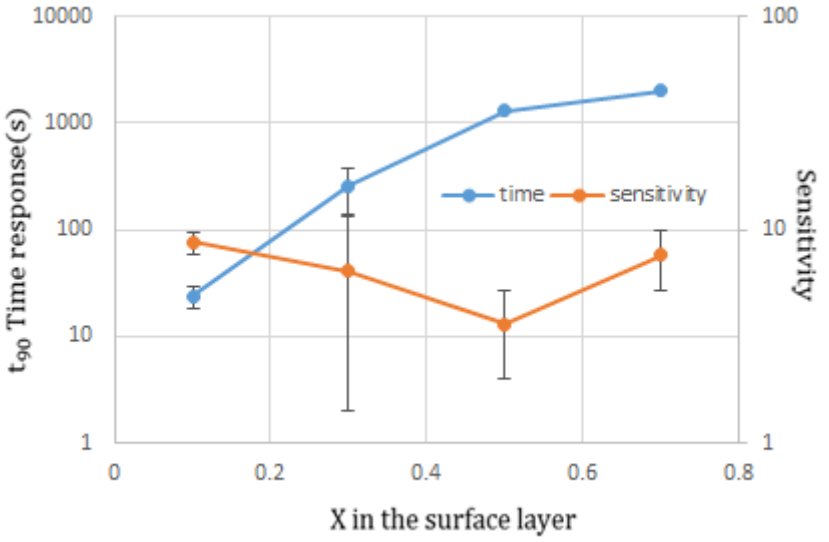

FIGURE 6.6: Time response of composition-modulated alloy composition $Pd_{1-x}Ni_x$ (x=0.3) Schottky barrier hydrogen sensor as function of Ni concentration x_s=0.1, 0.3, 0.5, and 0.7 in surface layer.

$Pd_{1-x}Ni_x$ Schottky barrier hydrogen sensor with various Ni concentration in the barrier layer with a constant PdNi composition in surface and bulk layer was developed to explore the best sensitivity and time response with a suitable Ni concentration in the barrier layer. Based on the results from the previous chapter and section, the surface concentration was fixed at x_s=0.1 and the bulk concentration at x=0.3, as shown in Fig. 6.3.

Fig. 6.7 shows the back to back current-voltage characteristic of composition-modulated alloy composition Schottky barrier hydrogen sensor with various Ni concentration in barrier layer in the nitrogen ambient and under exposure to 0.1 bar 5% hydrogen-nitrogen mixture gas.

Fig. 6.9 shows that despite the obvious variation form sample to sample, the sensitivity is clearly largest for 40 % Ni. The explanation for this is not straight forward, but likely related to the number of dipole sites at the PdNi-Si interface where hydrogen can be trapped. The consequence of the higher Ni concentration in the barrier layer of the film is to expand the lattice which allows more hydrogen atoms to diffuse to the silicon traps at the interface. This effect causes the time response increase as compared to the other structures. This will be explained in more detail in section 6.4.

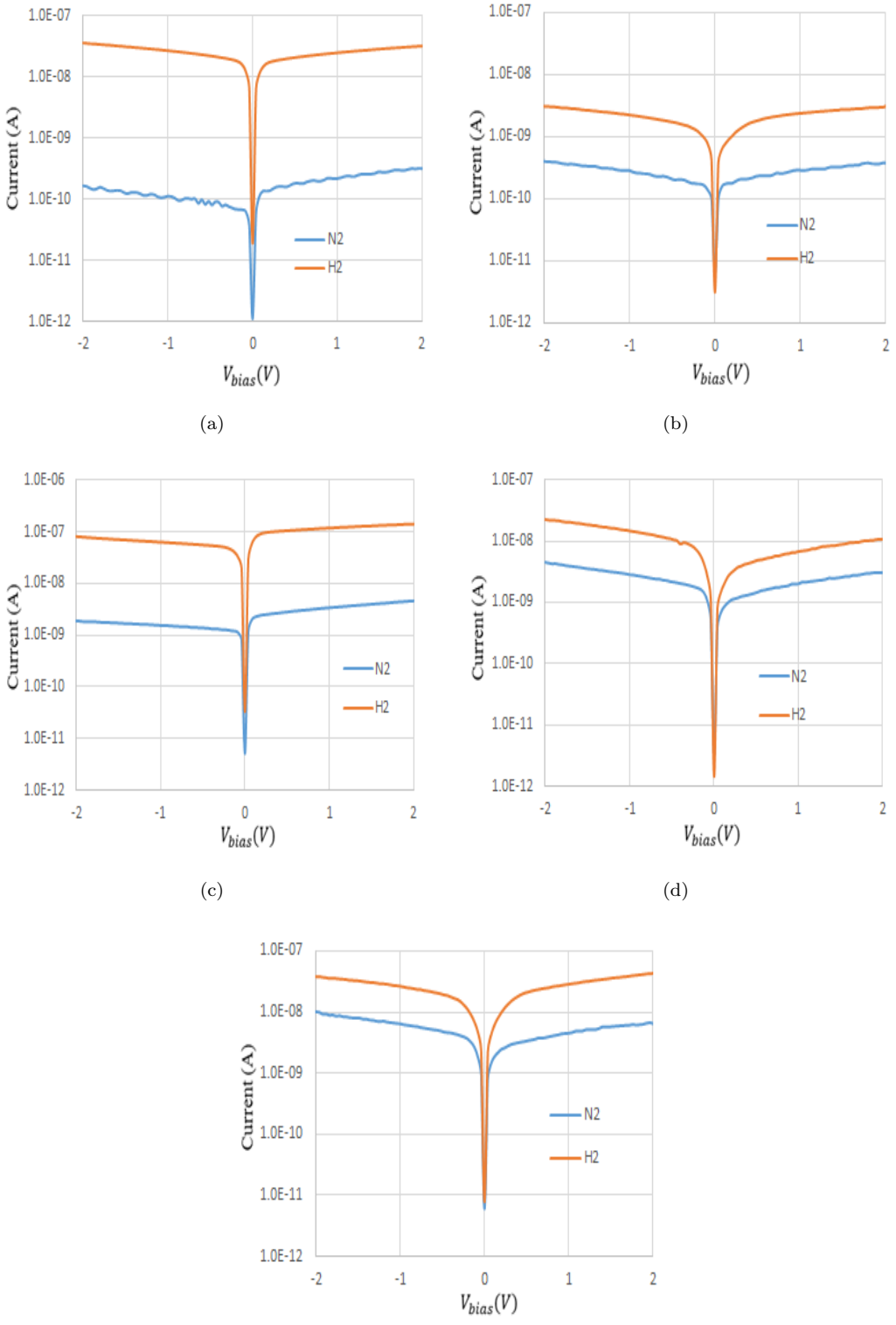

FIGURE 6.7: I-V characteristic of $Pd_{1-x}Ni_x$ Schottky barrier hydrogen sensor with x_s=0.1, x=0.3, and various Ni concentration in the barrier layer in both nitrogen and 5% hydrogen (5mbar partial pressure) ambient. (a) x_b=0.2, (b) x_b=0.3, (c) x_b=0.4, (d)x_b=0.5, (e) x_b=0.6.

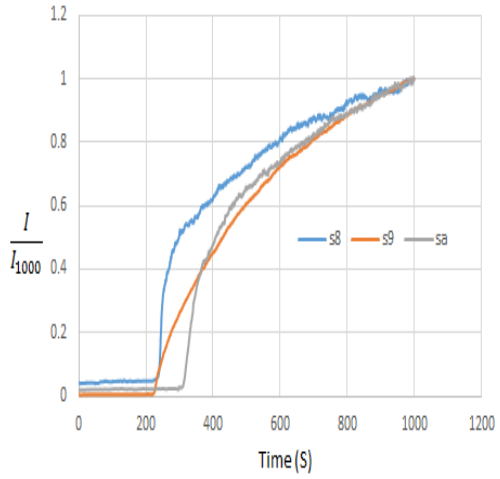

(a)

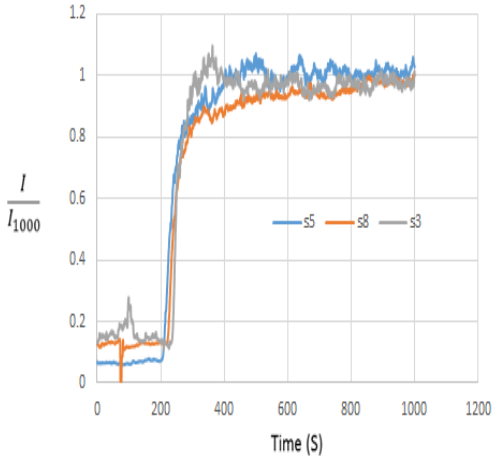

(b)

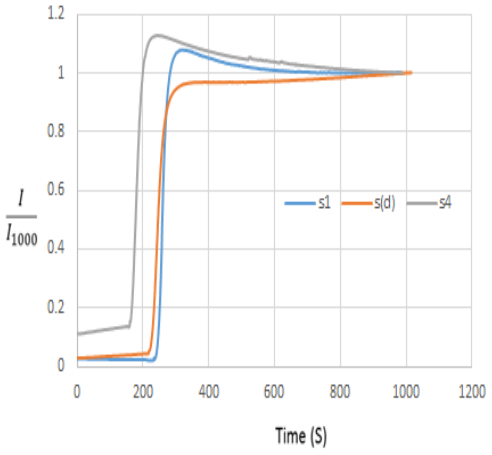

(c)

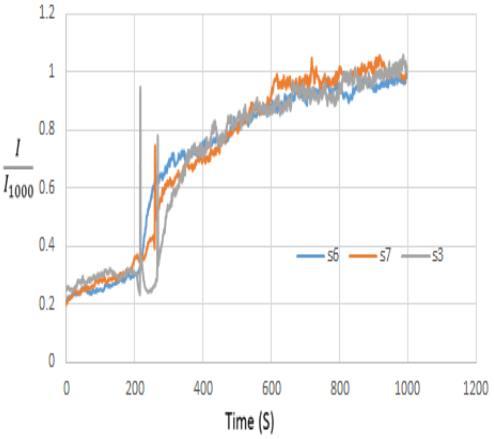

(d)

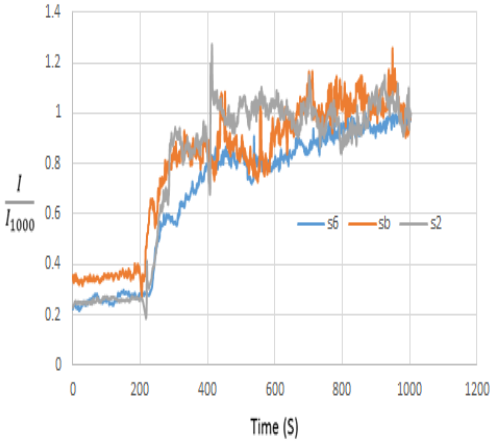

(e)

FIGURE 6.8: I-V-t characteristic of $Pd_{1-x}Ni_x$ (x_s=0.1, x=0.3) Schottky barrier hydrogen sensor with x_b=0.2 (a), 0.3 (b), 0.4 (c) , 0.5 (d), and 0.6 (e) in nitrogen and 5% hydrogen-nitrogen mixture (5mbar partial pressure) ambient after 200s. The numbers in these figures represent the labeled devices during the measurement.

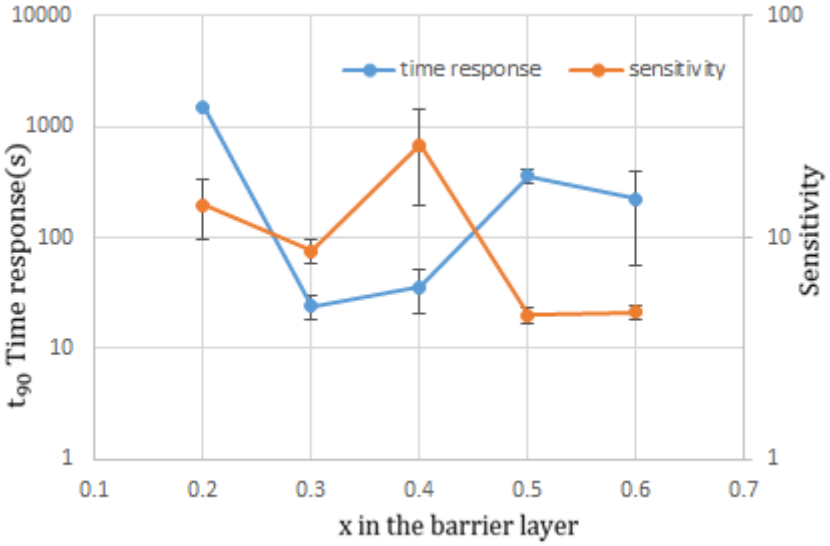

FIGURE 6.9: Time response and sensitivity of composition-modulated alloy composition $Pd_{1-x}Ni_x$ Schottky barrier hydrogen sensor with x_s=0.1, x=0.3 as function of Ni concentration x_b=0.2,0.3,0.4,0.5,0.6 in barrier layer. The numbers in figures denote to labeled sample.

6.3.2 Response Time

Fig. 6.8 shows the I-V-t characteristic of composition modulated Schottky barrier hydrogen sensor with various Ni concentration in barrier layer to a 0.1 bar 5% hydrogen-nitrogen mixture at room temperature corresponding to the I-V characteristic. In order to explicitly observe the I-V-t curve among the same structures, the data are normalized as $\frac{I}{I_{1000}}$. The time response and sensitivity can be extracted from these figures.

In theory, it is expected that the more Pd is in the Pd-Ni alloy at the barrier layer, the faster the hydrogen atoms will be trapped at the metal-semiconductor interface resulting in a fast response. However Fig. 6.9 clearly shows that the time response is slowest (tens of minutes) for the highest Pd concentration of 80% in the barrier layer. The Schottky barrier hydrogen sensor with 30% and 40% Ni concentration in the barrier layer possess the fastest time response (nearly 10 seconds) in this group in agreement with the measurements in the previous section. With the Pd concentration further decreasing in the PdNi barrier layer, the time response increases again to more than 10 minutes although these sensors still operate faster than those with 80% of Pd.

6.4 In-depth Analysis of Optimum Schottky Barrier Hydrogen Sensor

Based on the results of Chapter 5 and the preceding sections, it can be concluded that the $Pd_{1-x}Ni_x$ Schottky barrier hydrogen sensor requires as low as possible Ni concentration at the surface to accelerate the hydrogen dissociation, and a larger amount of Ni at the barrier layer to improve sensitivity. Based on those observations, we have concluded that the $Pd_{1-x}Ni_x$ Schottky barrier hydrogen with x_s=0.1, x=0.3, and x_b=0.4 shows the best characteristics. The performance of these sensors has hence be studied in more detail. Full details of the characteristics of the $Pd_{1-x}Ni_x$ Schottky barrier hydrogen sensor with x_s=0.1, x=0.3, and x_b=0.4 can be found in Appendix B.

6.4.1 Schottky barrier height

Table 6.1 shows the Schottky barrier height as extracted from C-V measurements for the $Pd_{1-x}Ni_x$ Schottky barrier hydrogen sensor with x_s=0.1, x=0.3, and x_b=0.4. The Schottky barrier height decreases by approximately 0.40 V (from 0.9V to 0.5V) for the high frequency measurements when the sensor is exposed to hydrogen. This value is compared to the data from the I-V measurements on the sample sensor in Table 6.2. It is evident that the Schottky barrier height in nitrogen as extracted from the C-V curves is significantly larger than the value extracted from the I-V curves. It has been explained at chapter 5 that the C-V value relates to the average over the depletion layer while the I-V measurements are determined by the part of the barrier where the Schottky barrier is at its lowest. More importantly, it is observed here that the even though the change in average barrier height (0.4V) is very large upon the exposure to hydrogen, the change in the minimum barrier height (0.1V) is much smaller. The areas with lower barrier height in nitrogen are hence less susceptible to hydrogen exposure than the average of the film. This is a significant disadvantage in operation where the extraction happens through a current measurement. The inhomogeneity in the barrier height reduces the sensitivity of the device and leads to device to device variation in sensitivity. To make the sensors of commercial value, it is required to reduce this variation by further optimizing the initial growth stages, in particular the pulsed electrodeposition process to create the nuclei.

TABLE 6.1: $Pd_{1-x}Ni_x$ Schottky barrier height as a function of frequency for x_s=0.1, x=0.3, and x_b=0.4 in both nitrogen and 5% hydrogen (5 mbar partial pressure) as extracted from C-V curves.

Hz(KHz)	5	50	500	1000	5000
$\phi_{Bn}(N2)$	0.97	0.95	0.96	0.93	0.92
$\phi_{Bn}(H2)$	0.44	0.53	0.53	0.52	0.54
$\Delta\ \phi_B$	0.53	0.42	0.43	0.41	0.38

TABLE 6.2: Schottky barrier height extracted from I-V and 1MHz C-V characteristic of $Pd_{1-x}Ni_x$ Schottky barrier hydrogen sensor with x_s=0.1, x=0.3, and x_b=0.4.

method	ρ (Ω.cm)	ϕB_n (N_2) (V)	ϕB_n (H_2) (V)	$\Delta\phi_B$ (V)
C-V	1.28	0.93	0.52	0.41
I-V		0.73	0.62	0.11

6.4.2 Sensitivity and Response Time as function of Hydrogen Concentration

The sensitivity of a sensor is generally rather ill defined as it depends critically on the concentration of target gas. The objective of the measurement described here is to gauge the sensitivity of the sensor to different concentrations of hydrogen. We place the sensor in the vacuum chamber (see Fig. 4.11), and hydrogen is introduced into the chamber through a plastic pipe, with the lowest hydrogen concentration flow through the pipe corresponding to 250 ppm. The results are shown in Fig. 6.10. At low hydrogen concentration, the amount of hydrogen molecules which dissolves in the Pd follows Sievert's law. This law which predicts that the hydrogen concentration in the bulk of the film is proportional to the square root of the hydrogen partial pressure in the system [108]. The extracted sensitivity, displayed in Fig. 6.11, does indeed agree with this relation.

6.4.3 Response Time as function of Hydrogen Concentration

Before measuring the time response as function of hydrogen concentration, the statistical variation between different devices was tested. Table 6.3 shows the time response of 19 individual devices. The time response of all devices is very similar and the standard deviation is relatively small.

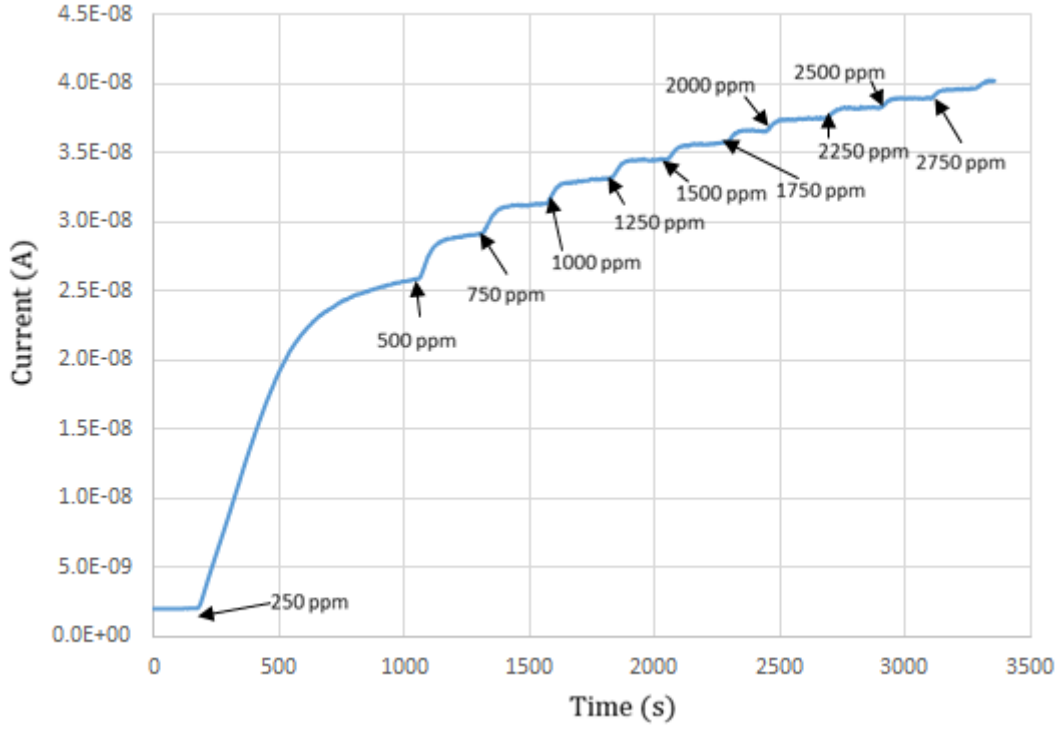

FIGURE 6.10: I-V-t curves of $Pd_{1-x}Ni_x$ sensor with x_s=0.1, x=0.3 and x_b=0.4 to hydrogen concentration from 250ppm to 3000 ppm.

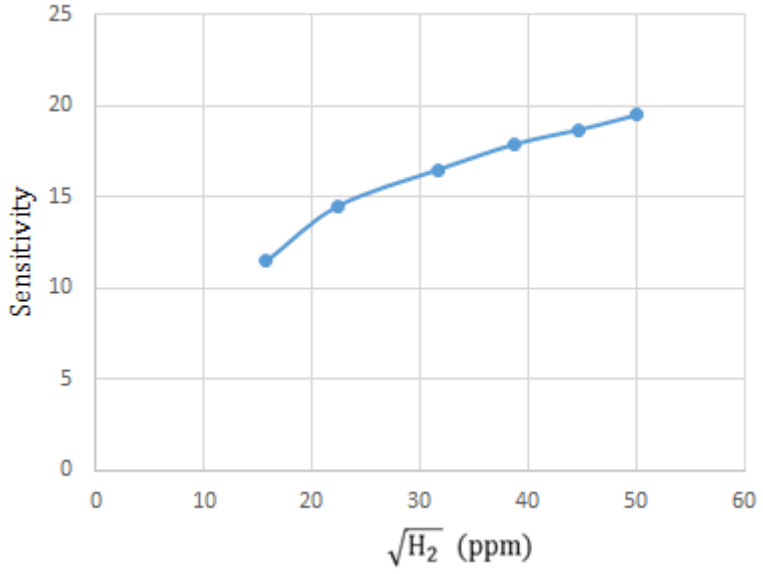

FIGURE 6.11: Sensitivity of $Pd_{1-x}Ni_x$ sensor with x_s=0.1, x=0.3 and x_b=0.4 at various of hydrogen concentration.

TABLE 6.3: Time response t_{90} of 19 individual $Pd_{1-x}Ni_x$ Schottky barrier hydrogen sensor with x_s=0.1, x=0.3 and x_b=0.4.

Samples	Time response (second)
1	14
2	18
3	16
4	22
5	10
6	10
7	14
8	14
9	15
10	9
11	18
12	19
13	29
14	19
15	10
16	15
17	14
18	13
19	16
average	15± 5

The time response of the Schottky barrier hydrogen sensor to hydrogen and nitrogen mixture gas with hydrogen concentration is plotted in Fig. 6.12 with the extracted response time given in Fig. 6.13. The time response to 5000 ppm is rather fast (30s) and the current increases about a factor of 32 times with respect to the current in the nitrogen. With increasing hydrogen concentration, the response time decreases. From 250 ppm to 1500 ppm, the time response decreases dramatically from 462 second to 82 seconds; With even higher hydrogen concentration, the response time keeps on decreasing but at a slower rate.

The time response is influenced by both the adsorption process and the interface trap filling process. If the adsorption process is considered as the rate restrictive step, the theoretical time response can be determined based upon the analysis of Lundstrom *et al.* [109] and Kimura [110]. Figure 6.14 illustrates the sites for absorption of hydrogen in the Pd film for both low and high hydrogen concentration. By Van der waals force, hydrogen attaches to the surface of PdNi film following by dissociation and diffusion. The chemical reaction of hydrogen at the Pd interface is given by:

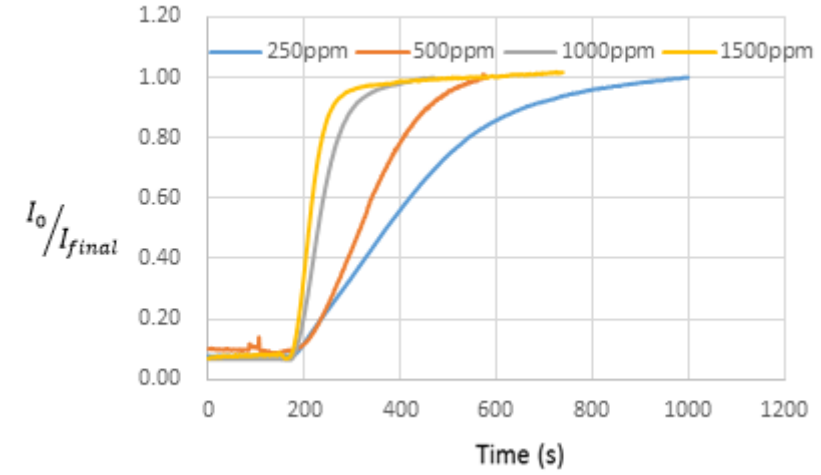

(a)

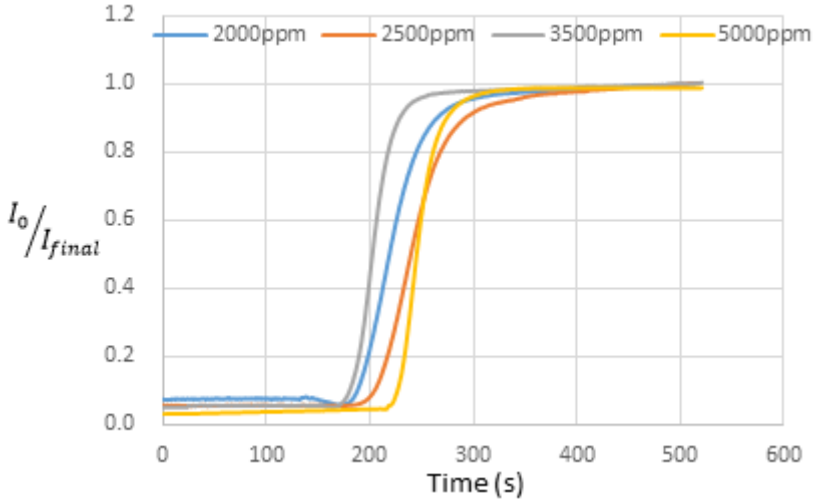

(b)

FIGURE 6.12: (a) Time response of $Pd_{1-x}Ni_x$ Schottky barrier hydrogen sensor with x_s=0.1, x=0.3 and x_b=0.4 upon exposure to hydrogen-nitrogen mixtures, measured at -1V. (a) from 250 ppm to 1500 ppm hydrogen . (b) from 2000 ppm to 5000 ppm hydrogen.

$$H_2 \underset{a_1}{\overset{b_1}{\rightleftharpoons}} 2H_a \tag{6.1}$$

in which both a_1 and b_1 are rate constants for the chemical reaction with Pd, and the rate equation for this reaction is:

$$\frac{\partial\theta}{\partial t} = a_1 P_{H2}(1-\theta)^2 - b_1\theta^2 \tag{6.2}$$

Where θ is the fractional coverage, which is defined as the number of interface

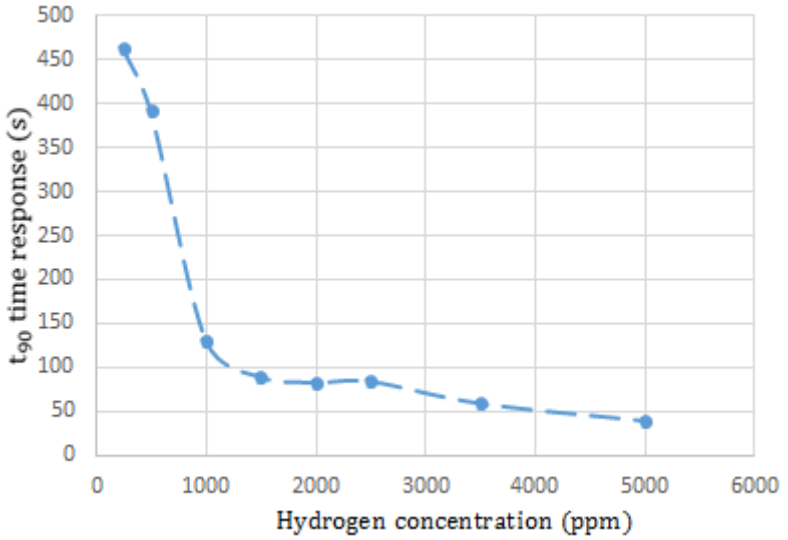

FIGURE 6.13: Time response (t_{90}) versus hydrogen concentration for $Pd_{1-x}Ni_x$ sensor with x_s=0.1, x=0.3 and x_b=0.4 on linear scale.

dipole sites per time unit divided by the total number of dipole sites at the PdNi and Si interface. In a steady state the fractional coverage θ_0 can be expressed as Eq. 6.3 6.4 6.5:

$$\theta_0/(1-\theta_0) = (a_1/b_1)^{1/2} P_{H2}^{1/2} \tag{6.3}$$

$$\theta_0 = \frac{\sqrt{\frac{a_1}{b_1} P_{H2}}}{1+\sqrt{\frac{a_1}{b_1} P_{H2}}} \propto \sqrt{P_{H2}} \tag{6.4}$$

$$\tau = \frac{\theta_0}{\frac{d}{dt}\theta|_{\theta=0}} = \frac{\sqrt{\frac{1}{a_1 b_1 P_{H2}}}}{1+\sqrt{\frac{a_1}{b_1} P_{H2}}} \propto \frac{1}{\sqrt{P_{H2}}} \tag{6.5}$$

Kimura *et al.* [110] utilized Eq. 6.5 to make a phenomenological model of hydrogen sensing according to which the catalytic metal leads to the dissociation of the hydrogen and the formation of an electric dipole layer on the semiconductor. According to their calculation from the rate equation, the time response at low hydrogen concentration should be inversely proportional to the square root of the hydrogen concentration. If the dissociation is not the restrictive step and every hydrogen atoms that impinges on the PdNi film will stick and diffuse, then the maximum sensitivity is limited by the amount of trap sites at the barrier inter-

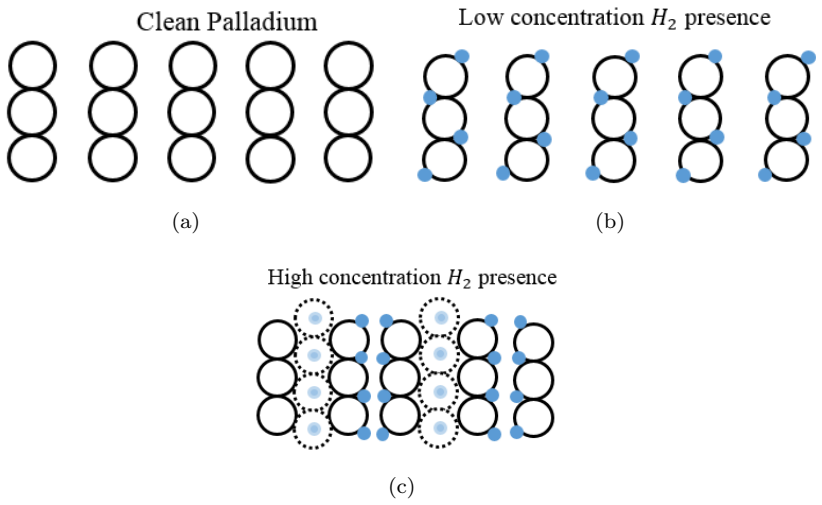

FIGURE 6.14: Sites for absorption of hydrogen in the Pd Film, (a) clean palladium lattice, (b) hydrogen atoms (blue dots) presence in Pd at low concentration (c) top view of hydrogen sites in the palladium and the dashed circle represents palladium as well, light blue dots is the hydrogen atoms below the solid circle. Modified from [111].

face. In this case, the time response is expected to be inversely proportional to the hydrogen concentration.

The plot of the time response on a double log scale is shown in Fig. 6.15. These points can be relatively well fitted with a straight line in the double exponential graph with a slope of -0.76. As discussed above, the slope of straight line dependence of the time constant versus the hydrogen concentration on the log-log scale should be equal to -0.5 if dissociation is the time limiting step, and equal to -1.0 if trapping is the time limiting step. Our result with slope of -0.76 is clearly in between these two extreme values which indicates that both dissociation and total number of traps at the barrier are of importance in the determination of the response time (and sensitivity). It is expected that at low concentration, the hydrogen sensing of the Schottky diode is controlled by the dissociation speed of hydrogen molecules by the Pd, and at high concentration by atom trapping between barrier layer and Si, and that the slope is not a constant over the entire hydrogen concentration range, but the data is too sparse to be able to confidently conclude this.

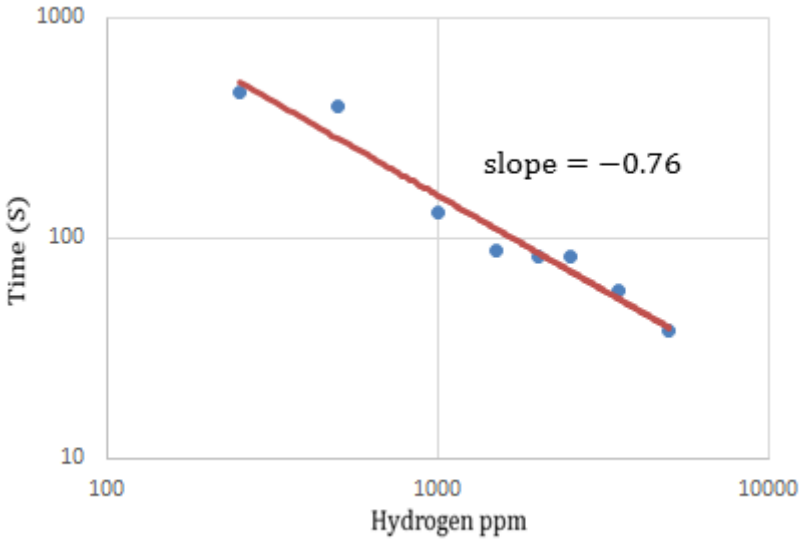

FIGURE 6.15: Time response (t_{90}) versus hydrogen concentration for $Pd_{1-x}Ni_x$ sensor with x_s=0.1, x=0.3 and x_b=0.4 on double logarithmic scale.

6.4.4 Temperature dependence of Schottky barrier height

Before the measurement, a hair drier was utilized to warm the chamber to ensure the aridity of the chamber. Normally, the hydrogen sensor operation is very dependent on the working temperature. Some times the hydrogen sensor would need to work in extreme conditions with either low temperature or high temperature. In order to extract these properties, the dependence of the Schottky barrier hydrogen sensor has been investigated at various temperature (232K-373K) in 5000 ppm hydrogen concentration.

The x_s=0.1, x=0.3, x_b=0.4 composition-modulated Schottky barrier hydrogen sensor was measured in the temperature controlled chamber. Before connecting the liquid nitrogen to the probe station, the chamber is pumped down to a good vacuum ($1x10^{-5}$ bar) to prevent ice forming on the surface of the sensor. Theoretically, the liquid nitrogen can decrease the temperature down to 70K in the chamber,but in reality only 80K was achieved. To stabilize low temperature measurement, the heating system of the probe station was used to maintain the vacuum chamber at the required temperature. For high temperature measurements, the heating system was used without the cryogenic operation.

Temperature dependent measurements do not only allow us to extract the operation of the sensor at different temperatures, it also allows more in depth analysis of the barrier properties. Based on the thermionic emission theory of the Schottky

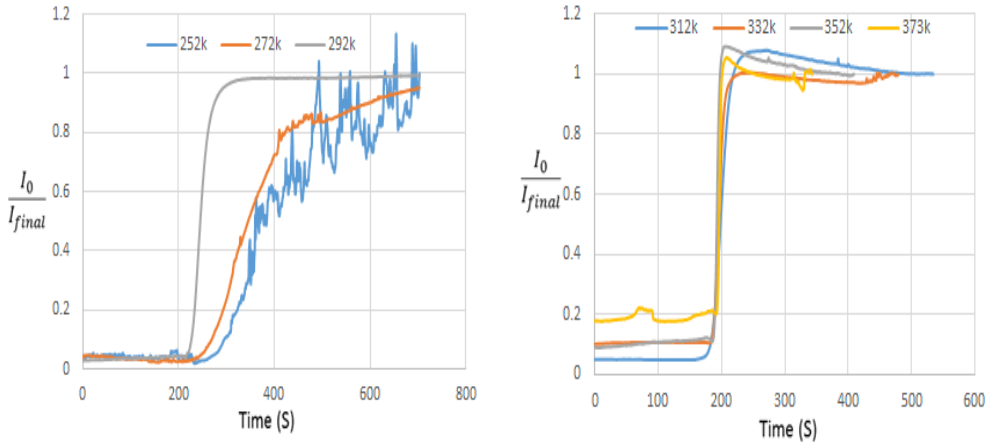

(a) (b)

FIGURE 6.16: I-V-t characteristic of $Pd_{1-x}Ni_x$ sensor with x_s=0.1, x=0.3 and x_b=0.4 at various temperatures (from 252K to 373K) when exposed to 5000ppm Hydrogen. (a) The time response at temperatures of 252K,272K, and 292K. (b) The time response at temperatures of 321K, 332K,352K,and 373K.

barrier as shown in equation Eq. 3.19, it is explained that with the temperature increasing, the reverse leakage current is increased as well. Figure 6.17 shows the I-V characteristic of the Schottky barrier hydrogen sensor $Pd_{1-x}Ni_x$ with x=0.1, 0.3, 0.4 for the surface, bulk, and barrier layer, respectively, for various temperature (from 252K to 373K) in 5000ppm hydrogen with the extracted sensitivity and time response shown in Fig. 6.18.

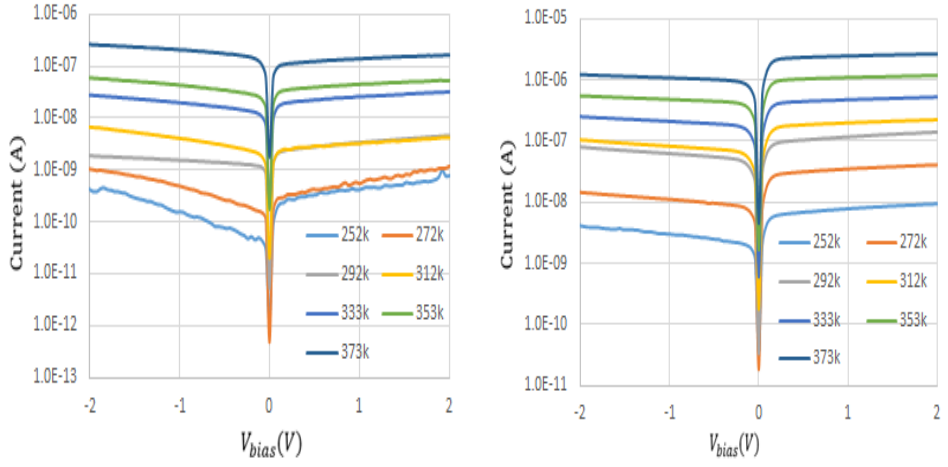

(a) (b)

FIGURE 6.17: (a,b) I-V characteristic of $Pd_{1-x}Ni_x$ sensor with x_s=0.1, x=0.3 and x_b=0.4 at various temperature (from 252K to 373K) in (left) nitrogen and (right) hydrogen ambient (5000 ppm).

The saturation current density was extrapolated from the I-V measurement in Hy-

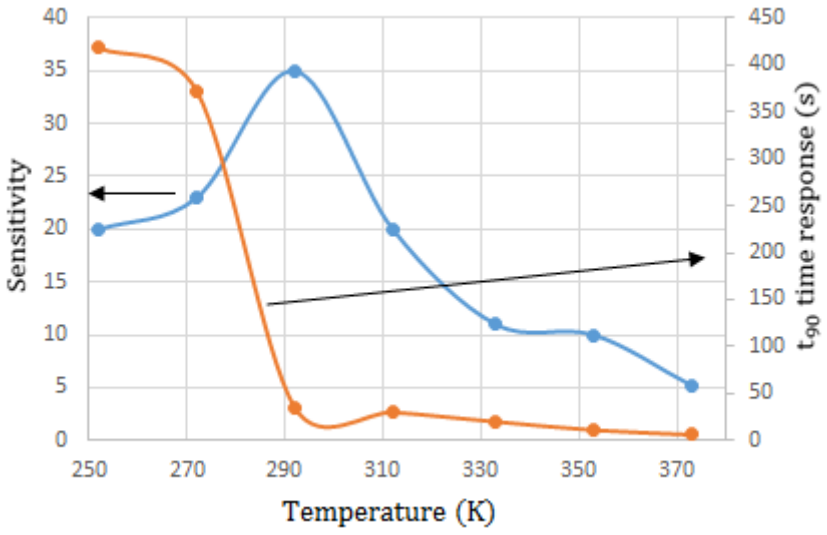

FIGURE 6.18: Sensitivity (blue) and time response (orange) of $Pd_{1-x}Ni_x$ sensor with x_s=0.1, x=0.3 and x_b=0.4 in 5000ppm hydrogen concentration as a function of temperature.

drogen ambient for different temperatures as shown in Fig. 6.19. As expected from the thermionic emission theory the saturation current decreases significantly with temperature. Theoretically, a temperature independent Schottky barrier height leads to a straight line on the activation energy diagram. The straight line fit with ϕ_B=0.32V is not particularly good.

In order to obtain a better fit an improved model has been used. The T_0 effect is often used to model the temperature dependent of Schottky barrier height [112]. In this model, the thermionic emission equation is expressed as:

$$J(V_A) = A^* \cdot T^2 \cdot e^{-\frac{q\phi B}{K\cdot(T+T_0)}} \cdot (e^{\frac{qV_a}{K(T+T_0)}} - 1) \tag{6.6}$$

By using the ϕ_B and T_0 as free parameters, a significant better fit than the temperature independent model is obtained. We use the last mean square method to minimize the sum of the squared residuals, S, as expressed in Eq. 6.7.

$$S = \sum_{i=1}^{n} r_i^2 \tag{6.7}$$

,where r_i is the residual being the difference between the experiment value and the fitting value from the model. In table 6.4 the residuals are given for a number of fits of barrier height and T_0. The smallest residual and hence best fit, corre-

sponds to ϕ_B=1.11V and T_0=144K. A physical interpretation of the To effect is given in Ref. [112] which explains it in terms of spatial variation in the Schottky barriers in which the current passes through the minimum value of the barrier. The analysis indicates that the barrier height between the PdNi alloy and the Si is not uniform across the entire area and that the sensitivity of the sensor is most likely determined by the area with the lowest Schottky barrier. We reached a similar conclusion previously based upon the comparison between I-V and C-V measurements.

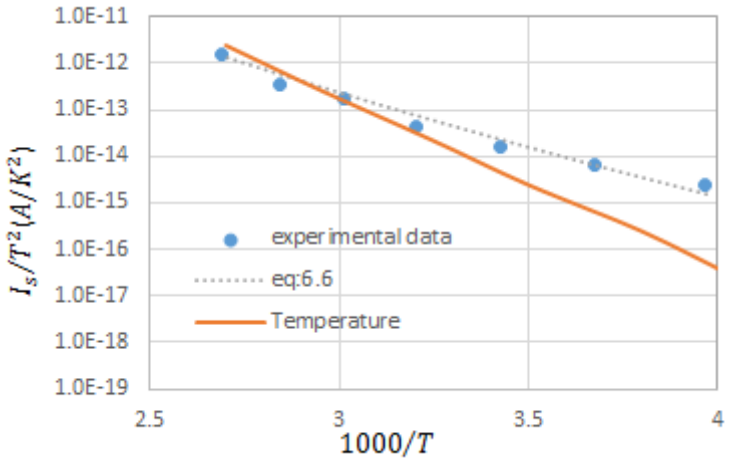

FIGURE 6.19: Activation energy diagram of x_s=0.1, x=0.3 and x_b=0.4 Schottky barrier hydrogen sensor in hydrogen ambient at different temperature as extracted from Fig. 6.17. These data are fitted by using a temperature independent Schottky barrier height thermionic emission model and the T_0 model.

ϕ_B (V)	T_0 (K)	$\sum_{i=1}^{n} r_i^2$
0.8	100	$4.53e^{-19}$
0.9	110	$6.40e^{-21}$
1	120	$7.92e^{-23}$
1.1	130	$3.41e^{-25}$
1.11	140	$2.13e^{-25}$
1.11	142	$1.52e^{-25}$
1.11	144	$1.24e^{-25}$
1.11	145	$2.09e^{-25}$
1.2	140	$3.24e^{-24}$

TABLE 6.4: The squared residuals between experimental data and T_0 effect model.

6.5 Conclusion

In this chapter, functional characterization of composition modulated electrodeposited films were presented in term of Schottky barrier hydrogen properties. The time response results for the $Pd_{1-x}Ni_x$ composition modulated surface layer and constant Pd-Ni ratio in the bulk layer prove that the speed of hydrogen dissociation at the surface scales near exponential with an increase of Pd concentration. Thus a high Pd concentration in the surface layer should be selected which is still compatible with the prevention of the β-phase during cycling. The sensitivity response results for the composition modulated barrier layer with constant Pd-Ni ratio in the bulk layer and 10% Ni in the surface layer agrees with the previous results on uniform films with x=0.4 giving the highest sensitivity. It is hence concluded that a $Pd_{1-x}Ni_x$ film with x=0.1, 0.3, 0.4 for the surface, bulk, and barrier layer, respectively, is the optimum composition.

The relation between response time and hydrogen concentration has been tested and showed a drastically fall with increasing hydrogen concentration. The quickest time response was achieved for a concentration of 5000ppm. The response time versus hydrogen concentration follows a power law relation with a slope of -0.76. A dissociation limited rate equation would follow Sievert's law and result in a slope of -0.5, while limitation in number of trap states at the PdNi-Si interface would result in a slope of -1.0. Our results hence indicate that both these processes are of importance in the determination of the sensitivity of the sensor.

The time response increases with decreasing the temperature, with the lowest temperature (253K) giving the slowest response time. The normalized current does not saturate below room temperature. When the temperature is elevated above 290K the sensor shows a fast time response (less than 20 seconds), which means this sensor should be operated preferable at room temperature or high temperature. The temperature dependence characteristic described in the final section show that the sensor have a good fit with the equation describing the current as function of temperature in terms of spatial variation of the barrier height. Minimizing this spatial variation is essential for reliable operation of the sensor.

Chapter 7

Summary and Outlook

The key property of hydrogen as renewable alternative to carbon-based fuels, is its clean combustion without harmful emission. Hydrogen sensors are critical to insure the safety of hydrogen systems due to hydrogen's combustion characteristics which include low minimum ignition energy, high heat of combustion, as well as wide flammable range. Hydrogen gas sensing technology has been applied in a broad market, such as for the safety in fuel cell automotive, in line fuel monitoring for hydrogen feed, safety in infrastructure and large scale power plants. Traditional sensing instruments such as gas chromatography and mass spectrometers are bulky and expensive for in-situ monitoring. A number of practical hydrogen sensing technologies based on micro-electronics and nanotechnology have emerged. Some of them demonstrate advantages such as size, cost, durability. However most of these sensors, such as electrochemical sensors, also have significant drawbacks like poor selectivity, and in particular high power consumption.

In this work a Schottky barrier based PdNi-Si hydrogen sensor is introduced which can compete with available sensors in terms of sensitivity and selectivity, and time response, while at the same time having extremely low power consumption.

The working principle of electrodeposition was firstly introduced as the primary step to form the metal alloy on semiconductor in the Schottky barrier hydrogen sensor. It is shown that with the right choice of solution, the setting of the electro-deposition potential is capable of creating PdNi alloys with the ratio of Pd to Ni spanning almost the entire range. Based on this possibility we present a new technique of composition-modulated PdNi films, in which each part of the PdNi film is separately optimized within a single electro-deposition process for use in a Schottky barrier hydrogen sensor. The rectifying properties of the electrode-

posited PdNi-Si Schottky barriers are analysed and compared with the theory of thermionic emission. Capacitance-Voltage and Current-Voltage measurement results reveal that the electrodeposited PdNi-Si Schottky barrier possesses excellent rectifying characteristics with high Schottky barrier height, low ideality factor, and most importantly, low reversed bias leakage which makes them extremely suitable for low power sensors.

Back-to-back PdNi-Si Schottky barrier hydrogen sensor have been fabricated in which a uniform layer of 50 nm PdNi alloy film was deposited on Si at current density between 3-5mA/cm^2. A controlled environment probe station is used to measure the Schottky barrier hydrogen sensor in both nitrogen and hydrogen ambient. The Current-Voltage measurements in both hydrogen and nitrogen ambient clearly demonstrate that the sensors have a good sensitivity to hydrogen.

A series of uniform $Pd_{1-x}Ni_x$-Si Schottky barrier hydrogen sensors were fabricated and characterized using Capacitance-Voltage and Current-Voltage measurements. It is shown that the pure Ni films do not show evidence of response to hydrogen and that adding a thin layer of Pd on top allows those sensors to function. This clearly indicates that Ni is not a catalyst for hydrogen dissociation at room temperature. For all sensors, the increase in current with hydrogen can be explained by a decrease of the Schottky barrier height due to the formation of interfacial dipoles. An increase in hydrogen concentration in the gas leads to a concurrent decrease in Schottky barrier height and an monotonic increase in current. It is shown that none of the sensors exhibits a response to nitrogen or air indicating excellent cross sensitivity behaviour for hydrogen. It is shown that sensitivity is optimum for $Pd_{1-x}Ni_x$ with x around 0.4 whereas time response is optimum for x around 0.1. This conundrum is solved by the composition-modulated technique.

We have consequently optimized the sensor device by specific layered deposition. This is first ever functional characterization of composition modulated electrodeposited films in term of Schottky barrier hydrogen properties. The time response results for the $Pd_{1-x}Ni_x$ composition modulated surface layer and constant Pd-Ni ratio in the bulk layer prove that the speed of hydrogen dissociation at the surface scales near exponential with an increase of Pd concentration. Thus a high Pd concentration in the surface layer should be selected which is still compatible with the prevention of the β-phase during cycling. The sensitivity response results for the composition modulated barrier layer with constant Pd-Ni ratio in the bulk layer and 10% Ni in the surface layer agrees with the previous results on uniform films with x=0.4 giving the highest sensitivity. It is hence concluded that a $Pd_{1-x}Ni_x$

film with x=0.1, 0.3, 0.4 for the surface, bulk, and barrier layer, respectively, is the optimum composition.

The relation between response time and hydrogen concentration was measured and showed a drastically decrease with increasing hydrogen concentration. The quickest time response was achieved as the concentration reach to 5000ppm and a power law relation of -0.76 was found. A dissociation limited rate equation would follow Sievert's law and result in a slope of -0.5 while limitation in number of trap states at the PdNi-Si interface would result in a slope of -1.0. Our results hence indicate that both these processes are of importance in the determination of the sensitivity of the sensor.

Temperature dependent measurements show that these sensors function properly at both slightly elevated and below zero temperature. The temperature dependence characteristic of the Schottky barrier height shows that the sensor have a good fit with the equation describing the current as function of temperature in terms of spatial variation of the barrier height. Minimizing this spatial variation is essential for reliable operation of the sensor.

As described in the thesis, the discrepancy between I-V and C-V data collected from same device indicate spatial variation of the Schottky barrier hieght. In order to achieve a more stable and reliable Schottky barrier hydrogen sensor, it is required to minimize this variation. The spatial variation of the Schottky barrier height is related to the size of the metal grains. By changing the parameters of the pulsed electrodeposition that is used for the initial nucleation, it should be possible to better control the Schottky barrier height. Another method to accomplish this would be the reduction in size of the Schottky barrier junctions from the current tens of μm to only tens of nm. This would both reduce the variation and facilitate integration in a CMOS process.

The detailed microstructure of the PdNi film, the PdNi-Si interface, and the surface dissociation layer are not known. Surface roughness measurements by atomic force microscopy, thickness measurements by cross-sectional scanning electron microscopy, and detailed interface studies by transmission electron microscopy would shed light on the detailed behaviour of the hydrogen within the film.

To take advantage of the low costs and low power consumption of the Schottky barrier hydrogen sensors, its use in ubiquitous distributed unpowered sensor networks seems to be the key application area. When integrated on a PCB board, the sensors are shown to function properly covered by an electrically insulating

gas permeable membrane,Polydimethylsiloxane (PDMS). This potentially allows distributed aqueous sensors.

Bibliography

[1] Paul E. Dodds and Will McDowall. The future of the UK gas network. *Energy Policy*, 60:305 – 316, 2013.

[2] Yang-Tse Cheng, Yang Li, Dan Lisi, and W. M. Wang. Preparation and characterization of Pd/Ni thin films for hydrogen sensing. *Sensors and Actuators B: Chemical*, 30(1):11–16, 1996.

[3] L. Boon-Brett, J. Bousek, G. Black, P. Moretto, P. Castello, T. Hert, and U. Banach. Identifying performance gaps in hydrogen safety sensor technology for automotive and stationary applications. *International Journal of Hydrogen Energy*, 35(1):373 – 384, 2010.

[4] Ching-Wen Hung, Han-Lien Lin, Huey-Ing Chen, Yan-Ying Tsai, Po-Hsien Lai, Ssu-I Fu, and Wen-Chau Liu. A nove $Pt/In_{0.52}Al_{0.48}As$ Schottky diode-type hydrogen sensor. *Electron Device Letters, IEEE*, 27(12):951–954, 2006.

[5] R. Vargas-Bernal. Techniques to optimize the selectivity of a gas sensor. In *Electronics, Robotics and Automotive Mechanics Conference, 2007. CERMA 2007*, pages 579–584, 2007.

[6] Lois Brett. The importance of fast responding hydrogen sensors in the detection of hydrogen leaks. Technical report, European Commission, DG JRC - Institute for Energy, 2010. also available as `http://www.hydrogenandfuelcellsafety.info/2010/jul/hydrogenSensors.asp`.

[7] L. Boon-Brett, G. Black, P. Moretto, and J. Bousek. A comparison of test methods for the measurement of hydrogen sensor response and recovery times. *International Journal of Hydrogen Energy*, 35(14):7652 – 7663, 2010.

[8] Ghenadii Korotcenkov, Sang Do Han, and Joseph R. Stetter. Review of electrochemical hydrogen sensors. *Chemical Reviews*, 109(3):1402–1433, 2009.

[9] `http://www.hysafe.org/download/1200/BRHS_Chap5_V1p2.pdf`.

[10] William J. Buttner, Matthew B. Post, Robert Burgess, and Carl Rivkin. An overview of hydrogen safety sensors and requirements. *International Journal of Hydrogen Energy*, 36(3):2462 – 2470, 2011.

[11] Joseph R. Stetter, William R. Penrose, and Sheng Yao. Sensors, Chemical sensors, Electrochemical sensors, and ECS. *Journal of The Electrochemical Society*, 150(2):S11–S16, 2003.

[12] Yente Chao, Sheng Yao, William J. Buttner, and Joseph R. Stetter. Amperometric sensor for selective and stable hydrogen measurement. *Sensors and Actuators B: Chemical*, 106(2):784 – 790, 2005.

[13] M. Sakthivel and W. Weppner. A portable limiting current solid-state electrochemical diffusion hole type hydrogen sensor device for biomass fuel reactors: Engineering aspect. *International Journal of Hydrogen Energy*, 33(2):905 – 911, 2008.

[14] C Huck, A Poghossian, P Wagner, and MJ Schöening. Combined amperometric/field-effect sensor for the detection of dissolved hydrogen. *Sensors and Actuators B: Chemical*, 187:168–173, 2013.

[15] T. Hübert, L.Boon-Brett, G. Black, and U. Banach. Hydrogen sensors-A review. *Sensors and Actuators B: Chemical*, 157(2):329 – 352, 2011.

[16] Joseph R. Stetter and Jing Li. Amperometric gas sensors-a review. *Chemical Reviews*, 108(2):352–366, 2008.

[17] L.P. Martin, A.-Q. Pham, and R.S. Glass. Electrochemical hydrogen sensor for safety monitoring. *Solid State Ionics*, 175(14):527 – 530, 2004.

[18] C. Ramesh, N. Murugesan, M. Krishnaiah, V. Ganesan, and G. Periaswami. Improved nafion-based amperometric sensor for hydrogen in argon. *Journal of Solid State Electrochemistry*, 12:1109–1116, 2008.

[19] Eui-Bok Lee, In-Sung Hwang, Jung-Ho Cha, Ho-Jun Lee, Won-Bae Lee, James Jungho Pak, Jong-Heun Lee, and Byeong-Kwon Ju. Micromachined catalytic combustible hydrogen gas sensor. *Sensors and Actuators B: Chemical*, 153(2):392 – 397, 2011.

[20] V.R. Katti, A.K. Debnath, S.C. Gadkari, S.K. Gupta, and V.C. Sahni. Passivated thick film catalytic type hydrogen sensor operating at low temperature. *Sensors and Actuators B: Chemical*, 84(23):219 – 225, 2002.

[21] Isolde Simon and Michael Arndt. Thermal and gas-sensing properties of a micromachined thermal conductivity sensor for the detection of hydrogen in automotive applications. *Sensors and Actuators A: Physical*, 97(0):104 – 108, 2002.

[22] Balakisnan B. Buttner WJ. Findlay MW. Maclay GJ. Stetter JR. Kelsch A. Low-power MEMS thermal conductivity sensors for hydrogen. *In: The 12th International Meeting on Chemical Sensors*, 2008.

[23] J. Watson. The stannic oxide gas sensor. *Sensor Review*, 14:20–23, 1994.

[24] Gary W Hunter. A survey and analysis of commercially available hydrogen sensors. *NASA STI/Recon Technical Report N*, 93:17777, 1992.

[25] Jianwei Gong, Quanfang Chen, Weifeng Fei, and Sudipta Seal. Micromachined nanocrystalline SnO_2 chemical gas sensors for electronic nose. *Sensors and Actuators B: Chemical*, 102(1):117–125, 2004.

[26] Jianwei Gong, Jianren Sun, and Quanfang Chen. Micromachined sol–gel carbon nanotube SnO_2 nanocomposite hydrogen sensor. *Sensors and Actuators B: Chemical*, 130(2):829–835, 2008.

[27] Namrata Dewan, S.P. Singh, K. Sreenivas, and Vinay Gupta. Influence of temperature stability on the sensing properties of SAW NO_x sensor. *Sensors and Actuators B: Chemical*, 124(2):329 – 335, 2007.

[28] A. D'Amico, A. Palma, and E. Verona. Surface acoustic wave hydrogen sensor. *Sensors and Actuators*, 3(0):31 – 39, 1982C1983.

[29] Duy-Thach Phan and Gwiy-Sang Chung. Surface acoustic wave hydrogen sensors based on ZnO nanoparticles incorporated with a Pt catalyst. *Sensors and Actuators B: Chemical*, 161(1):341 – 348, 2012.

[30] Constantinos Christofides and Andreas Mandelis. Operating characteristics and comparison of photopyroelectric and piezoelectric sensors for trace hydrogen gas detection. i. development of a new photopyroelectric sensor. *Journal of Applied Physics*, 66(9):3975–3985, 1989.

[31] M. A. Butler. Optical fiber hydrogen sensor. *Applied Physics Letters*, 45(10):1007–1009, 1984.

[32] Minghong Yang, Zhi Yang, Jixiang Dai, and Dongsheng Zhang. Fiber optic hydrogen sensors with sol-gel WO_3 coatings. *Sensors and Actuators B: Chemical*, 166-167(0):632 – 636, 2012.

[33] R.J. Westerwaal, J.S.A. Rooijmans, L. Leclercq, D.G. Gheorghe, T. Radeva, L. Mooij, T. Mak, L. Polak, M. Slaman, B. Dam, and Th. Rasing. Nanostructured Pd-Au based fiber optic sensors for probing hydrogen concentrations in gas mixtures. *International Journal of Hydrogen Energy*, 38(10):4201 – 4212, 2013.

[34] T.Graham. *On the Relation of Hydrogen to Palladium.* Royal Society of London, 1868.

[35] T.B. Flanagan and WA Oates. The palladium-hydrogen system. *Annual Review of Materials Science*, 21(1):269–304, 1991.

[36] T.B. Flanagan, B. Baranowski, and S. Majchrzak. Remarkable interstitial hydrogen contents observed in rhodium-palladium alloys at high pressures. *The Journal of Physical Chemistry*, 74(24):4299–4300, 1970.

[37] M Lee and R. Glosser. Pressure concentration isotherms of thin films of the palladium-hydrogen system as modified by film thickness, hydrogen cycling, and stress. *Journal of Applied Physics*, 57(12):5236–5239, 1985.

[38] Antonin Ollagnier, Arnaud Fabre, Thomas Thundat, and Eric Finot. Activation process of reversible Pd thin film hydrogen sensors. *Sensors and Actuators B: Chemical*, 186(0):258 – 262, 2013.

[39] JC Barton, FA Lewis, and I. Woodward. Hysteresis of the relationships between electrical resistance and the hydrogen content of palladium. *Trans. Faraday Soc.*, 59(0):1201–1207, 1963.

[40] DH Everett and P. Nordon. Hysteresis in the palladium+ hydrogen system. *Proceedings of the Royal Society of London. Series A. Mathematical and Physical Sciences*, 259(1298):341–360, 1960.

[41] Y. Sakamoto, T. Matsuo, T. Sakaki, and K. Baba. The diffusion of hydrogen in Pd-Ni solid solutions. *journal of Faculty of Engineering, Nagasaki University*, 18(30):61–67, 1988.

[42] H. Peisl. Lattice strains due to hydrogen in metals. In *Hydrogen in Metals I*, volume 28 of *Topics in Applied Physics*, pages 53–74. Springer Berlin/Heidelberg, 1978.

[43] Eunsongyi Lee, Jun Min Lee, Eunyoung Lee, Jin-Seo Noh, Jin Hyoun Joe, Bumsuk Jung, and Wooyoung Lee. Hydrogen gas sensing performance of

PdNi alloy thin films. *Thin Solid Films*, 519(2):880 – 884, 2010. Special Section: Romanian Conference on Advanced Materials 2009.

[44] I. Lundstrom, S. Shivaraman, C. Svensson, and L. Lundkvist. A hydrogen sensitive MOS field effect transistor. *Applied Physics Letters*, 26(2):55–57, 1975.

[45] Haoshuang Gu, Zhao Wang, and Yongming Hu. Hydrogen gas sensors based on semiconductor oxide nanostructures. *Sensors*, 12(5):5517–5550, 2012.

[46] G.C Bond. *Heterogenous Catalysis: Principles and Applications*. Clarendon Press, Oxford, 1974.

[47] Bum-Joon Kim, Jin-Ho Yoon, and Jung-Sik Kim. Gas sensing characteristics of low-powered dual MOSFET hydrogen sensors. *Materials Chemistry and Physics*, 142(2 - 3):594 – 599, 2013.

[48] Toshiyuki Usagawa and Yota Kikuchi. Device characteristics for Pt-Ti-O gate Si–MISFETs hydrogen gas sensors. *Sensors and Actuators B: Chemical*, 160(1):105 – 114, 2011.

[49] J. Fogelberg, M. Eriksson, H. Dannetun, and L.G. Petersson. Kinetic modeling of hydrogen adsorption/absorption in thin films on hydrogensensitive fieldeffect devices: Observation of large hydrogeninduced dipoles at the PdSiO2 interface. *Journal of Applied Physics*, 78(2):988–996, 1995.

[50] V.I. Filippov, A.A. Vasiliev, W. Moritz, and J. Szeponik. Room-temperature hydrogen sensitivity of a MIS-structure based on the Pt/LaF_3 interface. *Sensors Journal, IEEE*, 6(5):1250–1255, 2006.

[51] Martin C. Steele, John W. Hile, and Bernard A. Maciver. Hydrogen sensitive palladium gate mos capacitors. *Journal of Applied Physics*, 47(6):2537–2538, Jun 1976.

[52] Chi Lu and Zhi Chen. MOS hydrogen sensor with very fast response based on ultra-thin thermal SiO_2 film. *International Journal of Hydrogen Energy*, 35(22):12561 – 12567, 2010.

[53] Ingemar Lundström. Hydrogen sensitive MOS structures: Part 1: Principles and applications. *Sensors and Actuators*, 1(0):403 – 426, 1981.

[54] M. Crivellari, M. Mattevi, A. Picciotto, P. Bellutti, A. Collini, L. Torrisi, F. Caridi, S. Gennaro, and A. Gasparotto. Microfabrication of MOS hydrogen sensors based on Pd-gate deposited by pulsed laser ablation. *Sensors and Actuators B: Chemical*, 186(0):180 – 185, 2013.

[55] J. Schalwig, G. Mller, U. Karrer, M. Eickhoff, O. Ambacher, M. Stutzmann, L. Grgens, and G. Dollinger. Hydrogen response mechanism of PtGaN Schottky diodes. *Applied Physics Letters*, 80(7):1222–1224, 2002.

[56] Peng Zhang, A. Vincent, A. Kumar, Sudipta Seal, and Hyoung Jin Cho. A low-energy room-temperature hydrogen nanosensor: Utilizing the Schottky barriers at the electrode/sensing-material interfaces. *Electron Device Letters, IEEE*, 31(7):770–772, July 2010.

[57] Karel Zdansky and Roman Yatskiv. Schottky barriers on InP and GaN made by deposition of colloidal graphite and Pd, Pt or bimetal Pd/Pt nanoparticles for H2-gas detection. *Sensors and Actuators B: Chemical*, 165(1):104 – 109, 2012.

[58] Tsung-Han Tsai, Jun-Rui Huang, Kun-Wei Lin, Wei-Chou Hsu, Huey-Ing Chen, and Wen-Chau Liu. Improved hydrogen sensing characteristics of a Pt/SiO_2/GaN schottky diode. *Sensors and Actuators B: Chemical*, 129(1):292 – 302, 2008.

[59] Karl Skucha, Zhiyong Fan, Kanghoon Jeon, Ali Javey, and Bernhard Boser. Palladium/silicon nanowire Schottky barrier-based hydrogen sensors. *Sensors and Actuators B: Chemical*, 145(1):232 – 238, 2010.

[60] Aihua Zhong, Takashi Sasaki, and Kazuhiro Hane. Platinum/porous GaN nanonetwork metal-semiconductor Schottky diode for room temperature hydrogen sensor. *Sensors and Actuators A: Physical*, 209(0):52 – 56, 2014.

[61] ME Kiziroglou, AA Zhukov, X. Li, DC Gonzalez, PAJ De Groot, P.N. Bartlett, and CH de Groot. Analysis of thermionic emission from electrodeposited Ni–Si Schottky barriers. *Solid state communications*, 140(11):508–513, 2006.

[62] Jung Sik Kim Bum Joon Kim. Dual MOSFET hydrogen sensors with thermal island structure. *Key Engineering Materials*, 543:93–96, 2013.

[63] Hongyu Ma, Enjie Ding, and Wenjuan Wang. Power reduction with enhanced sensitivity for pellistor methane sensor by improved thermal insula-

tion packaging. *Sensors and Actuators B: Chemical*, 187(0):221 – 226, 2013. Selected Papers from the 14th International Meeting on Chemical Sensors.

[64] Cedric Perrotton, Nicolas Javahiraly, Alex Kazemi, and Patrick Meyrueis. Review of optical fiber sensor technologies for hydrogen leak detection in hydrogen energy storage. In *Proc. SPIE*, volume 8026, pages 80260O–80260O–11, 2011.

[65] V.V. Malyshev and A.V. Pislyakov. Sensitivity of semiconductor metal oxides (SnO_2, WO_3, ZnO) to hydrogen sulfide in dry and humid gas media. *Journal of Analytical Chemistry*, 69(2):123–135, 2013.

[66] Paunovic Milan and Schlesinger Mordechay. *Fundamentals of electrochemical deposition*. John Wiley and Sons, INC, 1998.

[67] F. A. Lowenheim. *Modern electroplating*. Wiley, New York, 1974.

[68] Ashwin R. Usgaocar. *Integration of electrodeposited PdNi alloys with Silicon and Carbon nanotube electronics*. PhD thesis, University of Southampton, 2011.

[69] Seung-Eun Nam, Sang-Hak Lee, and Kew-Ho Lee. Preparation of a palladium alloy composite membrane supported in a porous stainless steel by vacuum electrodeposition. *Journal of Membrane Science*, 153(2):163 – 173, 1999.

[70] Carmen Nila and Ignacio Gonzlez. The role of ph and cu(ii) concentration in the electrodeposition of cu(ii) in {NH4Cl} solutions. *Journal of Electroanalytical Chemistry*, 401(12):171 – 182, 1996.

[71] J. Goldstein. *Scanning electron microscopy and X-ray microanalysis*, volume 1. Springer, 2003.

[72] `http://en.wikipedia.org/wiki/Energy-dispersive_X-ray_spectroscopy`.

[73] Yaokun Xiao, Gang Yu, Juan Yuan, Jinyin Wang, and Zongzhang Chen. Fabrication of PdNi alloy nanowire arrays on HOPG surface by electrodeposition. *Electrochimica Acta*, 51(20):4218 – 4227, 2006.

[74] Hsin-Yi Huang and Po-Yu Chen. Voltammetric behavior of Pd(II) and Ni(II) ions and electrodeposition of PdNi bimetal in N-butyl-N-methylpyrrolidinium dicyanamide ionic liquid. *Electrochimica Acta*, 56(5):2336 – 2343, 2011.

[75] A. Dolati, M. Ghorbani, and M.R. Ahmadi. An electrochemical study of AuNi alloy electrodeposition from cyanidecitrate electrolytes. *Journal of Electroanalytical Chemistry*, 577(1):1 – 8, 2005.

[76] Mehdi Ebadi, Wan Jeffrey Basirun, Yatimah Alias, Mohammad Reza Mahmoudian, and Sim Yoke Leng. Investigation of electrodeposition of NiCoFeZn alloys in DMSO with MHD effect. *Materials Characterization*, 66(0):46 – 55, 2012.

[77] Da-ling Lu, Kazunari Domen, and Ken-ichi Tanaka. Electrodeposited AuFe, AuNi, and AuCo alloy Nanoparticles from aqueous electrolytes. *Langmuir*, 18(8):3226–3232, 2002.

[78] Jie Gong, Steve Riemer, Augusto Morrone, Venkatram Venkatasamy, Michael Kautzky, and Ibro Tabakovic. Composition gradients and magnetic properties of 5–100 nm thin CoNiFe films obtained by electrodeposition. *Journal of the Electrochemical Society*, 159(7):D447–D454, 2012.

[79] P. Leisner, C.B. Nielsen, P.T. Tang, T.C. Dorge, and P. Moller. Methods for electrodepositing composition-modulated alloys. *Journal of Materials Processing Technology*, 58(1):39 – 44, 1996.

[80] Joseph Yahalom and Ori Zadok. Formation of composition-modulated alloys by electrodeposition. *Journal of Materials Science*, 22(2):499–503, 1987.

[81] Byungjun Jeon, Sanghwa Yoon, and Bongyoung Yoo. Electrochemical synthesis of compositionally modulated Fe_xPd_{1x} nanowires. *Electrochimica Acta*, 56(1):401 – 405, 2010.

[82] DS Lashmore and MP Dariel. Electrodeposited Cu-Ni textured superlattices. *Journal of the Electrochemical Society*, 135(5):1218–1221, 1988.

[83] Raymond T. Tung. Recent advances in Schottky barrier concepts. *Materials Science and Engineering: R: Reports*, 35(1-3):1 – 138, 2001.

[84] S.M.Sze. *Semiconductor Devces: Physics and Technology 2nd Edition*. John Wiley and Sons, INC, 2001.

[85] E.H.Rhoderick. Transport processes in Schottky diode. In *Conference on metal-semiconductor contacts*, Manchester, Lans, UK, April,1974.

[86] E.H.(Emlyn Huw) Rhoderick and R.H.Williams. *Metal-semiconductor contacts 3nd Edition*. Clarendon, Oxford, 1988.

[87] A.F. Abd Rahim, M.R. Hashim, and N.K. Ali. High sensitivity of palladium on porous silicon MSM photodetector. *Physica B: Condensed Matter*, 406(4):1034 – 1037, 2011.

[88] AC Schmitz, AT Ping, I Adesida, et al. Schottky barrier heights of Ni, Pt, Pd, and Au on n-type GaN. In *MRS Proceedings*, volume 395, page 831. Cambridge Univ Press, 1995.

[89] J.W. Bae, T. Hossain, I. Adesida, K.H. Bogart, D. Koleske, A.A. Allerman, and J.-H. Jang. Low resistance ohmic contact to p-type GaN using Pd/Ir/Au multilayer scheme. *Journal of Vacuum Science Technology B: Microelectronics and Nanometer Structures*, 23(3):1072–1075, May 2005.

[90] W.F.Beadle. *Quick Reference manual for Semiconductor Enginner*. Wiley, INC, 1985.

[91] M.E. Kiziroglou, A.A. Zhukov, M. Abdelsalam, X. Li, P.A.J. de Groot, P.N. Bartlett, and C.H. de Groot. Electrodeposition of Ni-Si Schottky barriers. *Magnetics, IEEE Transactions on*, 41(10):2639–2641, 2005.

[92] MS Shivaraman and CM Svensson. Control of palladium adherence to silicon dioxide for photolithographic etching. *Journal of The Electrochemical Society*, 123(8):1258–1258, 1976.

[93] Peter C. Thomas, Srinivasa R. Raghavan, and Samuel P. Forry. Regulating oxygen levels in a microfluidic device. *Analytical Chemistry*, 83(22):8821–8824, 2011.

[94] Ghader Khanbabaei, Ebrahim Vasheghani-Farahani, and Ali Rahmatpour. Pure and mixed gas CH_4 and n-C_4H_{10} permeation in PDMS-fumed silica nanocomposite membranes. *Chemical Engineering Journal*, 191(0):369 – 377, 2012.

[95] Kyle Berean, Jian Zhen Ou, Majid Nour, Kay Latham, Chris McSweeney, David Paull, Andri Halim, Sandra Kentish, Cara M. Doherty, Anita J. Hill, and Kourosh Kalantar-zadeh. The effect of crosslinking temperature on the permeability of PDMS membranes: Evidence of extraordinary CO_2 and CH_4 gas permeation. *Separation and Purification Technology*, 122(0):96 – 104, 2014.

[96] Huey-Ing Chen, Yen-I Chou, and Chieh-Kang Hsiung. Comprehensive study of adsorption kinetics for hydrogen sensing with an electroless-plated PdInP Schottky diode. *Sensors and Actuators B: Chemical*, 92(12):6 – 16, 2003.

[97] T Mitsui, MK Rose, E Fomin, DF Ogletree, and M Salmeron. Dissociative hydrogen adsorption on palladium requires aggregates of three or more vacancies. *Nature*, 422(6933):705–707, 2003.

[98] Jrgen H. Werner and Herbert H. Gttler. Barrier inhomogeneities at Schottky contacts. *Journal of Applied Physics*, 69(3):1522–1533, 1991.

[99] J. Werner, A. F. J. Levi, R. T. Tung, M. Anzlowar, and M. Pinto. Origin of the excess capacitance at intimate Schottky contacts. *Phys. Rev. Lett.*, 60:53–56, Jan 1988.

[100] P. Chattopadhyay and B. RayChaudhuri. New technique for the determination of series resistance of Schottky barrier diodes. *Solid-State Electronics*, 35(7):1023 – 1024, 1992.

[101] İ. Yücedağ, Ş. Altindal, and A. Tatarğlu. On the profile of frequency dependent series resistance and dielectric constant in MIS structure. *Microelectronic Engineering*, 84(1):180 – 186, 2007.

[102] W.A. Hill and C.C. Coleman. A single-frequency approximation for interface-state density determination. *Solid-State Electronics*, 23(9):987 – 993, 1980.

[103] Sanjay Kumar Singh and Qiang Xu. Complete conversion of hydrous hydrazine to hydrogen at room temperature for chemical hydrogen storage. *Journal of the American Chemical Society*, 131(50):18032–18033, 2009.

[104] Sanjay Kumar Singh, Ashish Kumar Singh, Kengo Aranishi, and Qiang Xu. Noble-metal-free bimetallic nanoparticle-catalyzed selective hydrogen generation from hydrous hydrazine for chemical hydrogen storage. *Journal of the American Chemical Society*, 133(49):19638–19641, 2011. PMID: 22070579.

[105] R.C Hughes, W.K Schubert, and R.J Buss. Solid-state hydrogen sensors using palladium-nickel alloys: Effect of alloy composition on sensor response. *Journal of the Electrochemical Society*, 142:249, 1995.

[106] Chi Lu, Zhi Chen, and Kozo Saito. Hydrogen sensors based on Ni/SiO2/Si MOS capacitors. *Sensors and Actuators B: Chemical*, 122(2):556 – 559, 2007.

[107] S. Rane, S. Tatkare, S. Rane, and S. Gosavi. Thick film hydrogen sensor based on nanocrystalline nickel ferrite prepared using simple microwave oven. In *Physics and Technology of Sensors (ISPTS), 2012 1st International Symposium on*, pages 212–215, March 2012.

[108] S. Tosti, A. Basile, L. Bettinali, F. Borgognoni, F. Chiaravalloti, and F. Gallucci. Long-term tests of PdAg thin wall permeator tube. *Journal of Membrane Science*, 284(12):393 – 397, 2006.

[109] K. I. Lundström, M. S. Shivaraman, and C. M. Svensson. A hydrogen - sensitive Pd-gate MOS transistor. *Journal of Applied Physics*, 46(9):3876–3881, 1975.

[110] Taketomo Sato Takeshi Kimura, Hideki Hasegawa and Tamotsu Hashizume. Sensing mechanism of InP hydrogen sensors using Pt Schottky diodes formed by electrochemical process. *Japanese Journal of Applied Physics*, 45:3414, 2006.

[111] Nevin Taşaltin, Sadullah Öztürk, Necmettin Kilinç, and Zafer Ziya Öztürk. Temperature dependence of a nanoporous Pd film hydrogen sensor based on an AAO template on Si. *Applied Physics A*, 97(4):745–750, 2009.

[112] A.N. Saxena. Forward current-voltage characteristics of Schottky barriers on n-type silicon. *Surface Science*, 13(1):151 – 171, 1969.

Appendix A

Appendix of Frequency Dependent C-V Measurement

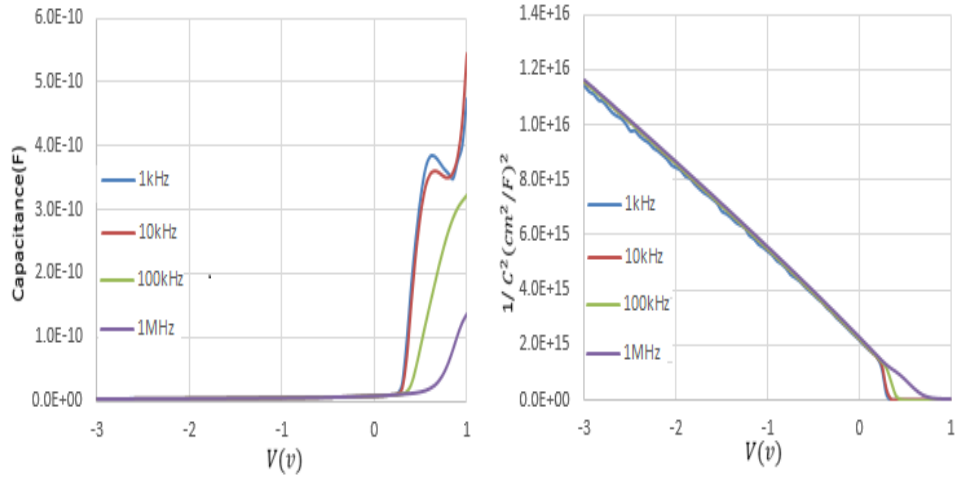

(a)

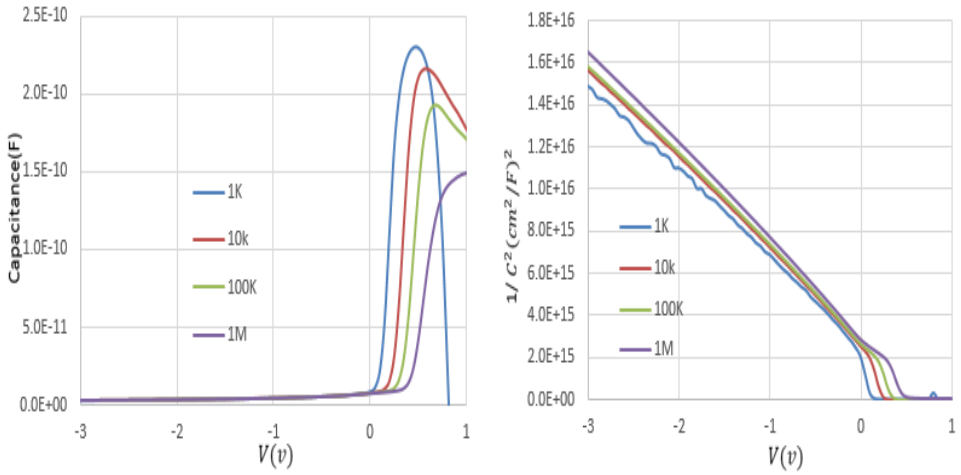

(b)

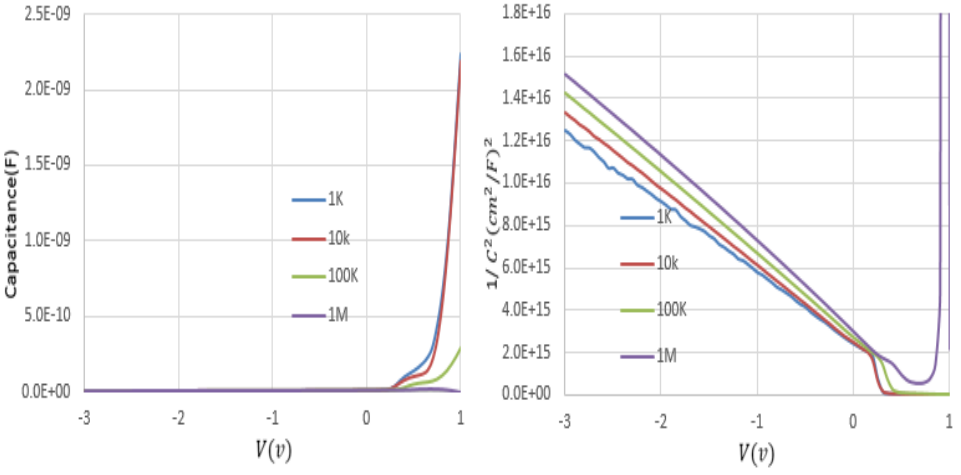

(c)

FIGURE A.1: Frequency dependent C-V measurements of $Pd_{1-x}Ni_x$ Schottky barrier hydrogen sensor and $1/C^2$-V characteristic of the same device for various frequencies at room temperature for (a) x=0, (b) x=0.3, and (c) x=0.4.

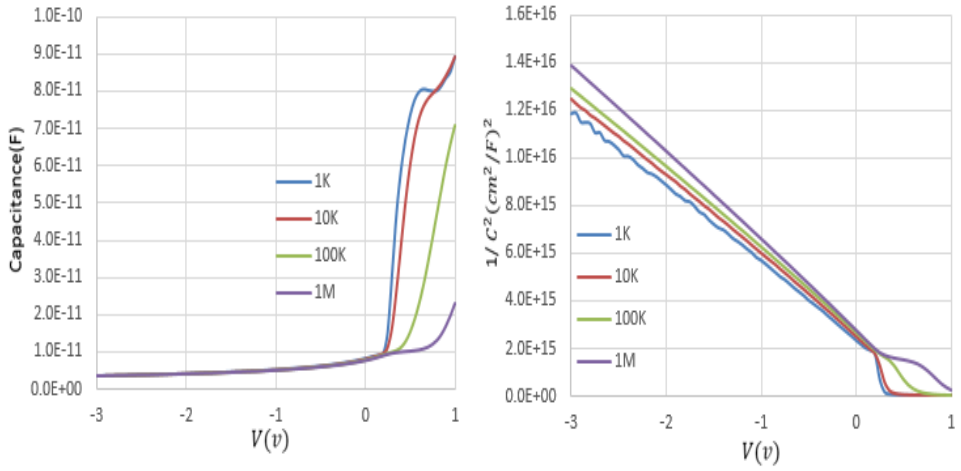

(a)

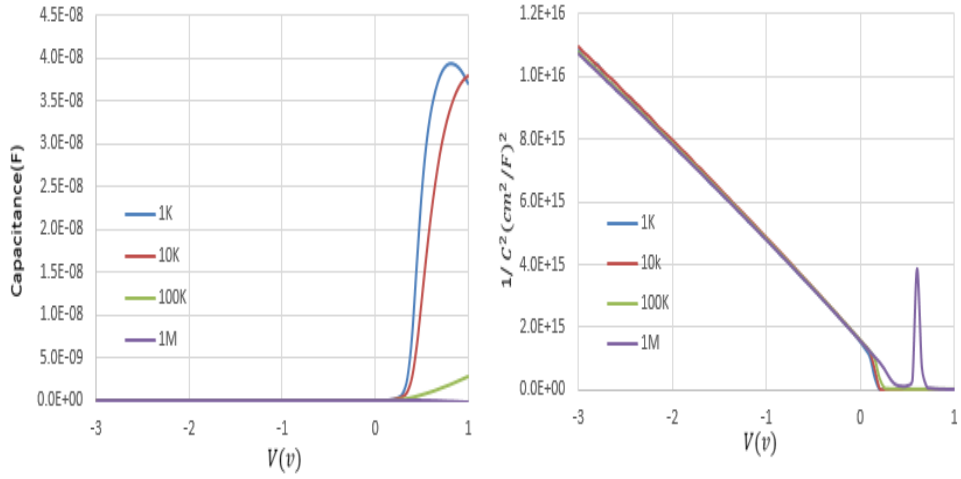

(b)

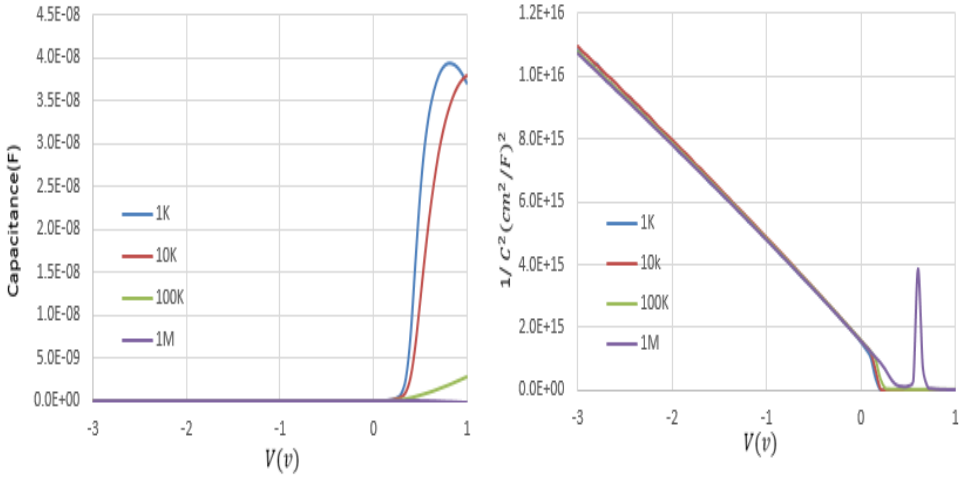

(c)

FIGURE A.2: Frequency dependent C-V measurements of $Pd_{1-x}Ni_x$ Schottky barrier hydrogen sensor and $1/C^2$-V characteristic of the same device for various frequencies at room temperature for (a) x=0.55, (b) x=1 and (c) x=1 with Pd cap.

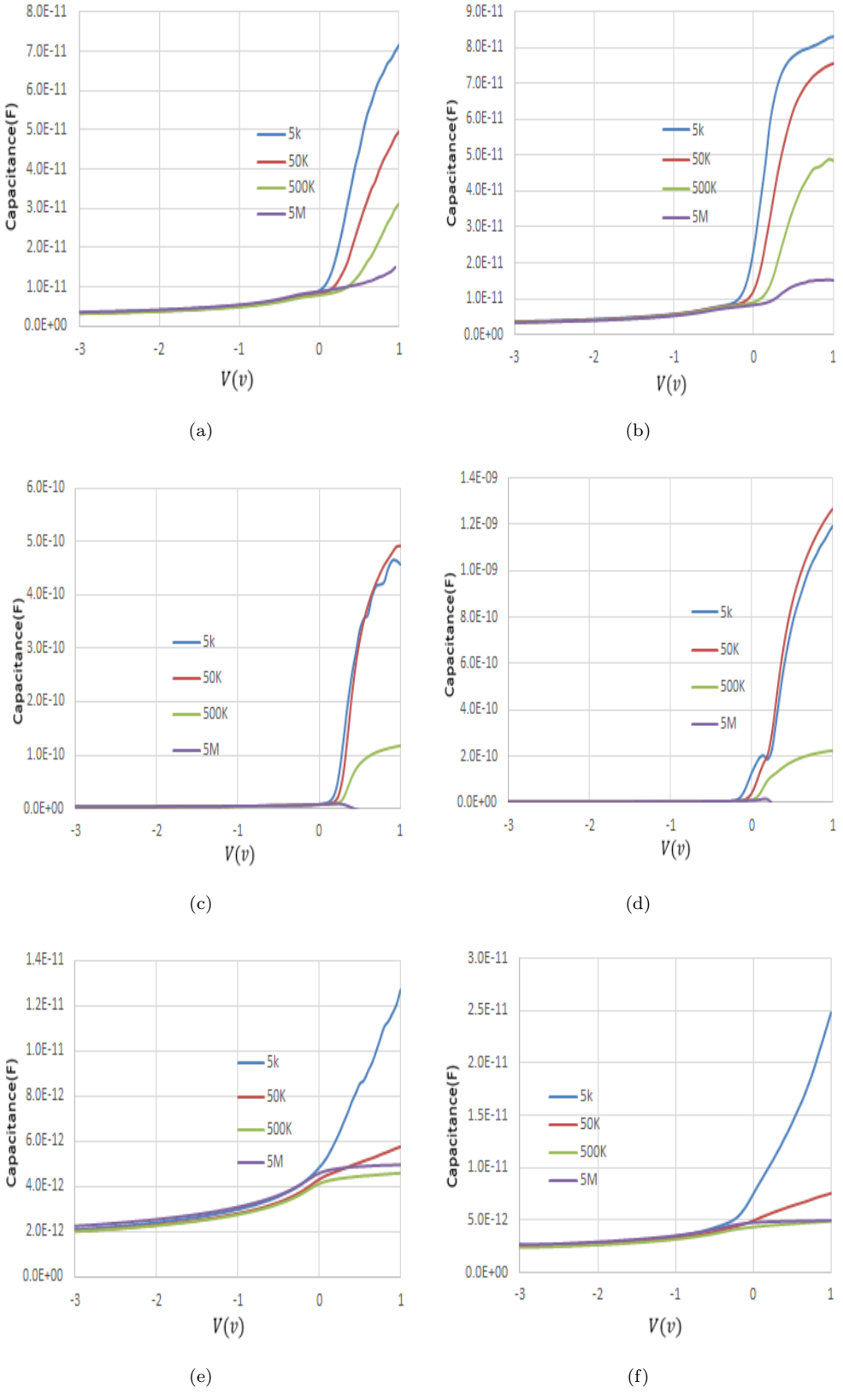

FIGURE A.3: Frequency dependent C-V characteristics of $Pd_{1-x}Ni_x$ Schottky diode hydrogen sensor in nitrogen (left) and 5 mbar hydrogen partial pressure (right) for (a,b) x=0 , (c,d) x=0.3 (Al voltage) , and (e,f) x=0.4 .

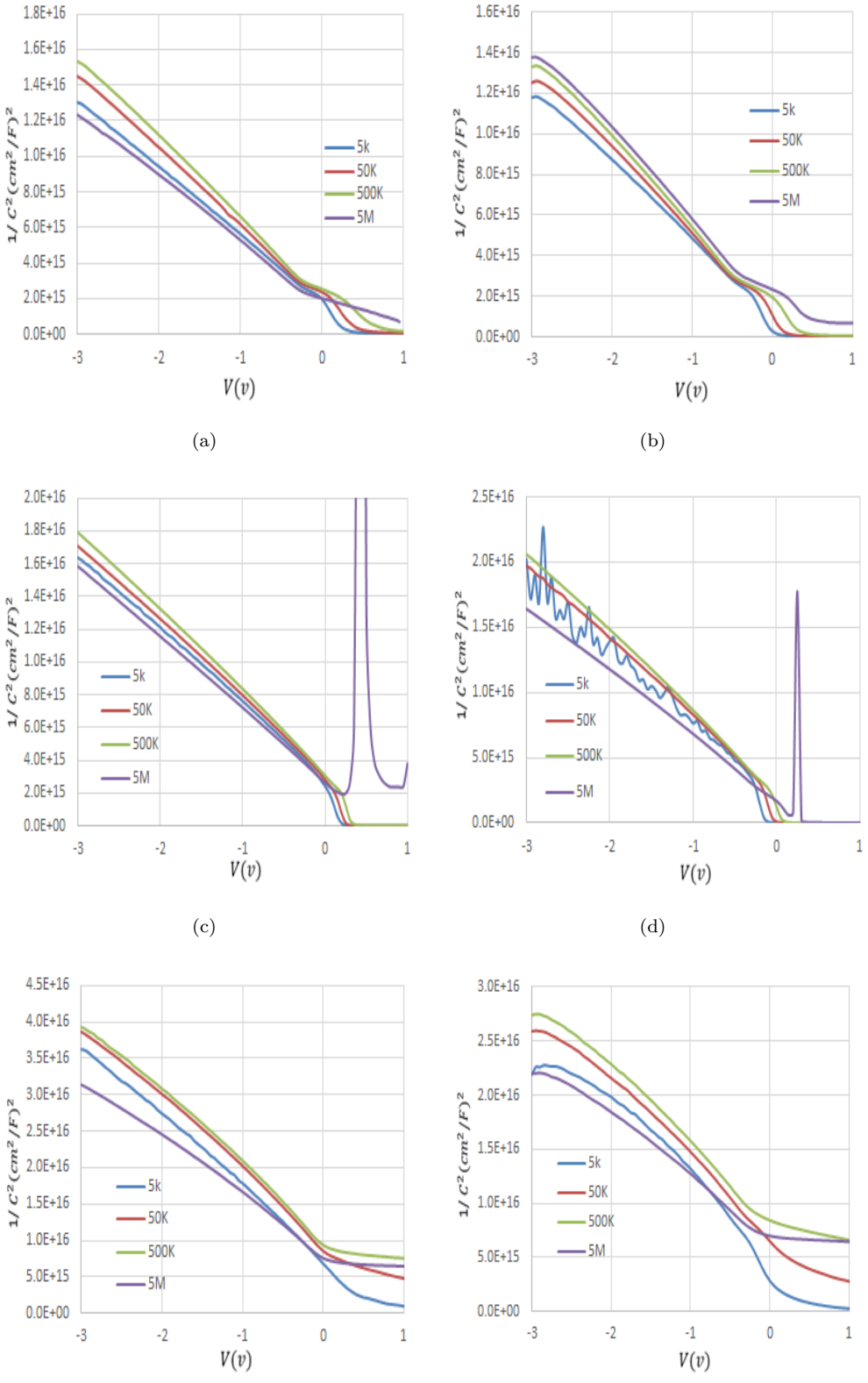

FIGURE A.4: Frequency dependent $1/C^2$-V characteristics of 50nm $Pd_{1-x}Ni_x$ Schottky diode hydrogen sensor in nitrogen (left) and 5 mbar hydrogen partial pressure (right) for (a,b) x=0 , (c,d) x=0.3 , and (e,f) x=0.4 . Data is based upon curves displayed in Fig A.3.

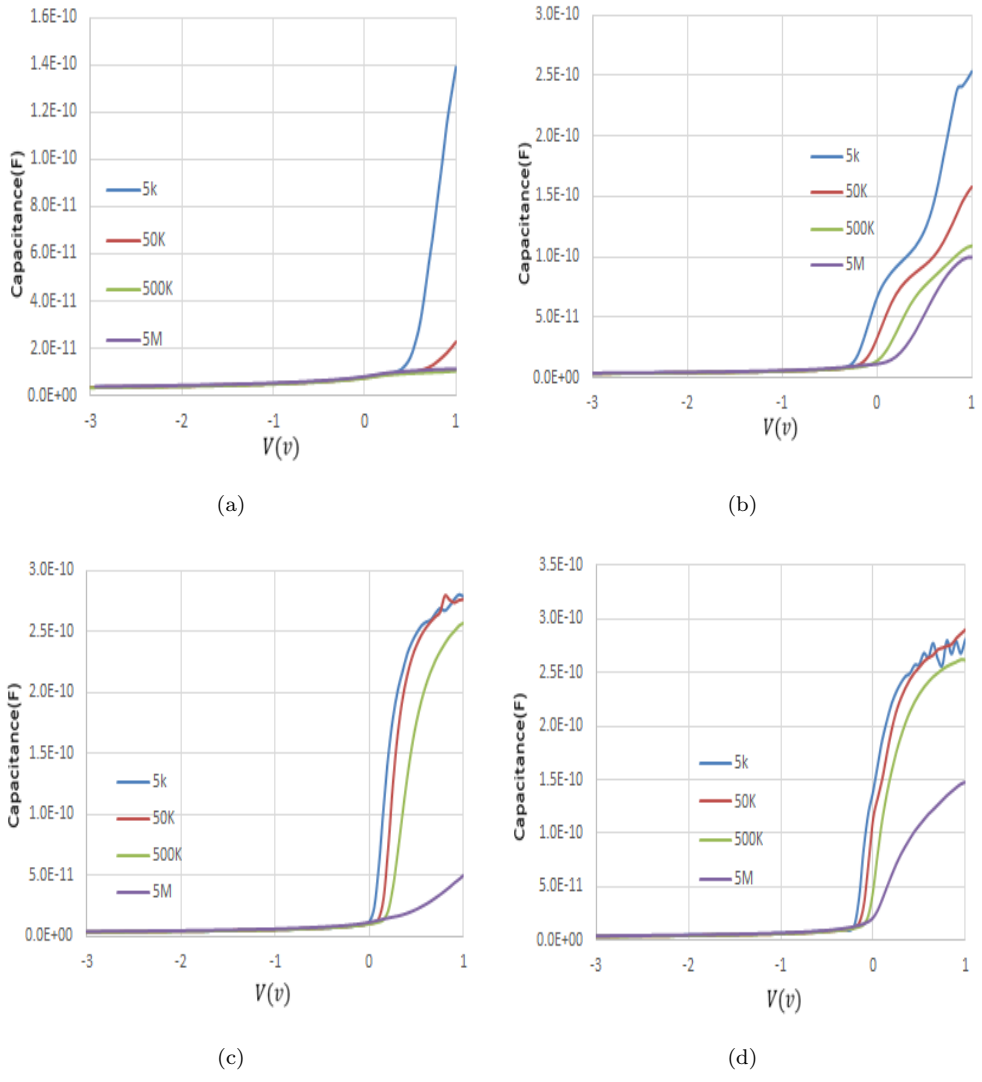

FIGURE A.5: Frequency dependent C-V characteristics of $Pd_{1-x}Ni_x$ Schottky diode hydrogen sensor in nitrogen (left) and 5 mbar hydrogen partial pressure (right) for (a,b) x=0.55 , and (c,d) x=1 with Pd cap.

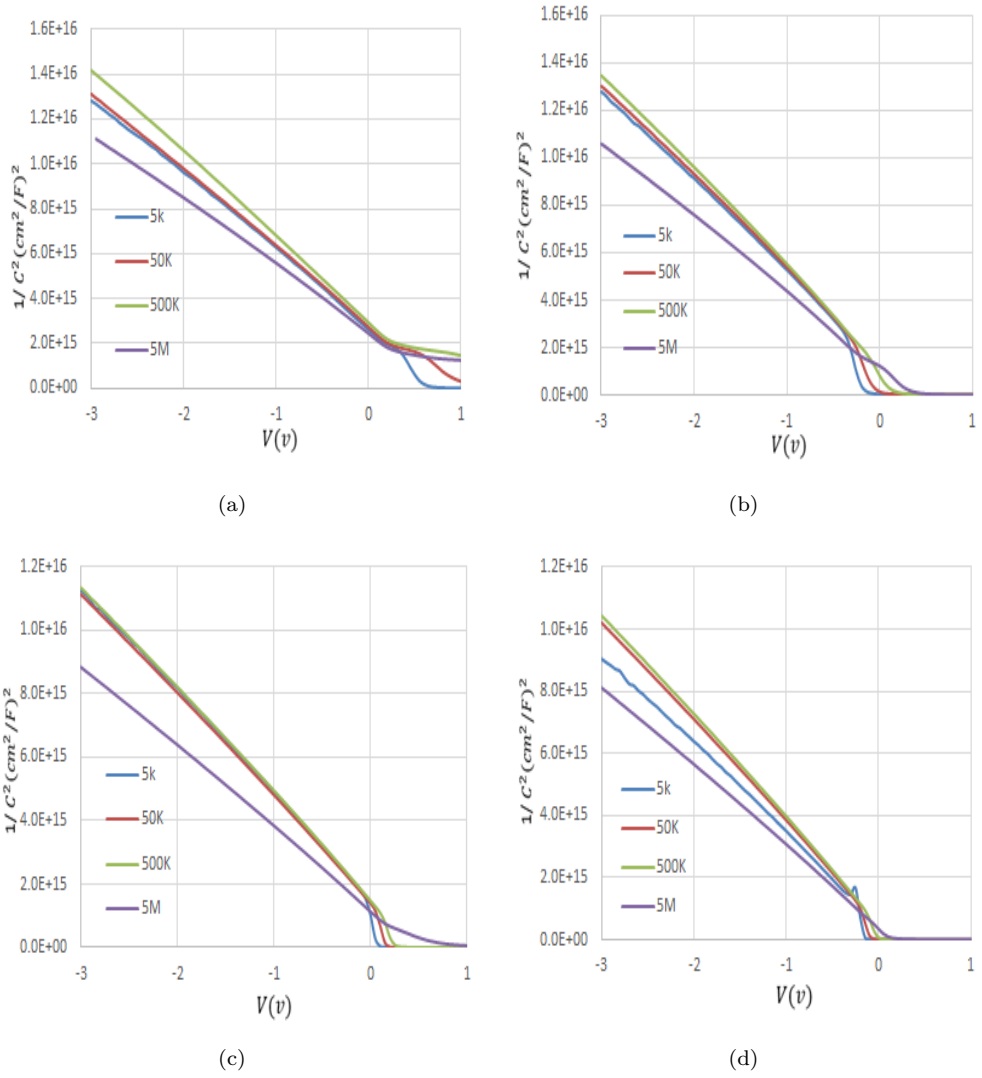

FIGURE A.6: Frequency dependent $1/C^2$-V characteristics of 50nm $Pd_{1-x}Ni_x$ Schottky diode hydrogen sensor in nitrogen (left) and 5 mbar hydrogen partial pressure (right) for (a,b) x=0.55, and (c,d) x=1 with Pd cap. Data is based upon curves displayed in Fig A.5.

Appendix B

Appendix of x_s=0.1, x=0.3 and x_b=0.4 Hydrogen Sensor

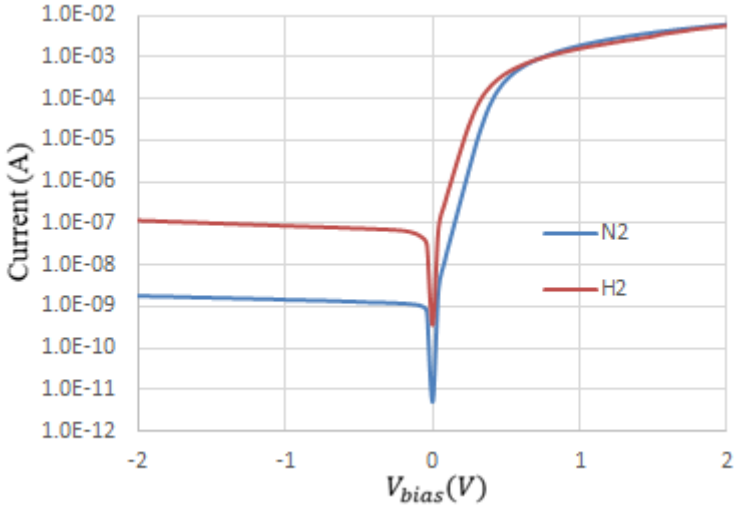

FIGURE B.1: Single I-V characteristics of x_s=0.1, x=0.3 and x_b=0.4 in barrier layer of composition modulated $Pd_{1-x}Ni_x$ Schottky barrier hydrogen sensor in nitrogen (0.3bar) and hydrogen-nitrogen mixture (5 mbar partial pressure).

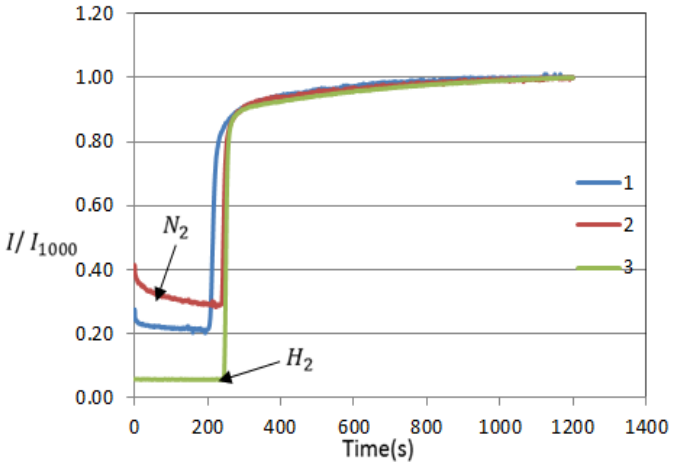

FIGURE B.2: Normalized time response of x_s=0.1, x=0.3 and x_b=0.4 in barrier layer $Pd_{1-x}Ni_x$ Schottky barrier hydrogen sensor after the exposure to 0.1bar of hydrogen.

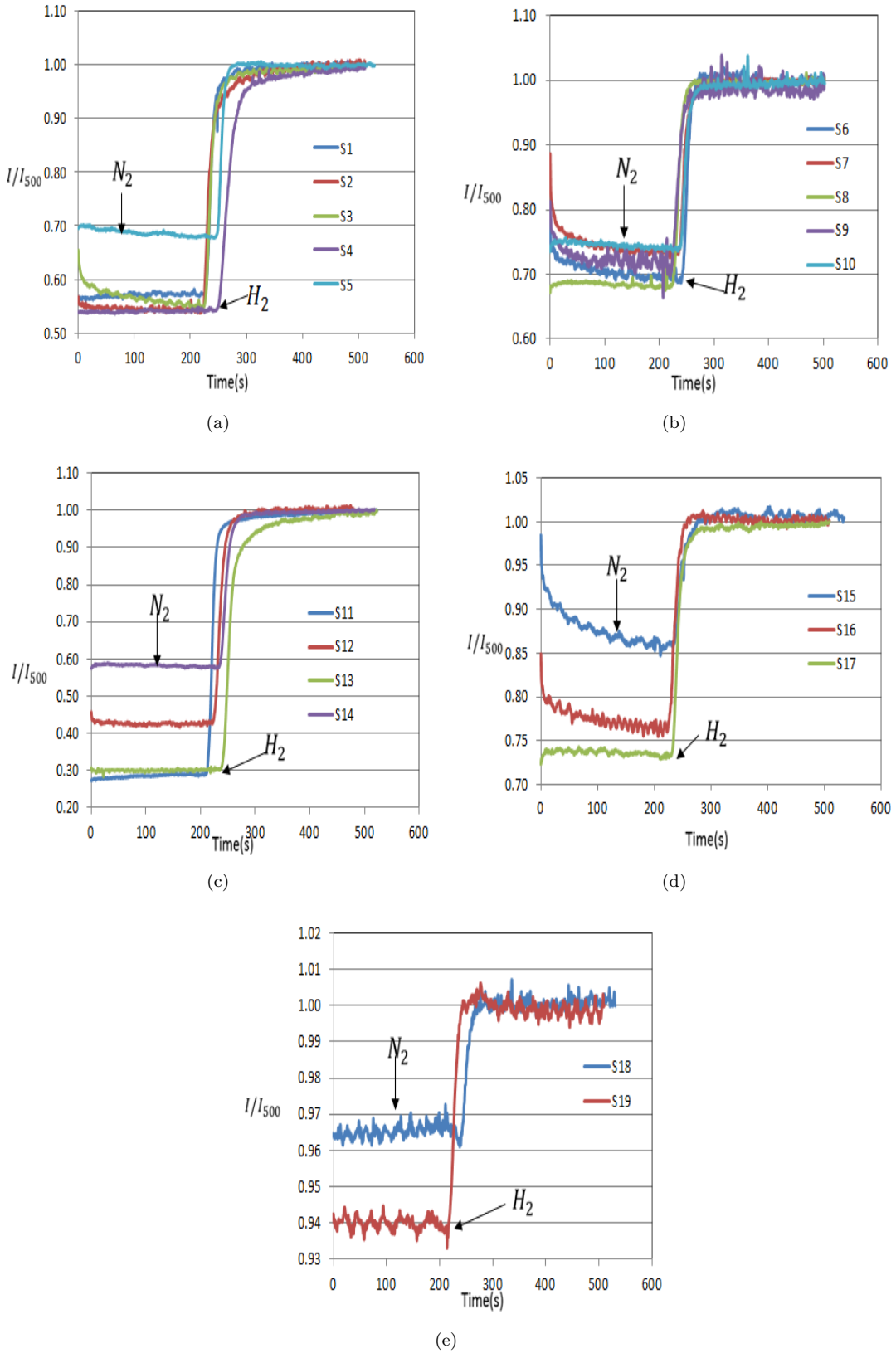

FIGURE B.3: 19 individual x_s=0.1, x=0.3 and x_b=0.4 in barrier layer $Pd_{1-x}Ni_x$ Schottky barrier hydrogen sensor I-V-t comparison under exposure to 0.1bar of 5%hydrogen-nitrogen mixture.

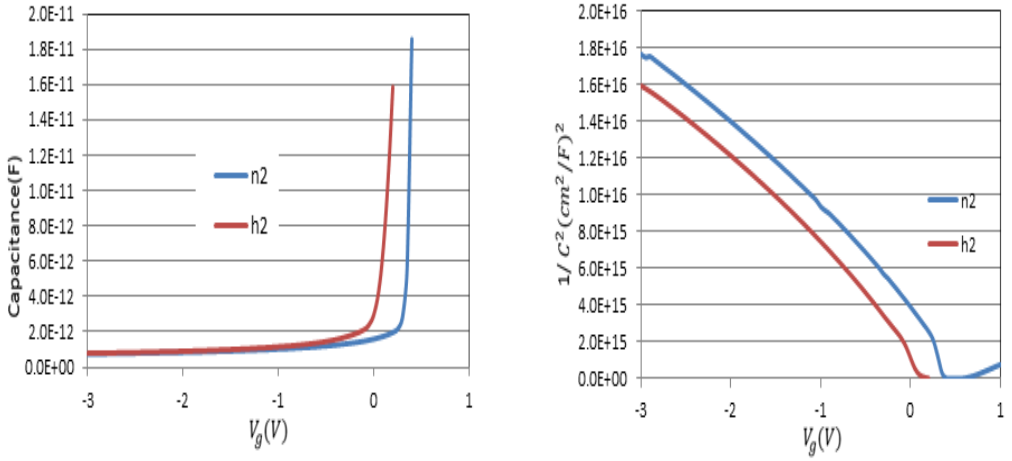

(a) (b)

FIGURE B.4: (a) C-V characteristic of x_s=0.1, x=0.3 and x_b=0.4 in barrier layer of $Pd_{1-x}Ni_x$ Schottky barrier hydrogen sensor in both nitrogen and 5% hydrogen-nitrogen mixture ambient at 1MHz. (b)$1/C^2$-V characteristic of the same device. The linear dependence reveals the formation of depletion region.

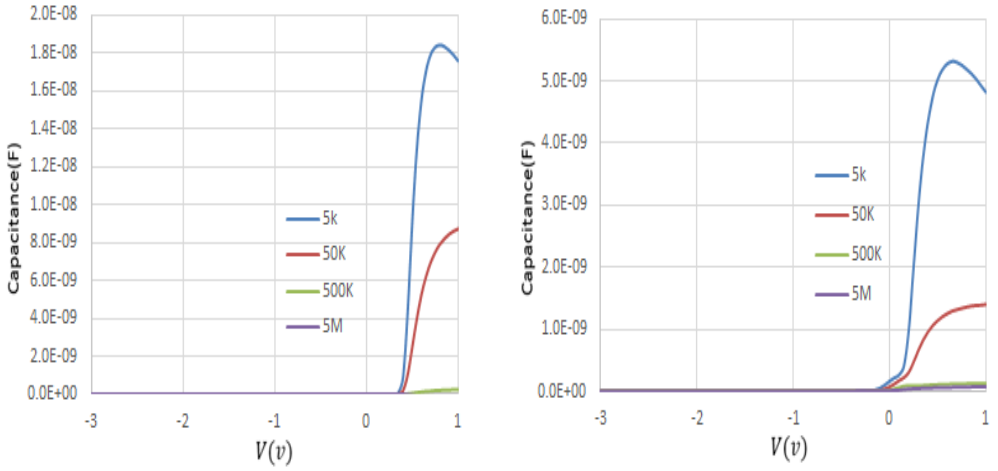

(a) (b)

FIGURE B.5: (a) Variable frequency C-V characteristic of x_s=0.1, x=0.3 and x_b=0.4 in barrier layer of $Pd_{1-x}Ni_x$ Schottky barrier hydrogen sensor in nitrogen ambient. (b)Variable frequency C-V characteristic of x_s=0.1, x=0.3 and x_b=0.4 in barrier layer $Pd_{1-x}Ni_x$ Schottky barrier hydrogen sensor in 5% hydrogen-nitrogen ambient.

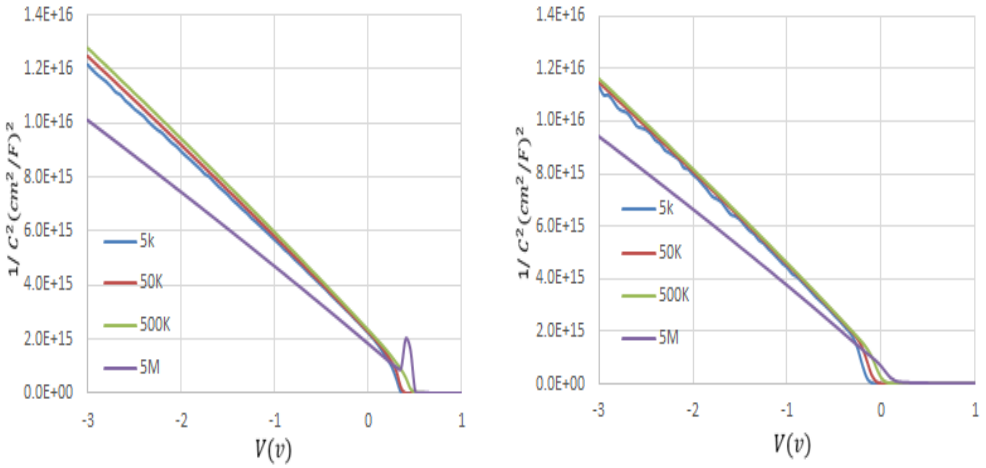

(a) (b)

FIGURE B.6: (a) Variable frequency $1/C^2$-V characteristic of x_s=0.1, x=0.3 and x_b=0.4 in barrier layer $Pd_{1-x}Ni_x$ Schottky barrier hydrogen sensor in the nitrogen ambient.(b) Variable frequency $1/C^2$-V characteristic of x_s=0.1, x=0.3 and x_b=0.4 in barrier $Pd_{1-x}Ni_x$ layer Schottky barrier hydrogen sensor in the hydrogen ambient.

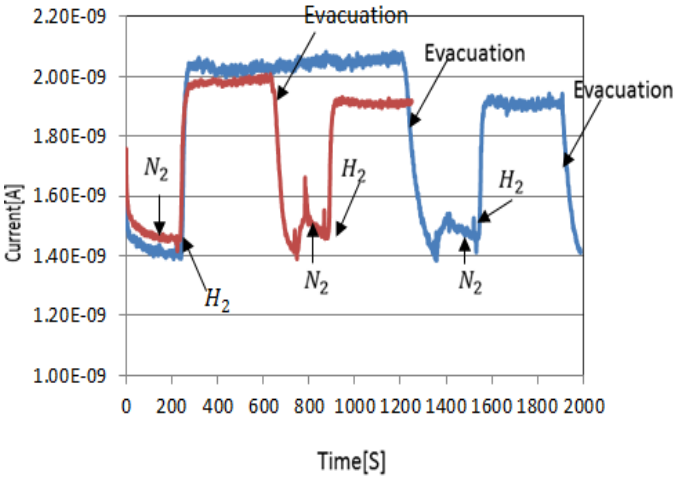

FIGURE B.7: Response of x_s=0.1, x=0.3 and x_b=0.4 in barrier layer $Pd_{1-x}Ni_x$ Schottky barrier hydrogen sensor expose under multiple changes in hydrogen and nitrogen ambient. This measurement contains evacuate gas from the chamber and re-introduce nitrogen and hydrogen in the chamber.